METALLIZATION AND MODIFICATION OF LOW-K DIELECTRIC MATERIALS

David M. Martini, B.S.

Dissertation Prepared for the Degree of

DOCTOR OF PHILOSOPHY

UNIVERSITY OF NORTH TEXAS

December 2008

APPROVED:

Jeffry A. Kelber, Major Professor
William E. Acree, Jr., Committee Member
Thomas Cundari, Committee Member
Mohammad Omary, Committee Member
Michael G. Richmond, Chair of the Department of Chemistry
Sandra L. Terrell, Dean of the Robert B. Toulouse School of Graduate Studies

Martini, David M. Metallization and Modification of Low-k Dielectric Materials. Doctor of Philosophy (Chemistry), December 2008, 108 pp., 6 tables, 38 illustrations, reference list, 121 titles.

Aluminum was deposited onto both Teflon AF and Parylene AF surfaces by chemical vapor deposition of trimethylaluminum. This work shows that similar thin film (100 Angstroms) aluminum oxide adlayers form on both polymers at the low temperature dosing conditions used in the studies. Upon anneal to room temperature and above, defluorination of the polymer surfaces increased and resulted in fluorinated aluminum oxide adlayers; the adlayers were thermally stable to the highest temperatures tested (600 K). Angle-resolved spectra showed higher levels of fluorination toward the polymer/adlayer interface region. Copper films were also deposited at low temperature onto Teflon AF using a copper hexafluoroacetylacetonate-cyclooctadiene precursor. Annealing up to 600 K resulted in the loss of precursor ligands and a shift to metallic copper. As with aluminum adlayers, some polymer defluorination and resulting metal (copper) fluoride was detected.

Parylene AF and polystyrene films surfaces were modified by directly dosing with water vapor passed across a hot tungsten filament. Oxygen incorporation into polystyrene occurred exclusively at aromatic carbon sites, whereas oxygen incorporation into parylene occurred in both aromatic and aliphatic sites. Oxygen x-ray photoelectron spectra of the modified polymers were comparable, indicating that similar reactions occurred. The surface oxygenation of parylene allowed enhanced reactivity toward aluminum chemical vapor deposition.

Silicon-carbon (Si-Cx) films were formed by electron beam bombardment of trimethylvinylsilane films which were adsorbed onto metal substrates at low temperatures in ultra-high vacuum. Oxygen was also added to the films by coadsorbing water before electron

beam bombardment; the films were stable to more than 700 K, with increasing silicon–oxygen bond formation at elevated temperatures. Copper metal was sputter deposited in small increments onto non-oxygenated films. X-ray photoelectric spectra show three-dimensional copper growth (rather than layer-by-layer growth), indicating only weak interaction between the copper and underlying films. Annealing at elevated temperatures caused coalescence or growth of the copper islands, with spectra indicating metallic copper rather than copper oxide.

Copyright 2008

by

David M. Martini

ACKNOWLEDGEMENTS

Financial support for this research was provided by the Semiconductor Research Corporation (SRC) through the Center for Advanced Interconnect Science and Technology (CAIST) and is gratefully acknowledged.

TABLE OF CONTENTS

Page

ACKNOWLEDGMENT iii

LIST OF TABLES vii

LIST OF ILLUSTRATIONS viii

Chapters

1. INTRODUCTION TO METAL/POLYMER INTERFACIAL INTERACTIONS 1
   - 1.1 Background 1
   - 1.2 Experimental Methods 2
     - 1.2.1 XPS and AES Analysis 3
     - 1.2.2 XPS for Nucleation Modes 4
     - 1.2.3 Other Surface Science Techniques 5
     - 1.2.4 Metal Deposition Techniques 6
   - 1.3 Metallization of Fluoropolymers 8
     - 1.3.1 Metal Evaporation 8
     - 1.3.2 Sputter Deposition 10
     - 1.3.3 Al MOCVD 10
     - 1.3.4 Cu MOCVD 12
   - 1.4 Introduction to SiC Films 14
   - 1.5 Conclusions 15
   - 1.6 Chapter References 16

2. METALORGANIC CHEMICAL VAPOR DEPOSITION OF ALUMINUM AND COPPER ON TEFLON® AF FILMS 20
   - 2.1 Background 20
   - 2.2 Experiment 22
   - 2.3 Results and Discussion 24
     - 2.3.1 XPS of the Neat Polymer Surface 24
     - 2.3.2 TMA on Teflon® AF Films 25
     - 2.3.3 Cu^{I}(hfac)(COD) on Teflon® AF Films 33
   - 2.4 Summary and Conclusions 36

2.5 Chapter References 37

3. CHARACTERIZATION AND ALUMINUM METALLIZATION OF A PARYLENE AF-4 SURFACE 39

3.1 Background 39

3.2 Experimental Methods 41

3.3 Results 44

3.3.1 Surface Analysis of Parylene AF-4 44

3.3.2 Exposure to TMA at 112 K 47

3.3.3 Effects of Annealing 49

3.3.4 Angle Resolved Spectra 55

3.4 Discussion 56

3.5 Summary and Conclusions 59

3.6 Chapter References 60

4. MODIFICATION OF PARYLENE AF-4 SURFACES USING ACTIVATED WATER VAPOR 63

4.1 Background 63

4.2 Experimental Methods 64

4.3 Results 67

4.3.1 Modification of Polystyrene 67

4.3.2 Neat Parylene AF-4 69

4.3.3 Modification of Parylene AF-4 71

4.3.4 Surface Roughness of Modified AF-4 74

4.3.5 Trimethylaluminum Deposited onto Modified AF-4 75

4.4 Discussion 77

4.5 Summary and Conclusions 81

4.6 Chapter References 82

5. FORMATION OF SI-C_X FILMS AND THEIR INTERACTIONS WITH H_2O AND Cu 84

5.1 Introduction 84

5.2 Experimental 85

5.3 Results and Discussion 88

5.3.1 Film Composition 88

5.3.2 Stability in Air/H_2O 89
5.3.3 Addition of Oxygen to Films 92
5.3.4 Annealing of Si(O)C Films 94
5.3.5 Cu Interactions with Si-C_x Films 96
5.4 Conclusions 99
5.5 Chapter References 100

LIST OF REFERENCES 102

LIST OF TABLES

Page

2.1 Selected Aluminum Bond Energies 28

3.1 AFM Surface Roughness Data for Parylene AF-4 44

3.2 Selected Aluminum Bond Energies 57

4.1 Carbon Balance for Polystyrene 69

4.2 Carbon Balance for Parylene AF-4 72

4.3 AFM Surface Roughness Data for Parylene AF-4 75

LIST OF ILLUSTRATIONS

Page

1.1 Schematic of “typical” UHV surface analysis chamber 3

1.2 Intensity vs. time plots of (a) Volmer–Weber (islanding), (b) Frank–van der Merwe (layer-by-layer), and (c) Stranski–Krastanov growth (monolayer then islanding).............5

1.3 CVD reaction mechanisms of (a) Cu(hfac)(COD) and (b) $Cu(hfac)_2$ on a metal substrate 13

2.1 Structure of Teflon® AF 1601 21

2.2 F(1s), O(1s), and C(1s) XPS spectra of neat Teflon® AF surface referenced to F(1s) binding energy of 689.0 eV 24

2.3 C(1s) and Al(2p) XPS spectra of Teflon®-AF surface dosed with TMA at 112 K and subsequently annealed to 300 K and 550 K (in series) in UHV 25

2.4 O(1s) and F(1s) XPS spectra of Teflon®-AF surface dosed with TMA at 112 K and subsequently annealed to 300 K and 550 K (in series) in UHV 26

2.5 Depth profiling using XPS angle resolution 31

2.6 Surface normal and 60° take-off angle-resolved Al(2p) spectra of TMA dosed and annealed Teflon® AF surface 32

2.7 Composition diagram of CVD aluminum adlayer on Teflon® AF 32

2.8 C(1s), O(1s), and F(1s) spectra of Cu(I)hfac(COD) on Teflon®-AF at 105 K, 300 K, and 600 K..33

2.9 Cu(2p) and Cu(L3VV) spectra of Cu(I)hfac(COD) on Teflon®-AF at 300 K and 600 K 34

3.1 Structure of Parylene AF-4 40

3.2 Atomic force micrograph of vapor deposited Parylene AF-4...43

3.3 F(1s) and C(1s) XPS spectra of neat Parylene AF-4 45

3.4 XPS spectra of TMA on Parylene AF-4 at dosing temperature and annealed to 300 K and 550 K: (a) F(1s) and C(1s) spectra and (b) Al(2p) and O(1s) spectra 48

3.5 (a) F(1s) and C(1s) XPS spectra and (b) Al(2p) and O(1s) XPS spectra of TMA on Parylene AF-4, surface normal and 60° angle resolved...53

3.6 Variations in Al/Al(112 K), O/Al, and non-polymeric C/Al signal ratios as a function of annealing temperature 54

3.7 Composition diagram of aluminum adlayer on Parylene AF-4 57

4.1 Structure of Parylene AF-4 64

4.2 XPS spectra of polystyrene (a) before and (b) after modification 67

4.3 XPS spectra of neat Parylene AF-4 surface 70

4.4 XPS spectra of Parylene AF-4 exposure to (a) 3,000 L and (b) 24,000 L "activated" water vapor 71

4.5 Atomic ratios of modified Parylene AF-4 73

4.6 AFM images of (a) neat and (b) modified Parylene AF-4 samples 74

4.7 XPS Al(2p) spectra of modified Parylene AF-4 sample (3,000 L modification) after exposure to TMA at 310 K. Exposures are (a) 3,000 L (b) 6,000 L (c) 9,000 L and (d) 15,000 L TMA 76

4.8 Al($2p_{3/2}$) XPS intensity versus exposure for (a) modified and (b) unmodified Parylene AF-4 exposed to activated water 76

5.1 Schematic of UHV/XPS chamber 85

5.2 XPS spectra of a typical Si-C_x film 88

5.3 Mass spectrum of ethenetrimethylsilane (vinyltrimethylsilane, or VTMS) 89

5.4 XPS spectra of 50 Å Si-C_x film on Cu substrate (a) in UHV and (b) after exposure to ambient environment for 30 minutes 90

5.5 Si-C_x Film (~100 Å) on Cu substrate (a) in UHV and (b) after 38 days in air 91

5.6 XPS spectra of films formed by 2-layer deposition sequences. (a) 30 L exposures with VTMS directly on Cu and (b) 30 L exposures with H_2O directly on Cu 92

5.7 XPS spectra of films formed by 4-layer deposition sequences. (a) 5 L exposures with VTMS directly on Cu and (b) 15 L exposures with H_2O directly on Cu 93

5.8 Si(2p) spectra of Si(O)C films made from coadsorbed VTMS and H_2O (alternating layers of 5 L each) 95

5.9 Deposition curve for Cu sputter deposited onto 50 Å Si-C_x 96

5.10 Cu (L_3VV) Auger peak after sputter deposition of Cu onto a Si-C_x film. (a) 4 min. (b) 8 min. (c) 12 min. (d) 16 min. (e) 20 min. (f) 24 min. (g) 28 min and (h) 32 min 97

5.11 Shift in Cu Auger parameter with annealing temperature (a)–(f) and bulk Cu foil (g) 98

CHAPTER 1

INTRODUCTION TO METAL/POLYMER INTERFACIAL INTERACTIONS

1.1. Background

The microelectronics industry has seen a rapid scaling of integrated circuits to produce smaller and faster integrated circuits (ICs) with lower power requirements, but further downscaling involves a variety of obstacles. Decreasing the pitch of metal lines and interconnects creates increased line resistance (R); decreasing line spacing leads to increased capacitance (C), which contributes to higher power dissipation and cross-talk between lines. At feature sizes below ~0.5 μm, the decreasing signal delay resulting from reduced gate lengths is overcome by resistance-capacitance (RC) delay.[1] In order to reduce the influence of RC delay on signal speeds and power loss, integration of materials with dielectric constants (k) lower than that of SiO_2 ($k \approx 4$) will be necessary.[1,2]

Many types of low-k materials are available, including polymers, fluoropolymers, fluorinated oxides, and porous dielectrics such as xerogels. Although many porous dielectrics have extremely low dielectric constants (k = 1.8–2.2),[1] capping layers may be necessary because their porous nature leads to problems from moisture absorption and diffusion of materials into the pores. Several fluoropolymers are available with $k \leq 3.0$, low moisture absorption, and temperature stabilities possibly high enough for back-end industrial processing ($T \leq 450$ °C).[3] Although most fluoropolymers are fairly inert, reactions with metals can occur that defluorinate the polymers, giving rise to fluorine out-diffusion and metal-fluoride bond formation. This M–F formation can increase the resistivity of metal lines, adding to the total RC delay, and may also enhance corrosion of lines and interconnects.

With device dimensions shrinking to below 90 nm, the challenges and limitations of integrating low-k materials into integrated circuits will largely depend on the interfacial properties of these materials. For example, it has been shown that alloying between Cu and Ta barrier layers can occur up to a depth of 50 Å,[4] which may constitute a major portion of the thickness of the barrier layers. In the same fashion, many of the interactions between metals and low-k materials (e.g., nucleation, adhesion, thermal stability) are dominated by interfacial properties. If intermixing or migration occurs between metals and low-k dielectric materials, a significant change in metal resistivity and/or dielectric capacitance may result. Characterization of metal/low-k interactions at the atomic and molecular levels will continue to yield insight into the strengths and weaknesses of the materials and their processibility.

1.2. Experimental Methods

Surface science studies typically take place, in whole or in part, under rigorously controlled ultra-high vacuum (UHV) conditions (below ~10^{-9} Torr), whereas actual IC manufacturing occurs in high vacuum (~10^{-7} Torr) or less-controlled conditions and often involves exposure to ambient. It is therefore reasonable to ask what relevance UHV studies actually have to understanding the behavior of "real world" systems. Although polymer surfaces are typically less reactive towards oxygen and water vapor than are clean transition metal or semiconductor surfaces, moisture absorption and impurity contamination from the ambient environment are possible factors of concern. The answer to the above question is that UHV surface science studies (1) permit detailed chemical and electronic information to be gained regarding polymer/metal interactions under ideal conditions, and (2) permit the examination of how such interactions are affected by systematically varied levels of various contaminants.

A typical UHV chamber setup for surface analysis is shown in Figure 1.1. This often consists of a main chamber evacuated by a pump (e.g., turbomolecular, sublimation, cryogenic, etc.), ports for electron beam or chemical introduction, surface analysis equipment, sample manipulator, and often an antechamber used for higher-pressure chemical dosing. Base pressures

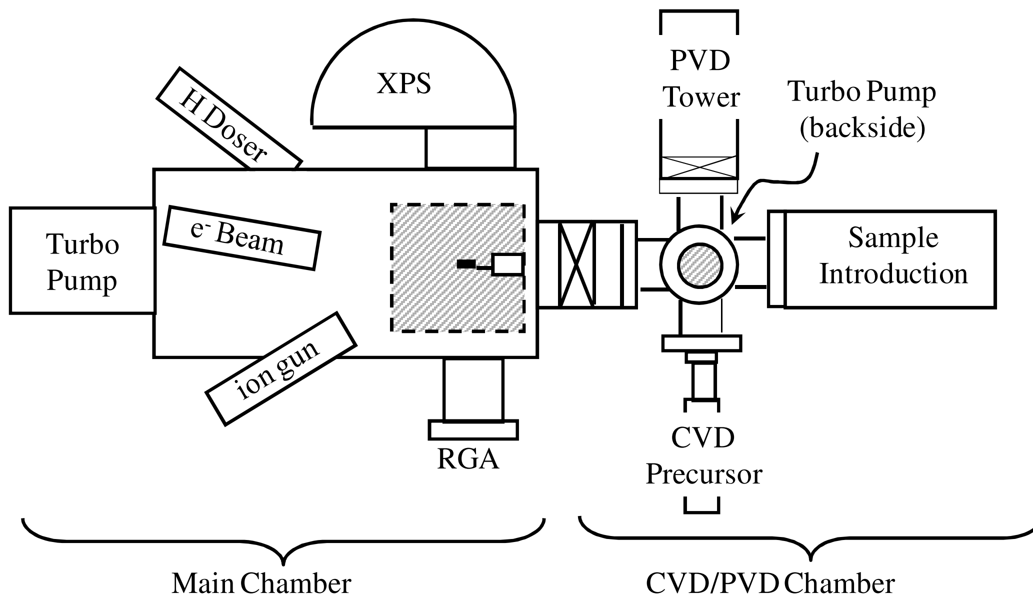

Figure 1.1. Schematic of a “typical” UHV surface analysis chamber.

in UHV systems are often 1 x 10^{-10} and 1 x 10^{-12} Torr.

1.2.1. XPS and AES Analysis

Both x-ray photoelectron spectroscopy (XPS) and Auger electron spectroscopy (AES) are surface-sensitive techniques that measure the kinetic energy of electrons ejected from a sample that is bombarded by x-ray radiation (for XPS) or a beam of electrons (for AES). Because of the relatively short inelastic mean free path lengths of ejected electrons (tens of angstroms), analysis depths for both XPS and AES are typically below 100 Å.[5,6] Because XPS uses a discreet energy source (Mg Kα or Al Kα x-rays), ejected core-level electrons are indicative of specific chemical

bonding environments and much of the characterization of surfaces can be made on the basis of XPS data alone. Due to the nature of the Auger electron transition, AES peaks tend to be broader and less sensitive to changes in chemical environment than those in XPS. Scan averaging over long periods of time is also often necessary in AES due to relatively low signal output. Damage to surfaces may result from typical electron beams used in AES (> 10^{-3} A/cm^2, 1–10 keV),[6] though damage can be reduced by utilizing lower current densities of the electron beam. For these reasons, XPS is often preferable to AES for analyzing insulating materials. Sample surface charging may shift the observed kinetic energies (peak positions) and broaden peaks in both XPS and AES, posing problems for peak identification. Even without extra equipment to neutralize charging, however, it is relatively simple to compensate for charging effects in XPS by referencing peaks to a known value, usually that of an inert metal or a hydrocarbon species.

1.2.2. XPS for Nucleation Modes

Different growth modes are possible during the initial stages of the deposition of an adsorbate (in this case a metal) onto a substrate, depending upon the strengths of the interactions between the metal and substrate atoms, and XPS and AES techniques have long been used to analyze such modes.[7,8] Volmer–Weber (V–W) growth involves the formation of small particles, or “islands,” on substrates without the formation of a continuous monolayer. This behavior occurs when metal–metal interactions are stronger than metal–substrate interactions, and that the metal adsorbate does not “wet” the surface. Islanding occurs when the surface tension of the substrate (γ_S) is less than the additive surface tensions of the metal (γ_M) and metal–surface interaction (γ_{MS}), or $\gamma_S < \gamma_M + \gamma_{MS}$. Frank–van der Merwe (F–M) growth is defined as layer-by-layer growth of the adsorbed metal; the substrate surface surface tension is greater than the metal

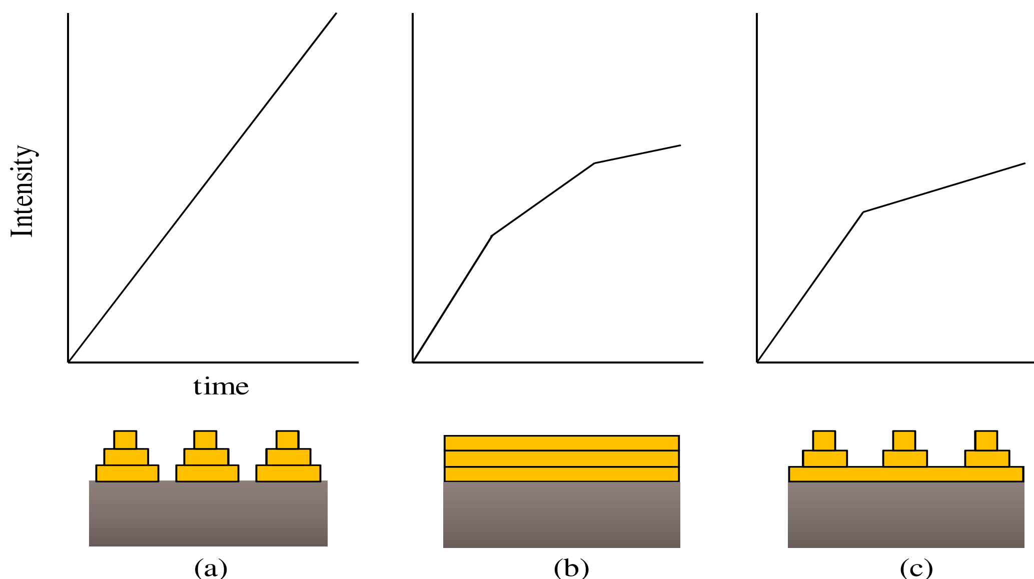

Figure 1.2. Intensity vs. time plots of (a) Volmer–Weber (islanding), (b) Frank–van der Merwe (layer-by-layer), and (c) Stanski–Krastanov growth (monolayer, then islanding). Adapted with permission from Argile and Rhead.[7]

overlayer and metal–substrate interaction, or where $\gamma_S > \gamma_M + \gamma_{MS}$. Stranski–Krastanov (S–K) growth is the formation of islands after the initial formation of one to three monolayers and is similar to F–M interactions. Typical plots of XPS or AES adsorbate intensity versus deposition time (I vs. t) are shown in Figure 1.2 for the three common growth modes. In general, V–W growth is characterized by an I vs. t plot with either a constant slope or a slight downward curve. The F–M growth mode typically has a plot with several segments of changing slope, with each break indicating the beginning of a new layer. The plot of S–K growth, though difficult to distinguish from F–M mode, has one or two breaks and typically begins to level off at higher coverages (when islanding occurs).[7,8]

1.2.3. Other Surface Science Techniques

Many other surface science methods exist that can be used to probe the metal/polymer interface region, only some of which will be mentioned here. Rutherford backscattering

spectroscopy (RBS) can be used to determine the masses and atomic concentrations of atoms versus sample depth. A beam of light ions (e.g., He^{+} or He^{++}) is projected onto the sample and the number and energy of the backscattering ions is recorded.[9,10] Some prior knowledge of the density of the sample is necessary. Mass resolution for lighter elements is better due to the transfer of energy between incident ion and sample atom, while sensitivity is greater for the heavier elements due to larger scattering cross sections.

High resolution electron energy loss spectroscopy (HREELS), uses a beam of low energy electrons (< 10 eV) to probe the outermost surface layers of metal or insulating samples. The energy loss of the electrons (0–0.5 eV) after interaction with the surface gives information about the molecular vibrations of adsorbed molecules equivalent to 0–4000 cm^{-1} in the IR spectrum.[10] The presence or absence of vibrational modes can be used to determine the bonding and orientation of adsorbed species. Surface charging makes HREELS difficult on insulating materials, though some methods have been developed to bypass this problem.

Secondary ion mass spectrometry (SIMS) is often performed in order to obtain depth profile information about a sample. An ion beam is used to slowly sputter away layers from the sample surface, and a time-of-flight mass spectrometer is used to detect the resulting ion fragments. SIMS results are plotted as the intensity of specific ions as a function of sample depth. Unknown ion fragments and sputter implantation (“knock-in”) of surface atoms can complicate analysis, and comparison with samples of known composition is often necessary.[10,11]

1.2.4. Metal Deposition Techniques

Several types of metal deposition are discussed in this chapter. Thermal evaporation, electron-beam evaporation, and sputter deposition are physical vapor deposition (PVD)

techniques that involve the deposition of metal atoms directly onto a substrate. These techniques are used for non-selective deposition (on both metallic and insulating materials) and typically produce very pure, low-resistivity metal layers. PVD processes involve line-of-sight deposition, however, and coverage is poor for features with high aspect ratios (height-to-width) or complex designs. Chemical vapor deposition (CVD) techniques involve the deposition of precursor molecules consisting of metal–organic complexes. The deposited molecules undergo surface-mediated reactions, resulting in loss of the ligand molecules and deposition of the pure metal. Because CVD involves deposition from a vapor, conformal coverage can be obtained across complex features.

Evaporative deposition is performed by either resistive or electron-beam heating of a pure metal in a high vacuum environment. High or ultrahigh vacuum environments are required because many of the metals have low vapor pressures and are highly reactive with atmospheric gases. Because metals have different vapor pressures, it is often not possible to evaporate stoichiometric mixtures of two different metals from the same source, although "dual-source" evaporators can be used for this purpose. Unfortunately, the high vacuum necessary for metal evaporation is often not compatible with industrial processing steps. Sample heating is typically not a factor with evaporative techniques since the sample is not in close proximity to the evaporator.

Sputter deposition is most often performed under low vacuum conditions (mTorr range), and is the main technique used in industry for the deposition of metal layers. A sputter target is bombarded with heavy ions from a plasma of inert gas, usually Ar^+ or Ne^+, and the metal atoms (and ions) that are dislodged travel toward the sample with energies in the range of 0.1–500 eV.[12,13] Because of the energetics of the metal species involved, some ablation and roughening

occurs, especially with polymer samples. Radiation damage and sample heating are also possible from the interaction of the plasma with the sample, which can be grounded or held at a bias potential with respect to the source. Sputter deposition of alloys and compounds is possible using complex target materials, and deposition of insulating materials is possible using direct current (d.c.) magnetron or radio frequency (r.f.) plasma sources.[14] Sputtering is commonly used to produce "seed layers" for Cu electroplating in high-aspect-ratio devices.

Metal-organic chemical vapor deposition (MOCVD) is ideally a surface-catalyzed reaction that produces low resistivity metal films with good step coverage and, in certain cases, selective deposition (conductive substrates preferred over insulators).[15–18] A good precursor material has a high vapor pressure; good thermal stability in the gas phase; and ligands that readily dissociate from the metal atoms upon contact with the sample surface, leaving only metal atoms and volatile ligand species.[15] The molecular mechanisms involved in the deposition are often quite complex, and ligands can decompose on the sample surface – leading to impurity incorporation and increased resistivity of metal layers. Ideally, precursor deposition and dissociation should also occur at temperatures low enough to be suitable for processing of microelectronics samples.

1.3. Metallization of Fluoropolymers

1.3.1. Metal Evaporation

A number of experiments have investigated metal/polymer interfaces by thermal and electron-beam evaporation of metals in UHV, and the reactivities of various metals (Al, Ti, Cr, Ni, Cu, Ag, and Au) with fluoropolymer substrates have been compared.[19–25] Both the formation of metal–polymer surface bonds and the penetration of the metals into the polymer play a role in

the formation of stable metal layers on fluoropolymers. In XPS studies of first-row transition metals (Ti, Cr, Ni and Cu), it has been found that Ti, Cr, and Ni all formed metal carbides upon reaction with fluoropolymer substrates, while only Ti and Cr formed appreciable fluoride species.[20–24] Both XPS and peel strength studies indicate that reactivities of these metals proceed as Ti > Cr (> Ni?) > Cu (no data given for Ni).[22] It has been suggested by at least one group[23] that differences in electronegativities between the metals and the fluoropolymer CF_n groups may be partly responsible for adhesion, where the largest electronegativity difference leads to the strongest bonding properties (electronegativities: Ti ~ Al < Cr < Ni ~ Cu < Au). The coinage metals (Cu, Ag, Au) all showed little or no M-C or M–F bonding and low peel strengths, indicating very little reaction with the fluoropolymer substrates. Although metal reactivity increases the adhesion and stability of the resulting metal-polymer interface, this bonding may result in an interface region of up to 40 Å of carbides, fluorides, and oxides, resulting in increased resistivity of the metal and higher capacitance of the dielectric material.[21]

The study of aluminum metallization of polymers has also been of particular interest to the semiconductor industry due to the use of Al, both exclusively and as an alloy, in conducting metal lines and interconnects. In general, Al is found to have weaker interactions with fluoropolymers than the more reactive transition metals such as Ti and Cr.[20–23] As with Ti, Cr, and Ni, evaporated Al has been found to produce carbide, fluoride, and oxide species on the surfaces of fluoropolymers, with Al–O arising from both polymeric and environmental oxygen.[19,21] Du and Gardella[19] have reported that Al–fluoropolymer bonding leads to defluorination of the polymer surface and diffusion of F^- ions into the bulk Al layer. Penetration of Al into the polymer also occurs, although this may be an artifact of “knock-in” from the sputter depth profiling technique. Others have reported that Al evaporation onto Teflon® PFA

samples results in the formation of ~20 Å of carbides, oxides, and fluorides, whereas Cr evaporation forms a layer of up to 40 Å.[21] The thinner layer of reacted Al and lower peel strengths on Teflon® PTFE and FEP indicate that Al is less reactive toward fluoropolymer substrates than transition metals such as Ti and Cr.

1.3.2. Sputter Deposition

Few studies are reported on the sputter deposition of metals onto polymers, possibly because the high energetics of sputter deposition can result in damage to polymer substrates. Sputter deposition of Cu and Ti onto the FLARE™ fluoropolymer has been reported by Du et al.[25] This group found that significantly more defluorination of the polymer was caused by sputter deposition than by metal evaporation. Although Ti sputter deposition produced Ti-F and Ti-C bond formation on the polymer surface, Cu sputter deposition resulted in no apparent Cu-F formation (and Cu does not form carbide species). Vasile et al.[26] previously reported that sputter deposition of Al on polyimide results in ~100-300 Å mixing of the metal and polymer. In contrast, other researchers[11] found that the sputter deposition of Cu onto Parylene-N substrates produced no metal-polymer intermixing, although partially-ionized beam (PIB) deposition of Cu resulted in ~90 Å of interface formation. Peel strengths for the PIB Cu were also much higher than those of evaporated or sputter deposited Cu, indicating that mechanical intermixing enhances the adhesion between metals and polymers.

1.3.3. Aluminum MOCVD

Due to low temperature processing and more uniform step-coverage on substrate features, especially high aspect ratio trenches and vias in semiconductor manufacturing, chemical vapor

deposition is often an attractive alternative to physical vapor deposition techniques.[15,17] CVD inherently necessitates chemical reaction, however, and a major problem of the technique is the reduction of precursor materials to pure metals – often precursors are not completely dissociated and carbon and/or oxygen contamination results.

Several precursor materials have been investigated for the purpose of Al metal deposition, with trimethylaluminum (TMA), dimethylaluminum hydride (DMAH) and triisobutylaluminum (TIBA) among the most common. Single crystal, metallic Al metal can be selectively deposited onto H-terminated Si holes (surrounded by SiO_2) from a DMAH precursor by low-pressure CVD at ~270°C.[18] Selective deposition results in a metallic Al layer with low resistivity (3 $\mu\Omega$ cm) and no apparent C or O incorporation into the bulk of the film, according to XPS depth profiling. Tsubouchi and Masu[18] have proposed that free electrons (conducting surface), H surface termination, and an asymmetric precursor (e.g., DMAH) are necessary conditions for the formation of metallic Al. They also note that, while DMAH will react with a conductive surface to form ordered Al metal and gaseous hydrocarbon products, an insulating surface must be supplied with free electrons (as from an r.f. plasma) in order to decompose the alkyl-aluminum bonds. Few reports of DMAH on oxides or polymers exist in the literature.

Triisobutylaluminum (TIBA) produces metallic Al films on both Si and Al substrates under various conditions.[27,28] Bent et al.[27] have found that, although showing very little reaction with clean Si substrates below 330 °C, room-temperature TIBA underwent β-hydride elimination reactions on both Al(111) and Al(100) surfaces at temperatures of 200-330°C to form epitaxial, carbon-free Al films. At temperatures above ~330°C, however, β-methyl elimination reactions occurred that led to incorporation of carbon in the films. Sekiguchi et al.,[28] reported that the low pressure CVD of TIBA on Si(100) could produce epitaxial Al(100) films by preheating the

precursor to 230ºC before deposition on a substrate held at ~400ºC. *Ab initio* molecular orbital calculations performed by Higashi, however, indicate that β-elimination reactions of alkyl-aluminum compounds are less likely on oxide surfaces (and, therefore, oxygen-containing polymers) due to increased activation energy for alkyl-aluminum compounds bound to oxygen.[29]

The possibility of producing metallic Al using trimethylaluminum (TMA) has had limited success, even on conductive substrates, although the use of low-power H_2/r.f. plasmas[18] and laser-induced CVD[30] have been demonstrated. Without plasma or laser assistance to dissociate TMA, researchers have reported the formation of Al–C and Al–O bonds on both metallic and polymer surfaces, with a distinct lack of Al metal formation.[31–34] From XPS measurements, Akhter et al.[34] have shown that TMA reacts with polyvinyl alcohol (PVA) at room temperature to produce an AlOC structure, with Al bridging the C-O bond in the polymer. In this reaction, TMA loses all three methyl groups, and no carbon is deposited onto the polymer surface.

1.3.4. Copper MOCVD

In general, two types of Cu β-diketonate precursors can be considered for CVD of Cu: Cu(I) compounds typically undergo "disproportionation" reactions—charge transfer resulting in both oxidation and reduction of the same species—to yield metallic Cu along with gaseous Cu(II) compounds; Cu(II) compounds must be heated to 250–300 °C in the presence of H_2 in order to form Cu metal (Figure 1.6). Two of the more widely studied Cu(I) compounds are 1,5-cyclooctadiene-Cu(I)-hexafluoroacetylacetonate (Cu[hfac][COD]) and trimethylvinylsilane-Cu(I)-hexafluoroacetylacetonate (Cu[hfac][TMVS]).[17,35–39] Copper(I) CVD reactions are particularly attractive due to the low deposition temperatures necessary (< 250 °C), the possibility of high deposition rates, and the lack of need for reducing agents such as hydrogen.[17]

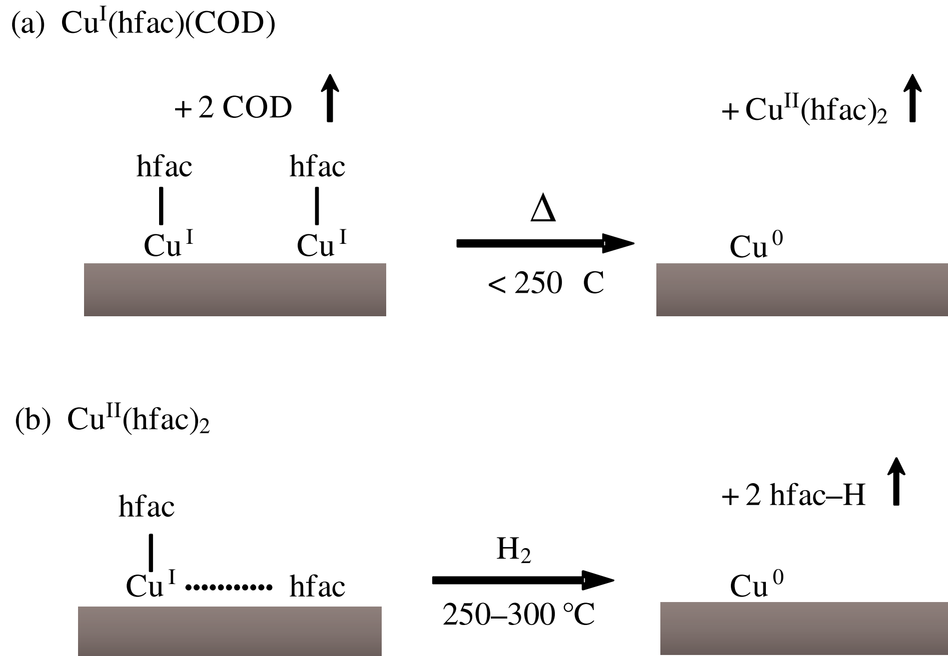

Figure 1.3. CVD reaction mechanisms of (a) Cu(hfac)(COD) and (b) Cu(hfac)$_2$ on a metal substrate.

One drawback of the Cu(I) mechanism is inefficiency due to loss of 50% of the surface Cu from disproportionation. Deposition rates remain high because there is no need to dilute the precursor with H_2 reducing agent, as with Cu(II) precursors.

Reports of CVD by Cu(I) precursors under both industrial[17,35] and UHV deposition conditions[36,38] on metal and TiN surfaces indicate that the disproportionation reaction to form clean Cu(0) occurs under typical processing pressures (10^{-3}–10^{-4} Torr) but rarely occurs in UHV. Naik et al.[17] reported the disproportionation of Cu^{I}(hfac)(TMVS) at 130–235 °C under typical MOCVD processing conditions (1–50 Torr) in sealed reactor tubes, with resulting formation of conductive Cu films. Since this reaction is a bimolecular process, it requires the presence of a mobile adsorbed Cu^{I}(hfac) species with surface coverages high enough for reaction to occur, which is an unlikely occurrence in UHV.[36,38] Rather than disproportionation, in UHV the hfac

ligands decompose upon annealing to 100–200 °C, leaving behind C, O, and F contamination in the Cu films.

$Cu(hfac)_2$ precursors also adsorb as $Cu^I(hfac)$, with the additional hfac molecule also adsorbed on the surface. Since there is an extra hfac molecule on the surface for each adsorbed $Cu^I(hfac)$, disproportionation reactions alone will not remove all of the hfac present, and hfac decomposition at temperatures > 300 °C have produced C, O, and F contamination of the Cu films.[17] The addition of reducing carrier gases such as H_2 at substrate temperatures of 310–360 °C causes the desorption of H-hfac molecules, with the resulting formation of low resistivity Cu films (~2.0-2.3 μΩ cm).[16] Cu metal has also been deposited, both under UHV and processing pressures, onto a variety of substrates using atomic-hydrogen assisted CVD of $Cu(hfac)_2$,[40] and Nuesca et al.[41] have shown that the removal of adsorbed hfac ligands by this technique allows the disproportionation of adsorbed $Cu^I(hfac)$ to occur, as with Cu(I) precursors.

1.4. Introduction to SiC Films

Recently, a number of investigators have reported the growth of hydrogen-containing amorphous silicon carbide (a-SiC:H) films for use in optoelectronics or as capping/passivation layers.[44–49] These depositions have been performed using either gas mixtures (e.g., $SiH_4 + CH_4$) or single gases (e.g., CH_3SiH_3) and are most commonly made by plasma-enhanced CVD (PECVD). Although an industry standard for low-k film deposition, PECVD often leads to fragmentation and decomposition of the precursor materials, resulting in difficult molecular characterization. Xu et al.[50] have reported the exposure of a CH_3SiH_3 precursor on Si substrates to an electron beam, forming a-$Si_{0.5}C_{0.5}$:H films that outgassed hydrogen and became tetrahedral a-SiC when annealed to 1283 K. Several companies in the IC industry currently utilize SiC films

as barrier or etch stop layers between Cu and low-k interlayer dielectric materials (carbon-doped oxides, or SiCOH, with k≈2.9). Although most recent research has focused on creating films analogous to a-SiC (with C:Si ≈ 1), others have shown that low-k films of the type $Si_{1-x}C_x$:H can also be made by plasma deposition techniques with a wide range of C:Si ratios.[51–53]

1.5. Conclusions

The above data indicate that the use of polymers, particularly fluoropolymers, as low-dielectric materials has certain systematic problems arising from the nature of interfacial metal-polymer interactions. The use of fluoropolymers is complicated by the ready formation of Al–F species,[19] and by the possible subsequent diffusion of F species into the metal upon thermal cycling. Copper shows a weaker tendency towards fluorine or carbon bond formation, resulting in lower adhesive strength.[22] The use of either Cu or Al with fluoropolymers would, therefore, seem to require an intermediate layer that could act as both a barrier to metal diffusion into the polymer and a barrier towards fluorine diffusion into the metal. Transition metals, including Ta and W, readily form fluorides so the possibility of fluoride diffusion is not eliminated. Ceramics such as TaN are possible candidates, but the complex interactions of such materials with fluoropolymers have yet to receive detailed attention. Data indicate that non-fluorinated polymers may be necessary to avoid the fluorine diffusion problem and that the use of a barrier will be required for integration with Cu. The studies reviewed here also indicate that while MOCVD of Cu diketonate precursors on polymer surfaces may result in metallic Cu formation, future studies should more properly be performed on intermediate barrier layers deposited on polymer substrates.

Current research on Si:C:H films indicates that adherent films can be deposited on metal substrates, including Cu, but that deposited Cu adatoms do not interact strongly with Si:C:H substrates. A possible reason for this is that the Si:C:H films are typically deposited on metal substrates via plasma deposition, where the metal is located at the active electrode, and the film/metal interface is subjected to charged particle bombardment during film growth. Similarly adherent films have been formed on Cu substrates via direct electron bombardment of Cu substrates.[54] It would seem that film/metal chemical interactions are enhanced by charged particle bombardment. Supporting this conclusion is the fact that Si:C:H films deposited on Au substrates at the active plasma electrode showed significantly better adhesion than films formed at the passive electrode, where negligible charged particle bombardment occurred.[55] It is apparent, then, that charged particle bombardment during the course of film/interface formation can significantly alter the interfacial interactions between Cu and Si:C:H films, for reasons as yet not well understood. This would appear to be a fruitful area of research for the immediate future of Cu/low-k integration.

1.6. Chapter References

1. Havemann, R. H.; Jain, M. K.; List, R. S.; Ralston, A. R.; Shih, W.-Y.; Jin, C.; Chang, M. C.; Zielinski, E. M.; Dixit, G. A.; Singh, A.; Russell, S. W.; Gaynor, J. F.; McKerrow, A. J.; Lee, W. W. Overview of Process Integration Issues for Low K Dielectrics. In *Low-Dielectric Constant Materials IV*; Chiang, C., Ho, P. S., Lu, T.-M., Wetzel, J. T., Eds.; MRS Symposium Proceedings 511; Materials Research Society: Warrendale, PA, 1998; p 3.

2. *International Technology Roadmap for Semiconductors,* 1999 Ed.; Semiconductor Industry Association: San Jose, CA, 1999.

3. Lee, W. W.; Ho, P. S. *Mater. Res. Soc. Bulletin* **1997**, *22*, 19.

4. Ryu, C.; Lee, H.; Kwon, K.-W.; Loke, A. L. S.; Wong, S. S. *Mater. Res. Soc. Symp. Proc.* **1998**, *14*, 75.

5. Moulder, J. F.; Stickle, W. F.; Sobol, P. E.; Bomben, K. D. *Handbook of X-ray Photoelectron Spectroscopy*; Physical Electronics: Eden Prairie, MN, 1995.

6. McIntyre, N. S.; Chan, T. C. Uses of Auger Electron and Photoelectron Spectroscopies in Corrosion Science. In *Practical Surface Analysis Vol. 1, Auger and X-ray Photoelectron Spectroscopy*, 2nd ed.; Briggs, D., Seah, M. P., Eds.; Wiley: New York, 1990; pp 485–529.

7. Argile, C.; Rhead, G. E. *Surf. Sci. Reports* **1989**, *10*, 277.

8. Rhead, G. E.; Barthès, M.-G.; Argile, C. *Thin Solid Films* **1981**, *82*, 201.

9. Fleming, R. The CEA Online Tutorial. http://www.cea.com/cai/rbstheo/cairtheo.htm (accessed May, 2000), Charles Evans & Associates.

10. Sacher, E. *Prog. Surf. Sci.* **1994**, *47*, 273.

11. Wu, P. K.; Dabral, S.; Yang, G.-R.; Gittleman, B.; Li, C.; McDonald, J. F.; Lu, T.-M. *J. Appl. Phys.* **1996**, *80*, 5759.

12. Drüsedau, T. P; Lohmann, M.; Klabunde, F.; John, T.-M. *Surf. Coat. Technol.* **2000**, *133*, 126.

13. Han, H. W.; Lee, N.-E. *Thin Solid Films* **2005**, *475*, 144.

14. Wasa, K.; Hayakawa, S. *Handbook of Sputter Deposition Technology*; Noyes: Park Ridge, NJ, 1992.

15. Creighton, J. R.; Parmeter, J. E. *Crit. Rev. Solid State Mater. Sci.* **1993**, *18*, 175.

16. Kim, D.-H.; Wentorf, R. H.; Gill, W. N. *J. Vac. Sci. Technol. A* **1994**, *12*, 153.

17. Naik, M. B.; Gill, W. N.; Wentorf, R. H.; Reeves, R. R. *Thin Solid Films* **1995**, *262*, 60.

18. Tsubouchi, K.; Masu, K. *Vacuum* **1995**, *46*, 1249.

19. Du, Y.; J. A. Gardella, J. *J. Vac. Sci. Technol. A* **1995**, *13*, 1907.

20. Shi, M.-K.; Lamontagne, B.; Selmani, A.; Martinu, L. *J. Vac. Sci. Technol. A* **1994**, *12*, 44.

21. Shi, M. K.; Lamontagne, B.; Selmani, A.; Martinu, L.; Sacher, E.; Wertheimer, M. R.; Yelon, A. *J. Vac. Sci. Technol. A* **1994**, *12*, 29.

22. Kim, Y.-K.; Chang, C.-A.; Schrott, A. G. *J. Appl. Phys.* **1990**, *67*, 251.

23. Chang, C.-A.; Kim, Y.-K.; Schrott, A. G. *J. Vac. Sci. Technol. A* **1990**, *8*, 3304.

24. Pan, F.-M.; Huang, J.-L.; Liaw, C.-F. *J. Vac. Sci. Technol. A* **1993**, *11*, 3076.

25. Du, M.; Opila, R. L.; Case, C. *J. Vac. Sci. Technol. A* **1998**, *16*, 155.

26. Vasile, M. J.; Bachman, B. J. *J. Vac. Sci. Technol. A* **1989**, *7*, 2992.

27. Bent, B. E.; Nuzzo, R. G.; Dubois, L. H. *J. Am. Chem. Soc.* **1989**, *111*, 1634.

28. Sekiguchi, A.; Kobayashi, T.; Hosokawa, N.; Asamaki, T. *J. Vac. Sci. Technol. A* **1990**, *8*, 2976.

29. Higashi, G. S. *Appl. Surf. Sci.* **1989**, *43*, 6.

30. Seki, K.; Frye, J. M.; Okabe, H.; Halpern, J. B. *J. Cryst. Growth* **1993**, *132*, 25.

31. Strongin, D. R.; Comita, P. B. *J. Phys. Chem.* **1991**, *95*, 1329.

32. Sutcliffe, R.; Martini, D.; Pavlica, D.; Kelber, J. MO-CVD of Aluminum and Copper on Teflon®-AF. In *Advanced Metallization and Interconnect Systems for ULSI Applications, 1996,* MRS Conference Proceedings Vol.12; Havemann, R., Schmitz, J., Komiyama, H., Tsubouchi, K., Eds.; Materials Research Society: Pittsburgh, 1997.

33. Sutcliffe, R.; Lee, W. W.; Gaynor, J. F.; Luttmer, J. D.; Martini, D.; Kelber, J.; Plano, M. A. *Appl. Surf. Sci.* **1998**, *126*, 43.

34. Akhter, S.; Zhou, X.-L.; White, J. M. *Appl. Surf. Sci.* **1989**, *37*, 201.

35. Cohen, S. L.; Liehr, M.; Kasi, S. *Appl. Phys. Lett.* **1992**, *60*, 50.

36. Donnelly, V. M. *J. Vac. Sci. Technol. A* **M. E. Gross**, *11*, 66.

37. Guinn, K. V.; Donnelly, V. M.; Gross, M. E.; Baiocchi, F. A. *Surf. Sci.* **1993**, *295*, 219.

38. Girolami, G. S.; Jeffries, P. M.; Dubois, L. H. *J. Am. Chem. Soc.* **1993**, *115*, 1015.

39. Nguyen, T.; Charneski, L. J.; Hsu, S. T. *J. Electrochem. Soc.* **1997**, *144*, 2829.

40. Lee, W. W. *Thin Solid Films* **1995**, *262*, 39.

41. Nuesca, G.; Prasad, J.; Kelber, J. A. *Appl. Surf. Sci.* **1994**, *81*, 237.

42. Jirka, I. *Surf. Sci.* **1990**, *232*, 307.

43. Benndorf, C.; Caus, H.; Egert, B.; Seidel, H.; Thieme, F. *J. Electron Spectrosc. Relat. Phenom.* **1980**, *19*, 77.

44. Lee, M.-S.; Bent, S. F. *J. Vac. Sci. Technol. A* **1998**, *16*, 1658.

45. Loboda, M. J.; Seifferly, J. A.; Dall, F. C. *J. Vac. Sci. Technol. A* **1994**, *12*, 90.

46. Kim, M. T.; Lee, J. *Thin Solid Films* **1997**, *303*, 173.

47. Stapinski, T.; Ambrosone, G.; Coscia, U.; Giorgis, F.; Pirri, C. F. *Physica B* **1998**, *254*, 99.

48. Seekamp, J.; Bauhofer, W. *J. Non-Cryst. Solids* **1998**, *227-230*, 474.

49. Giorgis, F.; Giuliani, F.; Pirri, C. F.; Tresso, E.; Conde, J. P.; Chu, V. *J. Non-Cryst. Solids* **1998**, *227*, 465.

50. Xu, J.; Choyke, W. J.; J. T. Yates, J. *Appl. Surf. Sci.* **1997**, *120*, 279.

51. Grill, A.; Patel, V. *J. Appl. Phys.* **1999**, *85*, 3314.

52. Lee, W.-Y. *J. Appl. Phys.* **1980**, *51*, 3365.

53. Catherine, Y.; Turban, G. *Thin Solid Films* **1979**, *60*, 193.

54. Chen, L. *J. Vac. Sci. Technol. A* **1999**, *17*, 1968.

55. Deplancke, M. P.; Powers, J. M.; Vandentop, G. J.; Salmeron, M.; Somorjai, G. A. *J. Vac. Sci. Technol. A* **1991**, *9*, 450.

CHAPTER 2

METALORGANIC CHEMICAL VAPOR DEPOSITION OF ALUMINUM AND COPPER ON TEFLON® AF FILMS[1]

2.1 Background

The metallization of materials with low dielectric constants is an area of rapidly growing interest because of applications to the multilevel metallization of integrated circuits. Incorporating a material with a lower dielectric constant (k) into integrated circuit (IC) manufacturing results in a reduction of capacitive coupling between metal lines and improved signal processing times and power consumption. Low dielectric constant polymers will yield the highest gains in signal processing speeds for architecture dimensions below 0.5 μm.[6]

Polytetrafluoroethylene (PTFE , Teflon®) has an extremely low dielectric constant with good mechanical strength as well as chemical and thermal stability, but problems have arisen with plastic creep (cold-flow deformation) associated with its high degree of crystallinity and low cross-linking. This has led to the introduction of amorphous fluoropolymers (AF), which incorporate functional groups designed to reduce or eliminate crystallinity.[2] One such species, known commercially as Teflon® AF 1601, is a co-polymer of 33 mol% PTFE and 66 mol% 2,2-bis(trifluoromethyl)-4,5difluoro-1,3 dioxole. Such films have been deposited on substrates via spin-coating, plasma deposition, thermal deposition and laser ablation.[2-5] The bulk structure of Teflon® AF 1601 films (Fig. 2.1) has been previously characterized by infrared spectroscopy, scanning electron microscopy, and x-ray diffraction.[2-5] For applications involving the deposition and adhesion of metal films, surface composition and resulting surface-metal interactions play a critical role.

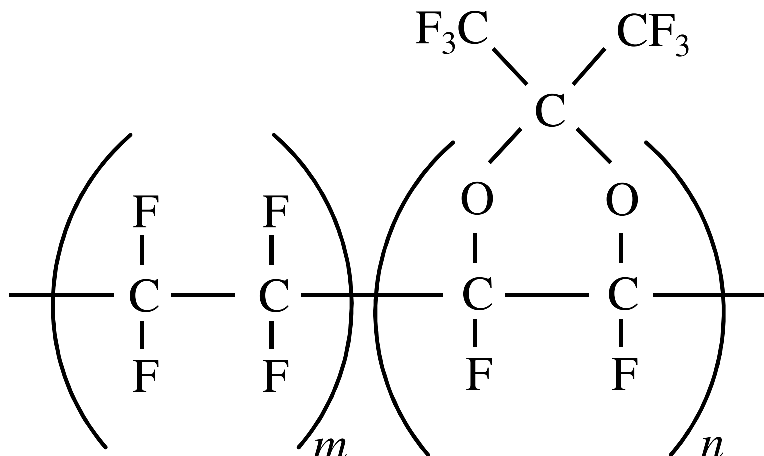

Figure 2.1. Structure of Teflon® AF 1601 films.

The selective deposition of metal films via metal-organic chemical vapor deposition (MOCVD) is of particular interest to the microelectronics industry with respect to the metallization of polymers. The improved step coverage of MOCVD over conventional sputter techniques is of critical importance, particularly if reflow techniques cannot be used due to polymer incompatibility with the required temperatures. In addition, sputter deposition frequently involves high kinetic energy (> 1 eV) bombarding species, which may result in surface roughening and metal atoms deep within the polymer substrate. Regardless of the deposition method, adlayer thermal stability and the interactions of the metal/polymer interface are of critical importance.

X-ray photoelectron spectroscopy (XPS) was used to characterize a Teflon® AF surface and subsequent interactions with two organometallic precursors: trimethylaluminum (TMA) and copper(I)hexafluoroacetylacetonate-cyclooctadiene (Cu^{I}[hfac][COD]). The neat polymer surface was exposed to the precursor at reduced temperature and subsequently annealed to higher temperature. These studies show that at 300 K or below, TMA will react with the Teflon® AF surface and water adsorbed from the ambient to form a thermally stable, fluorinated aluminum-

oxide adlayer with aluminum-carbide species at the adlayer/polymer interface. Annealing to higher temperature causes further polymer defluorination and increasing Al–F formation. Studies of the interaction between the neat Teflon® AF surface and Cu^{I}(hfac)(COD) show the loss of the neutral ligand (COD) by the copper precursor at or below room temperature. Upon annealing to higher temperature, the Cu(I) adsorbate undergoes a disproportionation reaction on the polymer surface resulting in the formation of a Cu(0) adlayer. Some Cu–F formation is also indicated.

2.2 Experiment

Thin films (3–5 μm) of Teflon® AF were formed by spin coating from a Teflon® AF 1601 S-6 (Dupont) solvent on Si(100) wafers with a native oxide. The films were then annealed in a nitrogen environment for five minutes at 300 °C. This procedure has been found to produce adherent films of consistent composition, comparable to those obtained by laser ablation and other methods.[4]

Experiments were carried out within an ultra-high vacuum (UHV) stainless steel surface analysis system with a base pressure of 5×10^{-10} Torr, evacuated by turbomolecular pumping. The system is equipped with a separate CVD chamber with a base pressure of 1×10^{-8} Torr. The analysis chamber was equipped with a dual-anode x-ray source, hemispherical analyzer and quadrupole mass spectrometer for residual gas analysis. Pressure in both chambers was monitored using a nude ion gauge calibrated for N_2. The ion gauge was mounted out of direct line of sight of the sample, in order to minimize electron damage to the sample. The sample temperature was controlled by a combination of resistive heating and liquid nitrogen cooling of the sample holder. Sample temperatures were monitored by a chromel-alumel thermocouple attached directly to the sample

holder. Annealing was carried out by ramping the sample to the required temperature for 30 minutes. The sample was allowed to return to base pressure prior to the acquisition of spectra.

XPS spectra were obtained using an unmonochromatized MgKα x-ray source operated at 15 keV and 300 W, and a commercial hemispherical analyzer operated in the constant pass energy mode (50 eV pass energy). Take-off angle resolved spectra were obtained by rotating the sample 60º off surface normal. The analyzer was calibrated using Au and Cu standards, according to established procedure.[7] XPS data were analyzed using a commercially available software package.[8] The exposure of fluoropolymers to x-ray flux is known to induce defluorination and cross-linking[8]; to minimize sample damage, x-ray exposure was limited to that needed for spectral acquisition. XPS binding energies were affected by sample charging during data acquisition; therefore, the data were referenced to a F(1s) binding energy of 689.1 eV, which is consistent with the published values for fluorine in a C–F environment.[4,10–14] The full width at half-maximum (FWHM) for the fitted spectra was kept constant with each atomic species for all spectra of that species. Differentiation between Cu(I) and Cu(0) oxidation states was accomplished using published methods of combining the Cu(L_3VV) line shape analysis and calculation of the modified Auger parameter.[14–16] For a Cu(0) oxidation state, the Cu(L_3VV) spectrum shows a narrow feature with a large asymmetry on the high binding energy side whereas Cu(I) gives a broader, more symmetric peak. The modified Auger parameter is determined by the distance (in eV) between the Cu($2p_{3/2}$) feature and the maximum of the Cu(L_3VV) Auger spectrum, added to the x-ray photon energy.[14–16] This parameter is then compared to tabulated parameters in order to determine the copper oxidation state.

Metal-organic chemical vapor deposition was carried out using TMA and Cu^{I}(hfac)(COD) obtained from commercial sources. The precursors were introduced directly into the CVD chamber using a metering valve. Composition of the organometallic precursors were verified by

measurements with a quadrupole mass spectrometer. The sticking coefficients of the precursors to the polymer were maximized by performing the exposures at reduced temperatures (< 115 K). Exposures are reported in Langmuirs (1 L = 10^{-6} Torr-sec), and have not been corrected for directional dosing effects or ion-gauge sensitivity. The samples were then transferred to the main UHV chamber for XPS analysis. Anneals were carried out in series in UHV, with spectra taken after each annealing. To minimize changes in x-ray flux, the sample was not moved after introduction into the UHV chamber other than rotation to obtain angle resolved spectra; the sample arm was equipped with a graduated rotational scale in order to precisely determine rotation angles.

2.3. Results and Discussion

2.3.1. XPS of the Neat Polymer Surface

The XPS spectra of the unmodified polymer are displayed in Figure 2.2. Spectra for the neat polymer show a single feature in the F(1s) spectrum. Charge-compensated studies of bulk

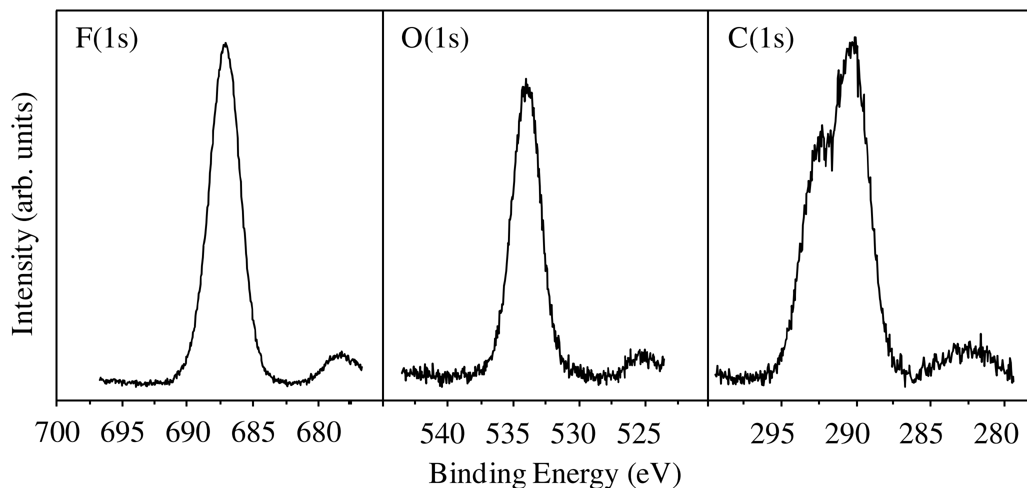

Figure 2.2. F(1s), O(1s), and C(1s) XPS spectra of neat Teflon® AF surface referenced to F(1s) binding energy of 689.0 eV.

and thin films show the F(1s) peak of the polymer to be at 689.1 eV, which is in good agreement with fluorine in a fluorocarbon environment.[4,10–14] The F(1s) feature seen here is therefore

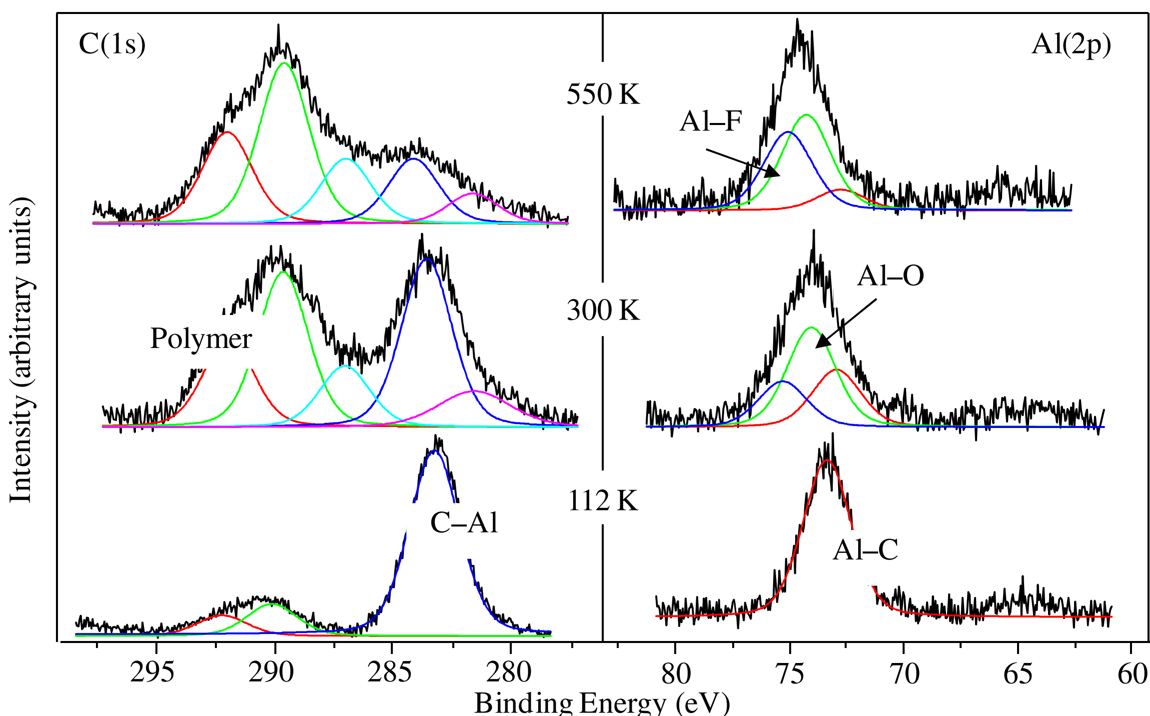

Figure 2.3. C(1s) and Al(2p) XPS spectra of Teflon®-AF surface dosed with TMA at 112 K and subsequently annealed to 300 K and 550 K (in series) in UHV.

assigned to a binding energy of 689.1 eV that is then used as an internal reference for all subsequent elemental spectra. The O(1s) spectrum also shows a single feature at 534.9 eV and is assigned to the oxygen in the dioxole ring.[4,10] The C(1s) XPS spectrum (Fig. 2.2) shows a large, unresolved doublet with environments at approximately 293 and 291 eV. These C(1s) binding energies are in good agreement with published values for Teflon® AF 1600 and 2400 films (67% and 82% dioxole ring segment, respectively).[4,10]

2.3.2. TMA on Teflon® AF Films

2.3.2.1. Exposure at 112 K

C(1s) and Al(2p) XPS spectra are displayed in Figure 2.3 for the polymer exposed to 30 L TMA at 112 K and subsequently annealed to temperatures up to 550 K. The corresponding F(1s) and O(1s) spectra are shown in Figure 2.4. In addition to the high binding energy doublet

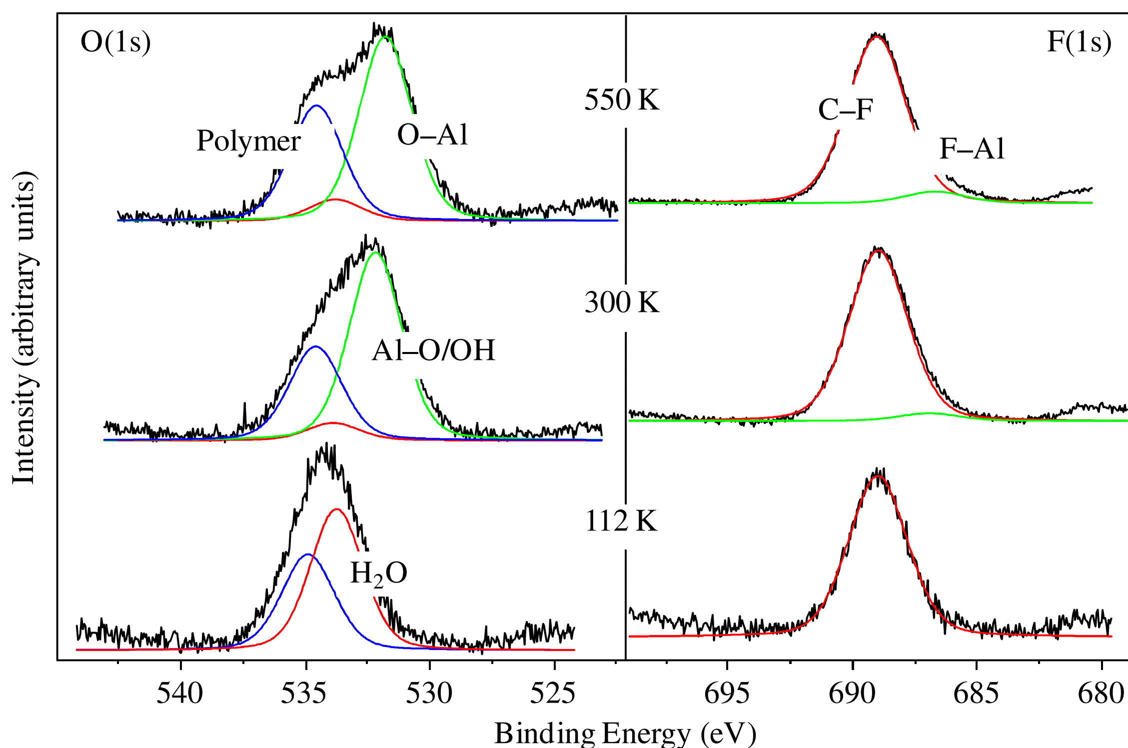

Figure 2.4. O(1s) and F(1s) XPS spectra of Teflon®-AF surface dosed with TMA at 112 K and subsequently annealed to 300 K and 550 K (in series) in UHV.

characteristic of the polymer, the C(1s) spectrum in Fig. 2.3 shows a large feature at low binding energy (283.5 eV). The published C(1s) binding energy for the Al–C bonds in TMA is 283.4 eV, which is in good agreement with the feature seen here.[17] The low binding energy feature (283.5 eV) is assigned to the methyl ligands of the unreacted precursor. A small peak centered at ~282.5 eV was added to the calculated spectrum in Figure 2.3 to compensate for the MgKα x- ray satellites from the C(1s) features of the polymer substrate. The Al(2p) spectrum (Fig. 2.3) shows a single feature at 73.7 eV, similar to the published value for condensed TMA (73.4 eV).[17]

The F(1s) spectrum at 112 K (Fig. 2.4) shows the large feature of the polymer substrate referenced to 689.1 eV. The low temperature O(1s) spectrum exhibits significant broadening and the appearance of an assymetry on the high binding energy side. The broadening of the O(1s) feature upon exposure to TMA indicates the presence of additional oxygen environments beyond that of the polymer. Using a FWHM of 2.5 eV for each component of the fitted O(1s) spectrum,

as determined from the spectrum of the neat polymer (Fig. 2.2), the exposed O(1s) spectrum is well fit by two environments: 534.7 eV (attributed to the polymer substrate) and 533.8 eV. Experiments involving the low temperature exposure of non-oxygenated fluoropolymers to the environment of the deposition chamber also show an O(1s) feature at ~533.5 eV, which is in the range of published binding energies for adsorbed water.[18,19] Given the relatively high working pressure of the deposition chamber (~5 x 10^{-7} Torr) and the low deposition temperature (112 K) used in these experiments, the physisorption of water on the polymer substrate is likely. The O(1s) feature at 533.8 eV is therefore assigned to adsorbed water (H_2O_{ads}).

2.3.2.2. Annealing to 300 K

The C(1s) spectrum of the TMA-exposed polymer surface annealed to 300 K (Fig. 2.3) shows a 54.6% decrease in relative signal intensity and a shift to higher binding energy – by about 1.0 eV – for the feature attributed to Al-C bonds (284.4 eV). These changes indicate the decomposition of the precursor and a reaction between aluminum and the carbon in the polymer surface. Additionally, there is an increase in the intensity of the doublet attributed to the polymer substrate, indicating substantial desorption of the methyl ligands from the decomposed precursor and a corresponding reduction of the signal attenuation of the underlying polymer.

The Al(2p) spectrum (Fig. 2.3) displays a shift to higher binding energy and significant broadening upon annealing to 300 K. The spectrum is well fit by three peaks: 76.1 eV, 74.9 eV, and 73.8 eV; assigned to Al–F, Al–O, and Al–C, respectively. In a study of the interaction between thermally deposited aluminum and fluoropolymers, Du and Gardella[11] reported binding energies for aluminum fluorides (76.4 eV to 76.8 eV), aluminum oxides (75.4 eV), and aluminum carbides (74.3 eV to 74.5 eV), which are approximately 0.5 eV higher than the values

seen in this research. Binding energy differences are likely due to differences in charge referencing; Du and Gardella[11] used the C(1s) signal for hydrocarbon contaminants, whereas this work uses the F(1s) of the polymer substrate. Other studies have reported similar assignments for the interaction between aluminum and fluorocarbons.[12,13]

The F(1s) spectrum for the TMA dosed surface, annealed to 300 K, is shown in Figure 2.4. The total F(1s) signal intensity experiences a marked increase due to the lessening of the signal attenuation from the desorption of the precursor decomposition products. Figure 2.4 also shows the appearance of asymmetric broadening on the low binding energy side of the F(1s) spectrum. The low binding energy asymmetry is in the region of the XPS spectrum where the F(1s) signal for metal-fluoride bonds are commonly found.[11-13,15,20,21] A good fit (Fig. 2.4) is obtained using a feature with a binding energy of 687.0 eV, which is in good agreement with published binding energies for aluminum fluorides.[11-13,15,20,21] The formation of aluminum fluorides has been observed during the evaporative deposition of aluminum on fluoropolymers and during the interactions of clean, metallic aluminum with perfluoroalkyl ethers, acyl fluorides, and fluorocarbon lubricants.[11–13] The presence of oxygen both in the polymer and on the surface presents the possibility of oxyfluoride (-OF) formation upon annealing. Published

Table 2.1. Selected aluminum bond energies.[22]

Bond Energies (kJ mol^{-1})			
Al–Al	186	Al–C	255
Al–O	512	FAl–O	582
Al–F	664	OAl–F	761

binding energies unambiguously assigned to oxyfluoride species are rare; however, published bond energy data (Table 2.1) show the Al-F bond energy to be approximately three times the that of O–F (664 kJ/mol vs. 222 kJ/mol). In addition, aluminum oxide fluorination increases the bond

energy of both the Al–F bonds (by 97 kJ/mol vs. AlF_x) and Al–O bonds (by 70 kJ/mol vs AlO_x). Thus, a fluorinated aluminum oxide (F–AlOx) is thermodynamically more likely to form than an aluminum oxyfluoride ($Al[OF]_x$). The low binding energy F(1s) feature at 687.0 eV is therefore tentatively assigned to Al–F in a fluorinated aluminum oxide.

Upon annealing to 300 K, the O(1s) spectrum (Fig. 2.4) exhibits significant broadening to lower binding energy and a shift of ~2.0 eV in the peak maximum to lower binding energy. Additionally, the spectrum shows a shoulder on the high binding energy side. The shift to lower binding energy is indicative of metal-oxide formation. A good fit is obtained using three oxygen environments: 534.6 eV, 533.9 eV, and 532.2 eV. The fitted feature at 534.6 eV can be attributed to the dioxole oxygen of the underlying polymer. Also, since the sample was allowed to return to low temperature prior to recording the spectra, the fitted feature at 533.9 eV is reasonable for re-adsorbed water. Given the reactivity of organo-aluminum compounds with water and the experimental conditions used in this study, aluminum oxide and/or hydroxide formation can be reasonably expected. In a study of the interaction between a clean aluminum surface and D_2O, Rogers reported an O(1s) binding energy for aluminum oxide/hydroxide mixed phase (Al–O/OH) at 532.5 eV, slightly higher than that of a pure bulk oxide (531.5 eV).[11–13,21–25] The fitted feature at 532.2 eV is therefore assigned to a mixed phase Al–O/OH.

2.3.2.3. Annealing to 550 K

Figures 2.3 & 2.4 also show the changes in the XPS spectra upon annealing to 550 K in UHV. The C(1s) spectrum shows a continued decrease (51.9%) in the relative signal intensity of the low binding energy feature at 285.0 eV and a corresponding increase in the high binding

energy doublet of the polymer substrate, indicating further desorption of methyl ligands from the precursor.

The Al(2p) spectrum of the aluminum/polymer system, annealed to 550 K, is also shown in Figure 2.3. The overall signal intensity of the Al(2p) feature remains constant upon annealing. The Al(2p) signal maximum has shifted by 0.7 eV to higher binding energy, indicating an increase in the formation of Al–F bonds. Also, the Al(2p) feature displays an overall narrowing, with only an asymmetry on the lower binding energy side, resulting from a decrease in the low binding energy Al–C signal. These changes are evidence of increased fluorination of the Al adlayer. The fitted Al–F feature at 75.9 eV has increased as a percentage of the total Al(2p) signal, from 22.8% to 40.5%, while the Al–C (73.6 eV) has decreased from 28.4% to 10.4%. The fitted peak attributed to Al–O (75.1 eV) remained constant (48.7% to 49.1%) upon annealing to 550 K.

Upon anneal to 550 K, the O(1s) spectral maximum exhibits a shift of ~0.5 eV to lower binding energy (Fig. 2.4). The high binding energy shoulder has also become more fully resolved. The spectrum is well fit by three environments: 534.6 eV, 533.8 eV, and 531.8 eV. Binding energies of 534.6 and 533.8 eV are attributable to the polymer substrate and adsorbed water (H_2O_{ads}), respectively, for reasons mentioned previously. The shift to lower binding energy of the spectral maximum and accompanying shift of the low binding energy fitted feature indicate a change from a mixed phase Al-O/OH to a bulk oxide (AlO_x). A similar phenomena has been reported for the interaction of methanol with a clean aluminum surface, where methanol was condensed on aluminum at low temperature and subsequently annealed;[25,26] by room temperature, the methanol partially decomposed to a chemisorbed methoxy species that formed a bulk aluminum oxide at higher temperatures (550 K).

The F(1s) spectrum shows a large increase in total signal intensity upon annealing to 550 K. Also, the contribution of the fitted peak attributed to Al–F (686.8 eV) shows a small increase as percentage of total F(1s) signal intensity (5.16% to 6.57%). This increase in the Al–F contribution to the F(1s) spectrum, combined with the increase in the Al(2p) spectrum, indicates increasing defluorination of the polymer substrate by the aluminum adlayer as a function of temperature.

2.3.2.4. Take-off Angle Resolved Measurements

XPS take-off angle resolution provides a non-destructive means of depth profiling. Given that XPS depth resolution is a function of the inelastic mean free path of the photoelectrons, changing the sample/analyzer angle (relative to surface normal) will decrease the effective electron escape depth by cosine θ (Fig. 2.5).[27] The 60° take-off angle resolved Al(2p) spectrum for the TMA dosed and annealed polymer is displayed in Figure 2.6. At the more surface-sensitive geometry, the Al(2p) feature exhibits significant broadening towards lower binding energy, indicating an increase in the relative contribution of one or more of the low binding energy environments (Al–C and Al–O). Curve fitting shows a marked increase in the relative

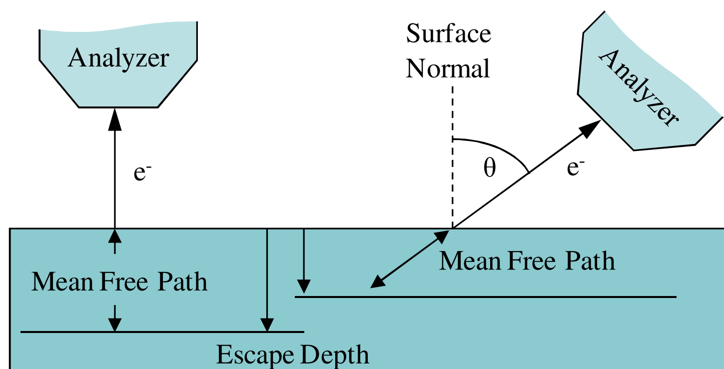

Figure 2.5. Depth profiling using XPS angle resolution.

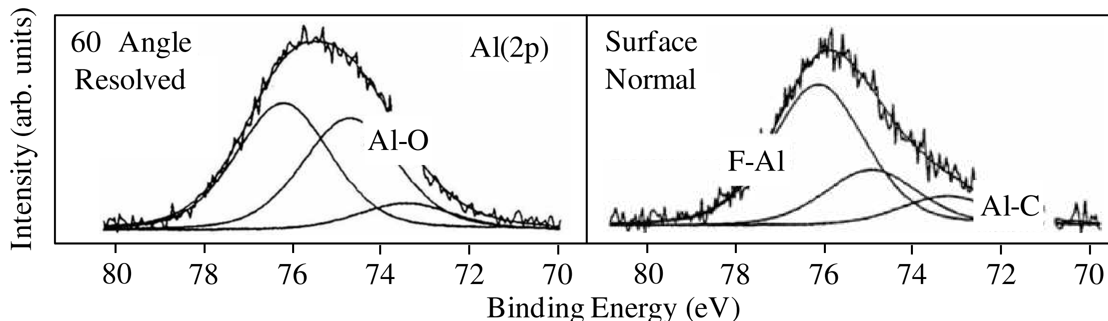

Figure 2.6. Surface normal and 60 take-off angle-resolved Al(2p) spectra of TMA dosed and annealed Teflon® AF surface.

intensity of the component attributed to Al–O (75.1 eV), while the fitted Al–C peak (73.6 eV) experiences a corresponding decrease. These changes indicate that the oxide in the Al adlayer is closer to the surface (i.e., the Al–vacuum interface) and attenuates the signal of the underlying Al–C. Based on the above evidence, the Al adlayer appears to be a fluorinated aluminum oxide

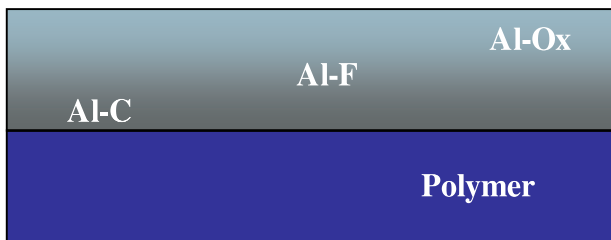

Figure 2.7. Composition diagram of CVD aluminum adlayer on Teflon® AF.

(F–AlOx), bound to the polymer surface through aluminum carbide bonds. The concentration of fluorine in the adlayer is greater toward the polymer surface, with defluorination of the polymer as the fluorine source, and may be thought of as a concentration gradient increasing toward the polymer/adlayer interface (Fig.2.7), though the adlayer thickness is less than 100 Å as calculated by XPS signal attenuation of the C(1s) signal from the underlying polymer.

2.3.3. Cu^{I}(hfac)(COD) on Teflon® AF Films

2.3.3.1. Exposure at 105 K

The XPS spectra for the neat Teflon® AF surface exposed to Cu^{I}(hfac)(COD) are given in Figures 2.8 and 2.9. CVD studies using Cu(I) β-diketonate precursors typically involve dissocitative chemisorption, where the organo-copper precursor loses the neutral ligand upon bond formation with the substrate.[14,28–30] The C(1s), O(1s), and F(1s) spectra (Fig. 2.8) for the dosed surface at 112 K show spectra characteristic of the hexafluoroacetylacetonate (hfac) and cyclooctadiene (COD) ligands.[14] This indicates complete attenuation of the photoelectron signal of the underlying polymer. The low temperature Cu(2p) and Cu(L_3VV) spectra (not shown) are featureless. Previous experience with the CVD system used in these experiments has shown

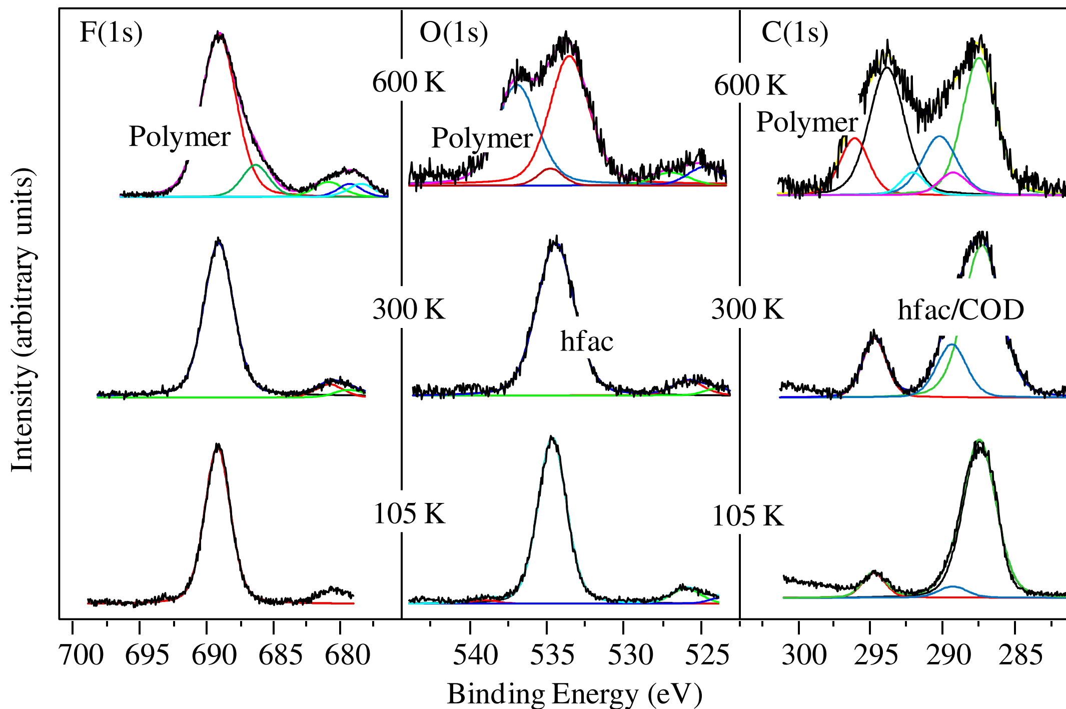

Figure 2.8. C(1s), O(1s), and F(1s) spectra of Cu^{I}(hfac)(COD) on Teflon®-AF at 105 K, 300 K, and 600 K.

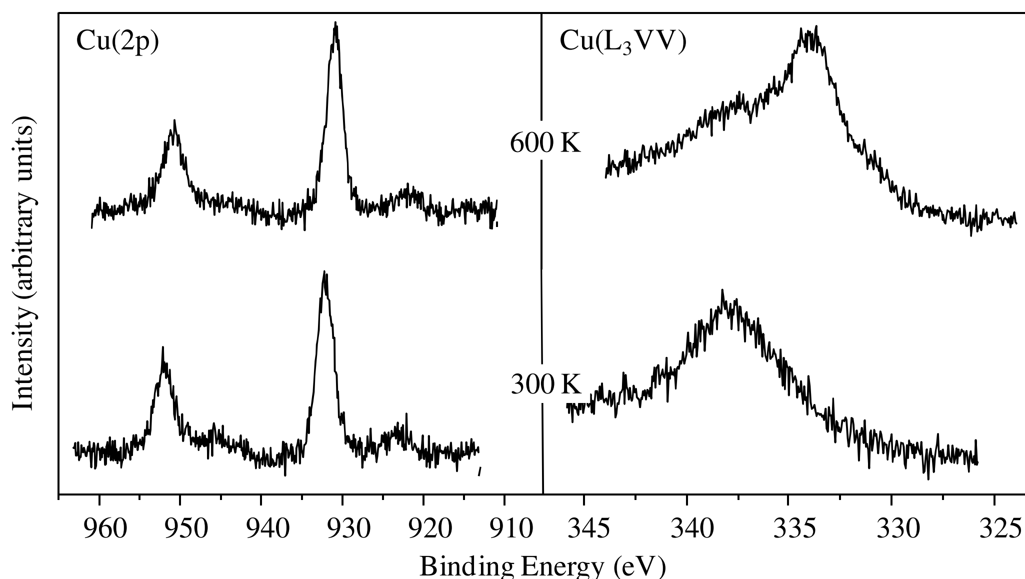

Figure 2.9. Cu(2p) and Cu(L_3VV) spectra of Cu^I(hfac)(COD) on Teflon®-AF at 300 K and 600 K.

substantial precursor decomposition in the introduction lines, which releases free ligands (primarily COD) into the CVD chamber. Due to the reduced temperature used during exposure, the free ligands are then co-adsorbed on the sample surface along with the precursor. The physisorption of the additional ligands causes total attenuation of the Cu photoelectron signal.

2.3.3.2. Annealing to 300 K

Upon annealing to 300 K, the C(1s) spectrum (Fig. 2.8) displays significant broadening of the low binding energy feature and an increase in the relative intensity of the high binding energy feature. These changes in the C(1s) spectrum indicate substantial desorption of COD ligands. Both the F(1s) and O(1s) spectra remain relatively constant upon annealing to 300 K.

The Cu(2p) and Cu(L_3VV) spectra for the annealed surface are shown in Figure 2.9. After annealing to 300 K, The Cu(2p) spectrum shows two well-resolved peaks at 951.8 eV and 932.2 eV, corresponding to Cu($2p_{1/2}$) and Cu($2p_{3/2}$) respectively. The Cu(L_3VV) shows a single broad peak at 338.5 eV (KE = 915.1 eV). The overall shape of the Cu(L_3VV) spectrum indicates

the copper to be in the form Cu(I).[15,16,31] Further evidence for a Cu(I) is given by the modified Auger parameter of 1847.3 eV, which is within the range of 1847–1849 eV normally seen for Cu(I).[15,16,31]

2.3.3.3. Annealing to 600 K

Annealing to 600 K causes substantial changes in the C(1s) spectrum (Fig. 2.8). The low binding energy portion of the spectrum (attributed to the hfac/COD ligands of the precursor) experiences a large decrease in relative signal intensity, which indicates further desorption of the precursor ligands. Corroboration of this is seen in the re-emergence of the high binding energy features attributed to the underlying polymer. Additionally, the O(1s) spectrum shows the signal to have split into a partially-resolved doublet. Curve fitting shows the O(1s) signal to be a combination of the underlying polymer (534.9 eV) and the hfac ligand (531.3 eV).

The copper XPS spectrum of the dosed and annealed surface are shown in Figure 2.9. The Cu($2p_{3/2}$) spectrum shows a 1.2 eV shift to lower binding energy (931.0 eV). The Cu(L_3VV) spectrum shows narrowing and a shift to lower binding energy of 3.7 eV, to 334.8 eV (KE = 918.8). The narrowing of the overall lineshape of the Cu(L_3VV) spectrum indicates reduction to Cu(0). Copper reduction is corraborated by the change in the modified Auger parameter to 1849.8 eV, which is within the range expected for Cu(0).[15,16,31] Studies involving MOCVD of copper using Cu(I) or Cu(II) β-diketonate precursors on TiN and other surfaces indicate Cu(0) formation through disproportionation, which involves a 50% loss in total copper on the surface.[16,28–31] In this study, disproportionation should be manifest as a 50% reduction in the total Cu signal intensity; however, due to signal attenuation effects of the adsorbed ligands, determination of total copper is difficult. Total Cu determination is further complicated by the

similarity in chemical composition of the polymer substrate and the hfac ligand, which necessitates the calculation of signal attenuation using an internal standard. For these reasons it is unclear whether Cu(0) formation is through disproportionation.

The F(1s) spectrum (Fig. 2.8) shows the presence of an asymmetry on the low binding energy side. Curve fitting reveals a new environment at 686.3 eV that is within the range expected for metal fluorides. This indicates that, like aluminum, copper may also defluorinate the Teflon® AF surface.

2.4. Summary and Conclusions

XPS was used to study the interaction between trimethylaluminum and Teflon® AF films. The data demonstrate that aluminum deposited on unmodified Teflon® AF samples by low temperature CVD is stable to elevated temperatures. At low temperature, the TMA precursor and ambient water condenses on the polymer surface. Upon annealing to 300 K, the precursor decomposes and reacts with both carbon and fluorine from the polymer surface, in addition to oxygen from the adsorbed water. The TMA/polymer/water reaction forms a thermally stable aluminum oxide film bonded to the polymer surface through aluminum-carbon bonds. A difference in fluorine concentration exists across the adlayer with decreasing fluorine toward the adlayer/vacuum interface. Upon annealing to higher temperature (550 K), aluminum reacts preferentially with fluorine at the expense of carbon. Aluminum defluorinates the polymer at all temperatures studied, with fluorine diffusion into the adlayer film.

The interaction between Cu^{I}(hfac)(COD) and a neat Teflon® AF surface was also studied using x-ray photoelectron spectroscopy. The data show that low temperature CVD results in Cu(0) on the fluoropolymer surface by 600 K, with some metal fluoride formation. The Cu(I)

precursor condenses on the Teflon® AF surface at low temperature and reacts with the polymer by 300 K, with the resulting loss of the neutral cyclooctadiene ligand. Annealing to 600 K results in some Cu(I) to Cu(0) reduction and the desorption of substantial amounts of the hfac ligands. The F(1s) spectra of the annealed surface indicates some metal fluoride formation by 600 K.

2.5. Chapter References

1. Originally printed in *Advanced Metallization and Interconnect Systems for ULSI Applications, 1996, MRS Conference Proceedings Vol.12*; Havemann, R., Schmitz, J., Komiyama, H., Tsubouchi, K., Eds.; Materials Research Society: Pittsburgh, 1997; pp 437–447.

2. Blanchet, G. B. *Appl. Phys. Lett.* **1993**, *52*, 479.

3. Nason, T. C.; Moore, J. A.; Lu, T.-M. *Appl. Phys. Lett.* **1992**, *60*, 186.

4. Cho, C.-C.; Wallace, R. M.; Files-Sesler, L. A. *J. Electron. Mater.* **1994**, *23*, 827.

5. Buck, W. H.; Resnick, P. R. Properties of Amorphous Fluoropolymer Based on 2,2-Bistrifluoromethyl-4,5-Difluoro-1,3-Dioxole. *Proceedings of the183rd Meeting of the Electrochemical Society*, Honolulu, HI, May 16–23, 1993.

6. *The National Technology Roadmap for Semiconductors,* 1994 ed.; Semiconductor Industry Association: San Jose, 1994.

7. Powell, C. J. *Surf. Int. Anal.* **1995**, *23*, 121.

8. *ESCATools*, v.4.2; Surface/Interface, Inc.: Mountain View, CA.

9. Rye, R. *J. Polym. Sci. B*. **1993**, *31*, 357.

10. Matienzo, L. J.; Zimmerman, J. A.; Egitto, F. D. *J. Vac. Sci. Tech. A.* **1994**, *12*, 2662.

11. Du, Y.; Gardella, J. A., Jr. *J. Vac. Sci. Tech. A* **1995**, *13*, 1907.

12. Shi, M.-K.; Lamontagne, B.; Belmani, A.; Martinu, L. *J. Vac. Sci. Tech. A* **1994**, *12*, 44.

13. John, P. J.; Liang, J. *J. Vac. Sci. Tech. A* **1994**, *12*, 199.

14. Nuesca, G. M.; Kelber, J. A. *Thin Solid Films* **1995**, *262*, 224.

15. *Handbook of X-Ray Photoelectron Spectroscopy*; Wagner, C. D., Riggs, W. M., Moulder, J. S., Davis, L. E., Eds.; Perkin Elmer: Eden Prarie, MN, 1979.

16. Benndorf, C.; Caus, H.; Egert, B.; Seidel, H.; Thieme, F. *J. Electron Spec. Rel. Phenom.* **1980**, *19*, 77.

17. Akhter, S.; Zhou, X. -L.; White, J. M. *Appl. Surf. Sci.* **1989**, *37*, 201.

18. Wagner, C. D.; Zatko, D. A.; Raymond, R. H. *Anal. Chem.* **1980**, *52*, 1445.

19. Wren, A. G.; Phillips, R. W.; Tolentino, C. U. *J. Colloid Interface Sci.* **1979**, *70*, 544.

20. Chang, C.-A.; Kim, Y.-K.; Schrott, A. G. *J. Vac. Sci. Tech. A* **1990**, *8,* 3304.

21. McGuire, E.; Schweitzer, G. K.; Carlson, T. A. *Inorg. Chem.* **1973**, *12*, 2450.

22. Dean, J. A.; Lange's Handbook of Chemistry, 14th ed.; McGraw-Hill: New York, 1992.

23. Kishi, K.; Ikeda, S. *Bull. Chem. Soc. Jpn.* **1972**, *46*, 341.

24. Carley, A. F.; Roberts, M. W. *Proc. R. Soc. London A* **1978**, *363*, 403.

25. Rogers, J. W., Jr. An Electron Spectroscopic Investigation of the Interaction of Methanol and Ammonia with Clean and Partially Oxidized Aluminum Surfaces. Ph.D. Thesis, The University of Texas, 1979.

26. Rogers, J. W., Jr.; Hance, R. L.; White, J. M. *Surf. Sci.* **1980**, *100*, 388.

27. Briggs, D.; Rivière, J. C. Spectral Interpretation. In *Practical Surface Analysis Vol. 1, Auger and X-ray Photoelectron Spectroscopy*, 2nd ed.; Briggs, D., Seah, M. P., Eds.; Wiley: New York, 1990; pp 86–141.

28 Perry, W. L.; Chi, K. M.; Kodas, T.; Hampden-Smith, M.; Rye, R. Appl. Surf. Sci. **1993**, *69*, 94.

29. Donnelly, V. M.; Gross, M. E. *J. Vac. Sci. Tech. A* **1993**, *11*, 66.

30. Cohen, S. L.; Liehr, M.; Kasi, S. *Appl Phys. Lett.* **1991**, *60*, 50.

31. Jirka, I. *Surf. Sci.* **1990**, *232*, 307.

CHAPTER 3

CHARACTERIZATION AND ALUMINUM METALLIZATION OF A PARYLENE AF-4 SURFACE

3.1. Background

The study of low dielectric constant materials is an area of rapidly growing interest due to their applications in the microelectronics industry. The application of materials with lower dielectric constant (k) than the materials currently used in microelectronic applications would significantly reduce resistance-capacitance (RC) delay and enhance interconnect performance. A number of organic polymers have been investigated for use as interlayer dielectrics,[1–11] including fluoropolymers and parylenes (*p*-xylene polymers). Though fluoropolymers generally have lower dielectric constants (1.9–2.1), their application has thus far been limited by poor metal adhesion.[1,7,8,12]

While the dielectric constants for Parylene variants (k = 2.3–2.6) are slightly higher than fluoropolymers, they exhibit better adhesion properties and lower moisture uptake.[9,13] Parylenes can be vapor deposited, a process that is inherently cleaner than the conventional spin-on process used for fluoropolymers.[13] A fluorinated version called Parylene AF-4 has recently become available and has excellent thermal stability (melting point > 773 K) and a dielectric constant of 2.28.[13] Parylene AF-4 (also known simply as AF-4) is poly(α,α,α′,α′-tetrafluoro-*p*-xylylene) and is shown in Figure 3.1. In addition to its low dielectric constant, AF-4 exhibits a low dissipation factor for electric power loss (< 0.001) and very low moisture absorption (< 0.1%).[13]

Metallization by metal-organic chemical vapor deposition (MOCVD) is of particular interest to the microelectronic industry with respect to the use of low dielectric constant polymers. Low dielectric polymers will yield the highest gains in signal processing speeds for

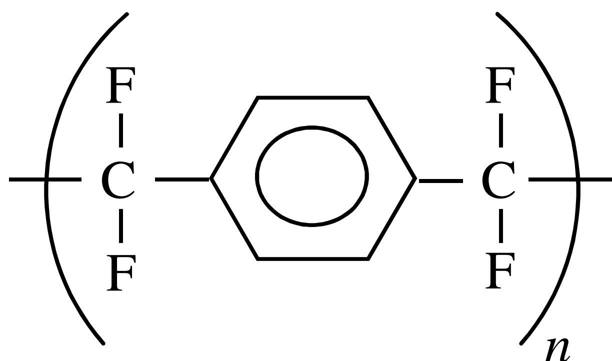

Figure 3.1. Structure of Parylene AF-4.

architecture dimensions below 0.5 microns.[14] In addition, the improved step coverage of MOCVD compared to sputtering techniques is of critical importance, particularly if reflow techniques cannot be used due to polymer incompatibility with the required temperatures. Also, sputter deposition of metals on polymer surfaces can result in metal atoms deep within the polymer and surface roughening due to ablation of the polymer surface by the high kinetic energy bombarding species. Whatever method of metal deposition is used, the thermal stability of the metal/polymer interface is a critical requirement.

In this work, atomic force microscopy (AFM) and x-ray photoelectron spectroscopy (XPS) were used in the surface characterization of Parylene AF-4 polymer. The polymer surface was then exposed to trimethylaluminum (TMA) at reduced temperature and subsequently annealed to higher temperatures. These studies show that TMA will react with the polymer surface and water adsorbed from the ambient at or below 300 K. The reaction forms a thermally stable adlayer on the polymer surface with aluminum-carbide species at the metal/polymer interface, aluminum-oxide toward the adlayer surface, and fluorinated aluminum species in the adlayer "bulk"; this result is similar to studies performed on Teflon® AF4 surfaces.[15] Annealing to higher temperatures causes further defluorination of the polymer surface and increasing Al–F

bond formation. Neither the presence of metallic aluminum nor diffusion of aluminum into the bulk polymer was observed.

3.2. Experimental Methods

The Parylene AF-4 films used in this study were vapor-deposited by pyrolitic decomposition of the cyclic dimer in an experimental deposition system at Novellus Systems using the Gorham process.[16] This process involves vaporizing the solid dimer to a pressure of ~100 mTorr, then allowing the gas to flow down a pressure gradient into a pyrolizer (923 K) where dimer cracks into the monomer (tetrafluoro-*p*-xylylene). The monomer gas proceeds into the deposition chamber (20 - 40 mTorr) and condenses onto a cold (273 K) wafer surface where it polymerizes to give the AF-4 film. Previously published studies by Plano et al.[17] have examined the effects of deposition conditions on AF-4 films. The AF-4 polymer samples used in this study were deposited at a rate of 150 Å/min to a thickness 5000 Å on 1000 Å plasma-enhanced tetraethoxysilane (PETEOS) deposited on silicon. The refractive index of the as-deposited film was measured using a variable angle, variable wavelength ellipsometer and found to be 1.5584 in-plane and 1.4393 out-of-plane.

Atomic force microscopy (AFM) was performed at the Texas Instruments Materials Science Laboratory and was used to determine the surface roughness of the polymer sample. The AFM (Digital Instruments) uses a photodetector to monitor a laser beam reflected from a spring cantilever mounted to the probe tip. During image acquisition, the instrument was operated in "tapping mode", where the oscillating probe encounters the surface and changes the amplitude of the vibration. The probe height is then adjusted to maintain a constant amplitude of oscillation across the surface. By mapping the voltage applied to the piezoelectric used for probe height

adjustment as a function of x–y position, a topographical map is obtained. Scan areas were 1.00 μm^2, 25.00 μm^2, and 100.00 μm^2.

X-ray photoelectron spectroscopy (XPS) and chemical vapor deposition (CVD) experiments were carried out in an ultra-high vacuum (UHV) surface analysis system at the University of North Texas. The UHV system was evacuated with a turbomolecular pump and had a base pressure of 5 x 10^{-10} Torr. The system was equipped with a separate CVD chamber with a base pressure of 1 x 10^{-8} Torr. Sample transport between chambers was achieved without exposure to atmosphere by mounting the sample on the end of a manipulator coupled to a linear drive. The two chambers were isolated from each other by a gate valve in combination with a differentially pumped Teflon® seal. Pressure in both chambers was monitored with nude ion gauges calibrated for N_2, mounted out of direct line of sight to minimize electron damage to the sample. The sample was mounted on a Ta foil sample holder spot-welded to Ta leads. Sample temperature control was maintained by a combination of resistive heating and liquid nitrogen cooling of the sample holder. Temperatures were monitored by a chromel-alumel thermocouple spot-welded to the sample holder. The sample was cooled by liquid nitrogen for approximately 5 minutes (to ensure consistent sample temperature) before dosing with TMA and was annealed by ramping the sample to the required temperature and maintaining that temperature for 10 minutes. The sample was allowed to return to base temperature prior to the taking of spectra.

XPS spectra were obtained using an unmonochromatized MgKα x-ray source (PHI model 1427) operated at 15 keV and 300 W and a hemispherical analyzer (VG 100AX) operated in the constant pass energy mode (50 eV pass energy). Take-off angle resolved spectra were obtained by rotating the sample 60° off surface normal, relative to the analyzer. The analyzer energy scale was calibrated using Au, Ag, and Cu standards, according to established

procedure[18] and XPS data were analyzed using commercially available software.[19] The variation in absolute signal intensity for the XPS system used in these experiments has been determined experimentally to be ≤ 4%. The exposure of fluoropolymers to x-rays is known to induce defluorination and cross-linking;[6] to minimize x-ray induced damage, exposure of the sample to x-ray flux was limited to that needed for the acquisition of spectra. The observed binding energies were affected by sample charging during data acquisition. Therefore, the XPS data were referenced to a F(1s) binding energy of 689.1 eV, which is consistent with the published values[4,5,8] for fluorine in a fluorocarbon environment. The full width at half-maximum (FWHM) for the fitted spectrum was kept constant within each atomic species for all spectra of that species.

Semiconductor grade (99.999% pure) TMA was obtained from Akzo Nobel Chemicals, Inc. (TMAL-9577) and was introduced directly into the CVD chamber using a metering valve. The composition of the organometallic precursor was verified by measurements with a quadrupole mass spectrometer. Exposures were performed at both elevated (540 K) and reduced

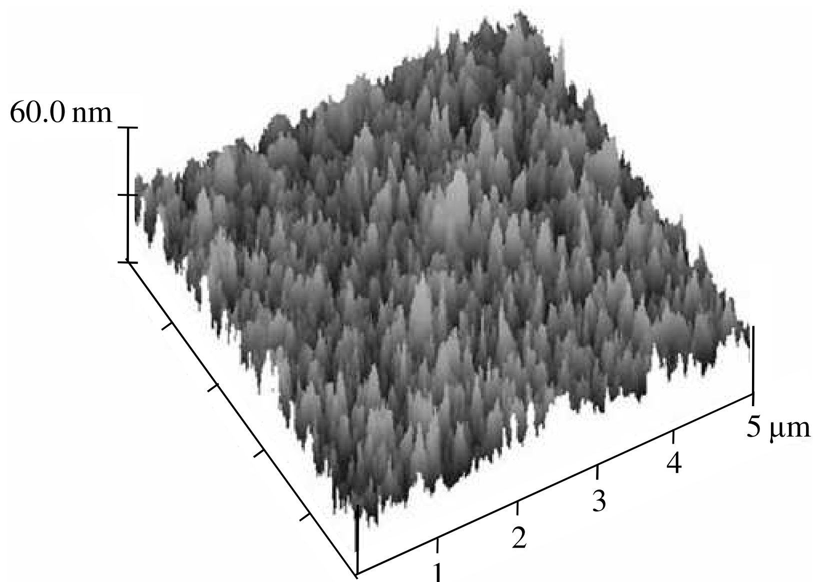

Figure 3. 2. Atomic force micrograph of vapor deposited Parylene AF-4.

(112 K) temperatures. Precursor exposures are reported as a product of background pressure and time of exposure (1 Langmuir [L] = 10^{-6} Torr-sec). Exposures have not been corrected for effects of directional dosing or ion gauge sensitivity. The sample was subsequently transferred to the UHV chamber for analysis by XPS. Anneals were carried out in the UHV chamber with XPS spectra taken after each annealing. To minimize changes in the x-ray flux, the sample was not moved after introduction into the UHV chamber other than rotation to obtain angle resolved spectra.

3.3. Results

3.3.1. Surface Analysis of Parylene AF-4

The atomic force micrograph for the 5.00 x 5.00 μm scan is shown in Figure 3.2 and surface roughness data for all AFM scans are given in Table 3.1. The average root-mean-square (rms) of the Parylene AF-4 surface profile (5.54 nm) compares favorably with that of spin-coated Teflon® AF (6.27 nm).[5] Water contact angle measurements show a contact angle of 97°; this

Table 3.1. Atomic Force Microscopy surface roughness data for Parylene AF-4 films used in this study.[a]

Scan Size $(\mu m)^2$	Z_{max} (nm)	R_{avg} (nm)	R_{rms} (nm)
1	32.82	3.857	4.800
1	54.13	5.407	4.648
5	53.85	4.608	5.825
5	57.14	4.513	5.782
10	68.42	4.624	5.926
10	57.88	4.632	5.919
50	81.92	4.015	5.128
50	120.68	4.115	5.303
Average	65.854	4.349	5.542
Std. Dev.	26.141	0.303	0.416

[a]Zmax is the maximum height of the profile, Ravg is the average of the deviations from the mean height, and Rrms is the root-mean-square of the roughness.

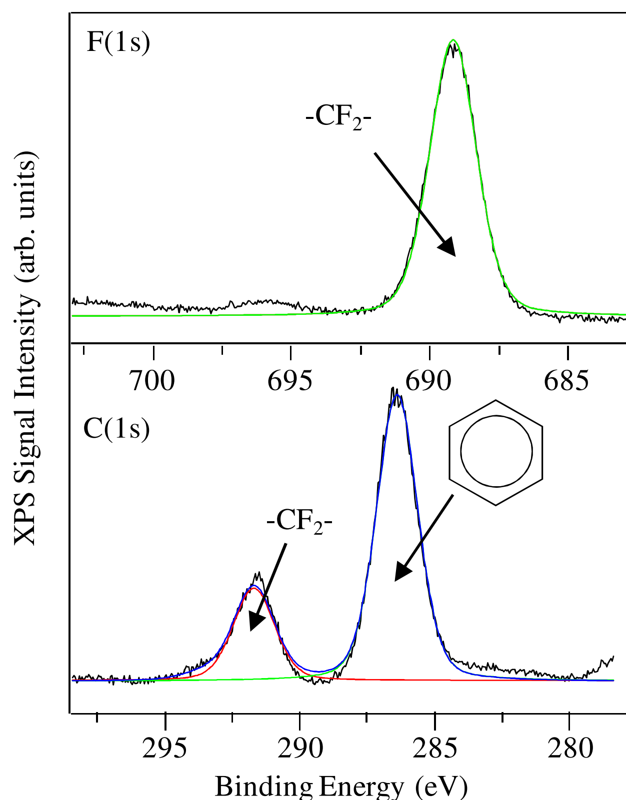

Figure 3.3. F(1s) and C(1s) XPS spectra of a neat Parylene AF-4 film.

indicates the Parylene surface is hydrophobic, though somewhat less so than amorphous Teflon® surfaces (118°).[5]

The x-ray photoelectron spectra for the neat Parylene AF-4 surface are given in Figure 3.3. The observed binding energies were affected by sample charging during the acquisition of spectra. Published charge compensation studies of fluoropolymers[4,5, 20,21] report F(1s) binding energies of 689.0–689.1 eV for fluorine in a $–CF_2–$ environment. The single feature seen in the F(1s) spectrum is therefore assigned to a binding energy of 689.1 eV. The O(1s) spectrum for the neat polymer at room temperature (not shown) contained no observable features.

The C(1s) spectrum of the neat Parylene AF-4 surface (Fig. 3.3) shows two well-resolved features at 291.8 eV and 286.6 eV. The published C(1s) binding energies for poly(tetrafluoroxylylene) are 290 eV ($–CF_2–$) and 285 eV (aromatic).[22,23] While the C(1s) peak-

to-peak spacing observed in this study (5.2 eV) is identical to the published values, the entire C(1s) spectrum of this study is 1.7 eV higher in binding energy. Differences in charge referencing is one possible explanation for this discrepancy; in neither previously published study is the method of charge compensation given. Comparison of the F(1s) to C(1s) [$–CF_2–$] peak spacing for this study with the literature values is also not possible because the F(1s) binding energy is not given for either published study.[22,23] Assignment of the high binding energy C(1s) peak seen in this study (291.8 eV) to the difluoride linkages ($–CF_2–$) gives a F(1s) to C(1s) [$–CF_2–$] peak spacing of 397.3 eV. Published XPS studies of non-oxygenated fluoropolymers[4–6,24,25] report F(1s) to C(1s) [$–CF_2–$] peak spacing in the range 396.8–397.0 eV, lower than that seen here (397.3 eV). An increase in the F(1s) to C(1s) [$–CF_2–$] peak spacing is indicative of a decrease in the electronegativity of the carbon environment as shown by the F(1s) to C(1s) [$–CF_2–$] peak spacing for poly(1,1-difluoroethylene) (398.8 eV), poly(1,2-difluoroethylene) (400.9 eV), and poly(monofluoroethylene) (401.3 eV).[26] An increase in the F(1s) to C(1s) [$–CF_2–$] peak spacing for Parylene AF-4, with respect to PTFE, is not unreasonable. Also, secondary fluorine effects resulting in C(1s) shifts to higher binding energy have been well documented[21,27] for both aliphatic and aromatic carbon. For example, Beamson and Briggs[21] list the binding energies for the C(1s) [$–CF_2–$] peak of poly(vinylidene fluoride) as 290.90 eV and the [$–CF_2–$] peak of poly(tetrafluoroethylene) as 292.48 eV. The addition of a fluorine atom to benzene also increases the binding energy of the C(1s) [$–CH_2–$] peak from 284.9 eV in benzene to 285.4 eV in monofluorobenzene.[27] The feature seen at 286.6 eV is therefore assigned to the aromatic ring of the xylene parent compound. The integrated intensity ratio of the 291.8 eV and 286.6 eV peaks is 3.0 ± 0.3, which agrees well with the theoretical structure of Parylene AF-4. The asymmetry seen on the low binding energy side of the 286.6 eV feature is

attributed to presence of x-ray satellites from the high binding energy C–F peak.[20] The asymmetry observed on the high binding energy side of the fitted peak at 291.8 eV is a shake-up satellite due to the aromatic $\pi \rightarrow \pi^*$ transition (relaxation resulting in the promotion of electrons in highest-filled energy levels into lowest-unoccupied ones).[20,28]

3.3.2. Exposure to TMA at 112 K

XPS spectra for the sample after exposure at low temperature (112 K) to 30 L trimethylaluminum are shown in Figure 3.4. The F(1s) signal (Fig. 3.4a) exhibits total signal attenuation due to the condensed TMA overlayer. The minimum overlayer thickness on the polymer can be estimated from the attenuation of the fluorocarbon F(1s) signal using the formula:

$$d_A = \lambda_A(E_B) \ln (I^{\infty}_B/I_B) \tag{3-1}$$

where I^{∞}_B/I_B is the ratio of the unattenuated signal of the substrate to the attenuated signal and $\lambda_A(E_B)$ is the mean free path of the substrate photoelectron of interest in the adlayer matrix.[28] Using a mean free path of 10–15 Å for a F(1s) photoelectron in an aluminum oxide matrix[29] and ~99.5% attenuation of the F(1s) signal gives an estimated minimum adlayer thickness of ≥ 53 Å.

The C(1s) spectrum also shows a large, asymmetric peak with a maximum at 284 eV. The asymmetry is indicative of the presence of more than one carbon environment. Using a FWHM of 1.8 eV (as determined from the C(1s) spectrum for the neat polymersurface), the feature is well fit by two peaks: 284.9 eV and 283.9 eV. The low binding energy feature (283.9 eV) is assigned to carbon in the methyl ligands of the TMA precursor.[30] The high binding energy component peak (284.9 eV) agrees well with the accepted value for hydrocarbons (285.0 eV). Previous experience with the chamber used in these experiments has shown that some

decomposition of the organometallic precursor invariably occurs prior to deposition on the sample; for this reason, the feature at 284.9 eV is assigned to adsorbed hydrocarbon from the partially decomposed precursor.

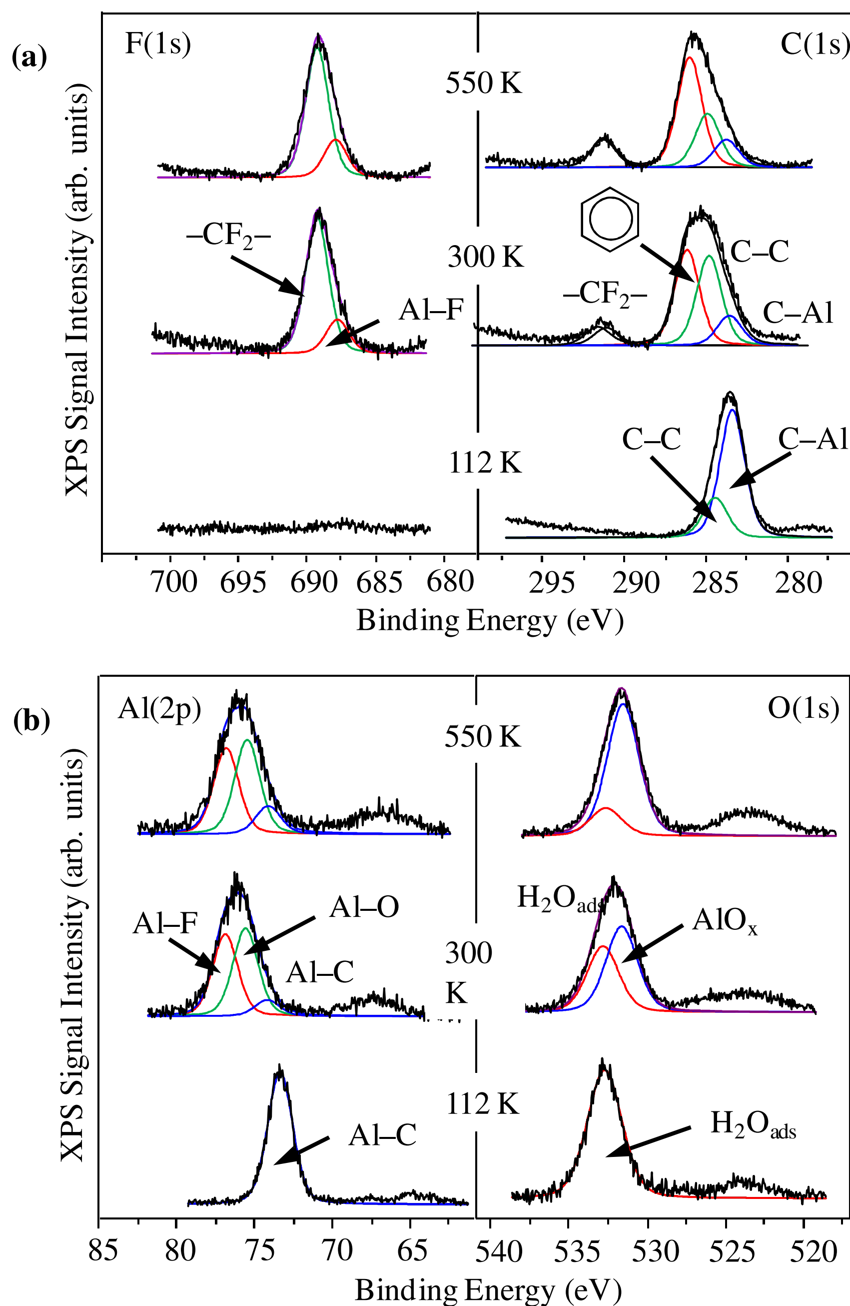

Figure 3.4. XPS spectra of TMA on Parylene AF-4 at dosing temperature and annealed to 300 K and 550 K: (a) F(1s) and C(1s) spectra and (b) Al(2p) and O(1s) spectra.

The Al(2p) spectrum shows a large single feature at 73.8 eV, 0.4 eV higher than the published[30] binding energy for trimethylaluminum (73.4 eV). However, the Al(2p) to C(1s) peak spacing of TMA observed in this study (210.1 eV) is in excellent agreement with that of Akhter and co-workers (210.0 eV).[30] Differences in observed binding energies may be attributed to differences in charge referencing: F(1s)[$–CF_2–$] for this study versus C(1s)[$–CH_2–$] for that of Akhter and co-workers.[30] The Al(2p) feature at 73.8 eV is therefore assigned to the TMA precursor.

After precursor deposition a large feature appears in the O(1s) spectrum at 532.7 eV (Fig. 3.4b) that is within the range of the published values of 532.6–533.3 eV for adsorbed water.[20,31–33] Given a base pressure for the CVD chamber of 1 x 10^{-8} Torr and the low deposition temperature used in these experiments, the physisorption of ambient water is unavoidable. For this reason, the O(1s) feature at 532.7 eV is assigned to adsorbed water (H_2O_{ads}).

3.3.3. Effects of Annealing

3.3.3.1. Annealing to 300 K

Figures 3.4 and 3.5 show the changes in the XPS spectra upon annealing of the TMA-dosed Parylene AF-4 sample in UHV. The F(1s) spectrum (Fig. 3.4a) exhibits a single, asymmetric feature with the centroid at 689.1 eV. The asymmetric broadening is indicative of multiple fluorine environments. Using a fixed FWHM of 2.0 eV (as determined from the neat polymer spectrum) the spectrum is well fit by two peaks: 689.1 eV and 687.7 eV; the former is attributed to the polymer substrate. Published studies[5,20,21] show the F(1s) binding energy for carbon-bound fluorine to be insensitive to changes in the local chemical environment. In a study of radiation-induced crosslinking of PTFE,[6] the F(1s) envelope exhibited negligible changes

upon exposure to x-rays for extended periods. It is, therefore, unlikely that the low binding energy fitted feature can be due to monofluoro- carbon species resulting from polymer defluorination. Additionally, the presence of a monofluoro- carbon species should give rise to a C(1s) feature with a binding energy ~3.0 eV lower than that of the $–CF_2–$ species;[21] no such feature is observed in the C(1s) spectrum for the TMA dosed and annealed AF-4 sample (Fig. 3.4a). The formation of aluminum fluorides has been observed during the evaporative deposition of aluminum on fluoropolymers[8,35] and during the interactions of clean, metallic aluminum with perfluoroalkyl ethers, acyl fluorides, and fluorocarbon lubricants.[34] The low binding energy fitted feature seen here (687.7 eV) is in good agreement with published binding energies for aluminum fluorides. [8,34–36]

After annealing to 300 K, the C(1s) spectrum (Fig. 3.4a) exhibits a shift of ~1.5 eV to higher binding energy and an increase in FWHM of the main feature by ~1.0 eV relative to the spectrum taken at 112 K. There is also a small additional feature at 292.0 eV, attributable to the C–F species from the polymer substrate. These changes are indicative of the desorption and decomposition of the TMA precursor and subsequent reaction with the polymer surface. Using a mean free path of 11–30 Å for a C(1s) photoelectron in an aluminum oxide matrix[29] (see Equation 3-1) an adlayer thickness of 17–47 Å is calculated after anneal to 300 K.[28] There is also a 52% decrease in the total signal intensity of the C(1s) spectrum upon annealing to 300 K, which is consistent with desorption of methyl ligands from the decomposed precursor. The increase in the FWHM of the main C(1s) feature is indicative of an increase in the number of carbon environments. Because of the reappearance of the high binding energy feature (292.0 eV) attributable to the fluoride species of the polymer substrate, a corresponding signal from the aromatic carbon from the polymer (at ~286.5 eV) can be inferred, with a signal intensity

approximately three times that of the fluoride signal. Other possible environments include hydrocarbons from the decomposition products, metal-carbides from either unreacted precursor or metal/polymer interactions, and carboxy species from interactions with the co-adsorbed water; however, the published C(1s) binding energies[21] for carbon species in oxygenated environments are 286.5 eV (alcohols and ethers) or greater. After compensation for the aromatic carbon of the polymer substrate, there is no spectral evidence for additional carbon species in the low binding energy feature with binding energies above ~285.5 eV. The large feature at low binding energy is well fit by three peaks: 286.6 eV, 285.2 eV, and 284.1 eV. The fitted peak at 286.6 eV is assigned to the aromatic carbon of the polymer substrate. The feature at 284.1 eV is within the range of published values for metal carbides.[1,30,34–36] The most probable sources of a carbide signal under these experimental conditions are unreacted precursor in the adlayer or interactions between the aluminum and carbon in the polymer substrate. Differentiation between these environments using C(1s) data alone would be highly subjective. However, the Al(2p) spectrum for the TMA-dosed surface (Fig. 3.4b) shows substantial changes upon annealing to 300 K. The changes observed in the Al(2p) and C(1s) spectra indicate near complete decomposition of the TMA precursor upon annealing to 300 K. The formation of Al–C bonds has been observed in a number of studies[1,8,34,35] involving the interactions of aluminum with fluorocarbons. The fitted feature at 284.1 eV is therefore assigned to aluminum bound to the polymer surface through Al–C bonds. The fitted feature at 285.2 eV is assigned to the remaining hydrocarbon species arising from the decomposition of the TMA precursor.

The Al(2p) spectrum exhibits significant broadening and a shift to higher binding energy upon annealing to 300 K (Fig. 3.4b). There is also very slight increase in total signal intensity. Using a fixed FWHM of 1.9 eV (as determined from the condensed precursor at 112 K), the

spectrum is well fit by three peaks: 76.8 eV, 75.6 eV, and 74.2 eV. In a study of the interaction between thermally deposited aluminum and fluoropolymers, Du and Gardella[8] reported binding energies for aluminum fluorides (76.4–76.8 eV), aluminum oxides (75.4 eV), and aluminum carbides (74.3–74.5 eV), which are very close to the binding energies of the fitted Al(2p) features in this study. Other studies[34,35] have reported similar assignments for the interaction between aluminum and fluorocarbons; thus, the fitted peaks in the annealed Al(2p) spectrum are assigned as follows: Al–F (76.8 eV), Al–O (75.6 eV), and Al–C (74.2 eV).

Upon annealing to 300 K, the O(1s) spectrum (Fig. 3.4b) exhibits a shift to lower binding energy and the appearance of an asymmetry on the high binding energy side of the main feature. The asymmetric broadening and decrease in binding energy are indicative of the formation of one or more additional oxygen environments. Curve fitting using a fixed FWHM (2.2 eV as determined from the low temperature O(1s) spectrum) gives a good fit with two peaks: a large peak centered at 531.7 eV and a smaller peak at 532.8 eV. While the former (531.7 eV) is well within the range of published values for aluminum oxides, previous studies[8,36–39] involving the interaction of aluminum with adsorbed water indicate some hydroxide formation at low temperature. The published O(1s) binding energy[37,38] for a mixed phase aluminum oxide/hydroxide (Al-O/OH) is 532.5 eV, relative to a bulk AlO_x signal of 531.5 eV. Annealing reportedly[37–39] causes a shift to lower binding energy in the O(1s) spectra as the mixed phase Al-O/OH is converted to a bulk AlO_x. In this study, no shift in the O(1s) binding energy is observed upon annealing to temperatures above 300 K, so the fitted feature at 531.7 eV is assigned to an AlO_x species. The smaller feature at 532.8 eV is assigned to the re-adsorption of water from the ambient upon returning the sample to 112 K after anneal and is in good agreement with the O(1s) spectrum (532.7 eV) taken at 112 K prior to anneal.

3.3.3.2. Annealing above 300 K

Figures 3.4 and 3.5 show the changes in the XPS spectra upon annealing to higher temperature in UHV. The total fluorine signal intensity increases as a function of temperature.

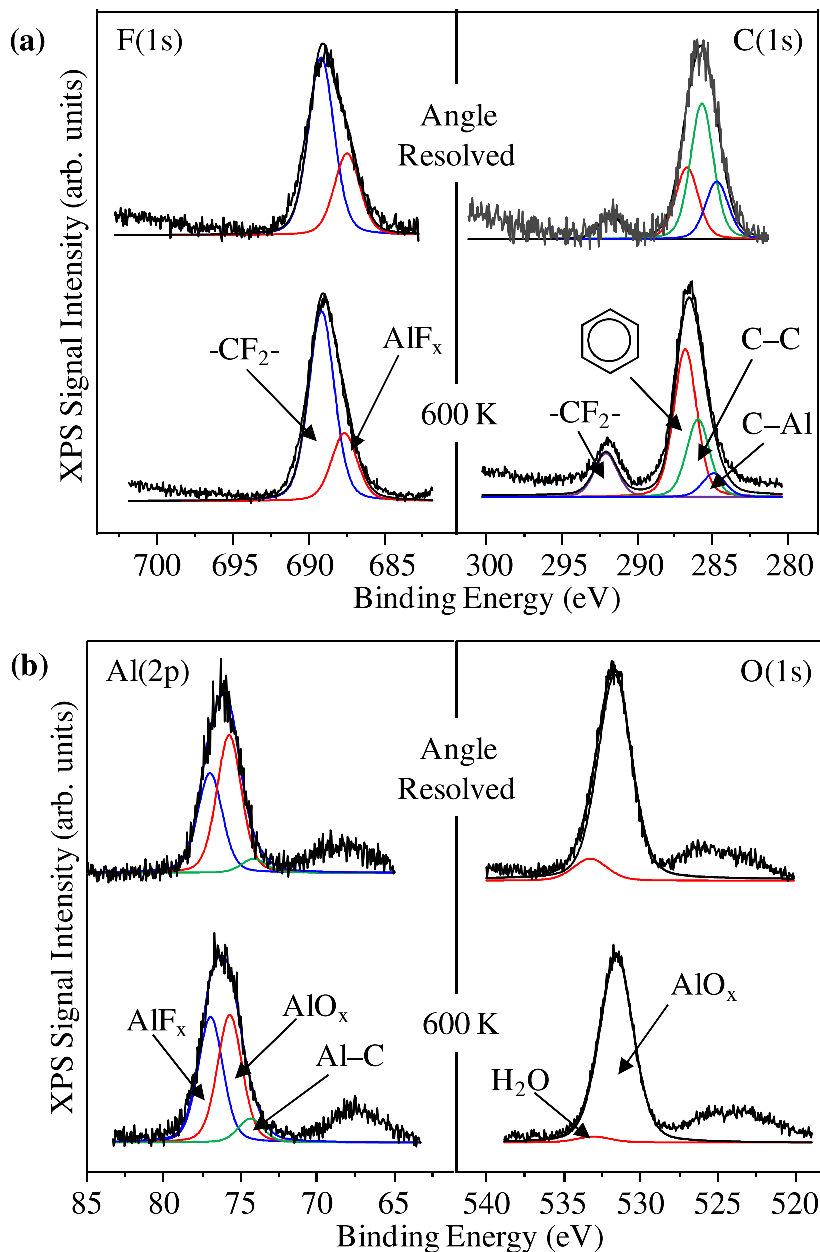

Figure 3.5. (a) F(1s) and C(1s) XPS spectra and (b) Al(2p) and O(1s) XPS spectra of TMA on Parylene AF-4, surface normal and 60° angle resolved.

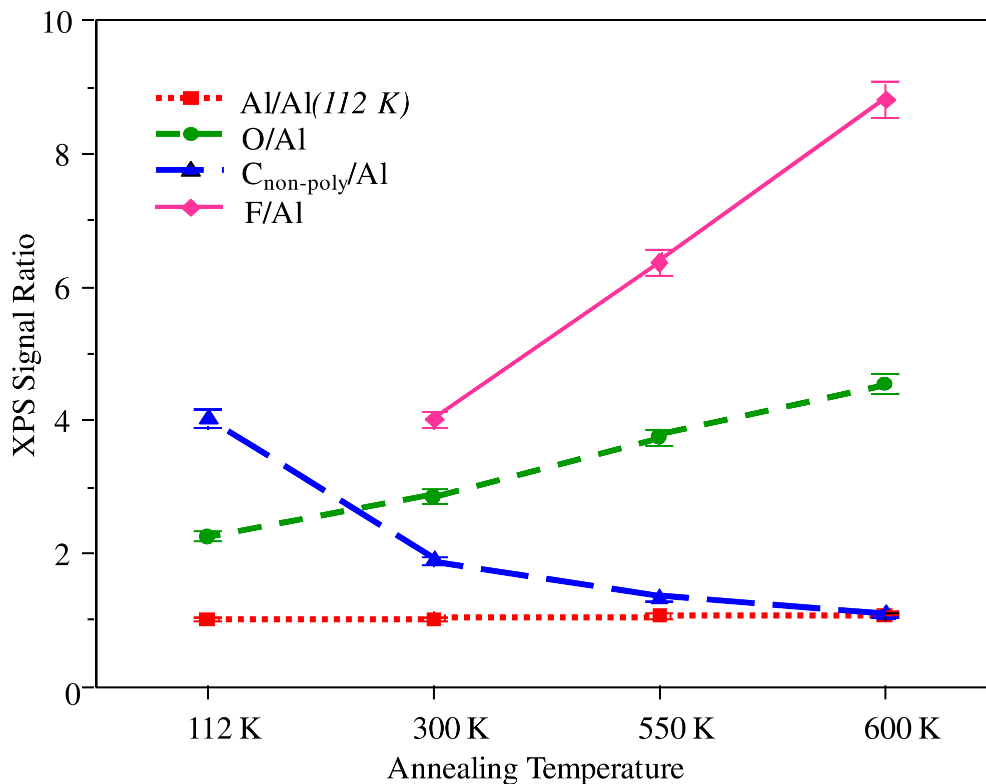

Figure 3.6. Variations in Al/Al*(112 K)*, O/Al, and non-polymeric C/Al signal ratios as a function of annealing temperature.

The F(1s) spectra of the sample show increasing asymmetry upon anneal to above 300 K (Figs. 3.4a & 3.5a); this indicates increasing aluminum-fluorine bond formation with respect to temperature. This increase in Al-F formation is represented graphically in Figure 3.6 by the increased intensity of the fitted feature attributed to Al–F (687.6 eV), as a function of temperature.

While the total carbon signal intensity decreases with respect to temperature, the intensity of the high binding energy (292.1 eV) component of the C(1s) spectra (assigned to C–F) increases. In addition, the low binding energy component narrows with temperature and shifts to higher binding energy (286.5 eV) by 550 K. These changes are indicative of further desorption of the hydrocarbon decomposition products produced in the initial reaction between the TMA precursor and the AF-4 surface.

The total Al(2p) signal intensity shows a slight increase upon annealing (Figs. 3.4a and 3.5a), which can be attributed to the desorption of the hydrocarbon decomposition products upon exposure of the sample to higher temperatures. The overall shape and position of the Al(2p) envelope remains constant upon annealing to temperatures above 300 K.

The O(1s) spectra (Figs. 3.4b & 3.5b) exhibit a steady increase in total signal intensity and decrease in the high binding energy asymmetry upon annealing. This can be attributed to the desorption of the hydrocarbon decomposition products from the aluminum adlayer (see above) and further reaction between the aluminum and water re-adsorbed on the adlayer surface upon cooling between anneals.

3.3.4. Angle Resolved Spectra

The relative roughness of a polymer surface, compared to that of a metal or semiconductor crystal, complicates the interpretation of take-off angle resolved spectra. Nonetheless, XPS take-off angle resolved studies have been reported for a variety of polymer films.[28,30,35] The fact that regular, monotonic changes are observed in XPS binding energies and/or relative atomic intensities is *prima facie* evidence that irregularities in polymer surface topography do not entirely obscure information to be obtained by variation of the take-off angle. For these reasons, take-off angle resolved studies were carried out on Parylene AF-4 samples exposed to TMA.

Take-off angle resolved spectra (taken at 60° off surface normal) for the sample annealed to 600 K are shown in Figures 3.5a and 3.5b. The F(1s) spectrum (Fig. 3.5a) experiences significant broadening to lower binding energy in the angle resolved spectrum. This is indicative of an increase in the relative contribution of the spectral component attributed to aluminum

fluorides (687.5 eV) when compared to the surface normal spectrum. Also, the C(1s) spectrum (Fig. 3.5a) shows a general decrease in the spectral features attributable to the C–F species of the underlying polymer (291.8 eV). The low binding energy peak shows signal broadening and a shift in the centroid to lower binding energy. These spectral changes indicate that the XPS sampling region is inhomogeneous over a range of about 30 Å. The relative concentrations of unfluorinated carbon and metal-carbide species are greater toward the outer border (vacuum/solid interface) of the sampling region.

The Al(2p) spectrum (Fig. 3.5b) shows a small (0.3 eV) shift to lower binding energy and a decrease in asymmetry on the low binding energy side at shallow angle (surface sensitive) geometry. The slight shift of the spectral maxima to lower binding energy is indicative of an increase in the signal attributed to the oxide species (75.7 eV) and the decrease in asymmetry indicates a decrease in the signal attributed to Al–C species (74.1 eV). These changes indicate that the aluminum oxide is toward the adlayer/vacuum interface, the Al–C species at the adlayer/polymer interface, and the aluminum fluoride species (76.9 eV) lies between. These results are similar to previously published studies of aluminum deposited on FEP and PFA polymers by Du and Gardella.[8] The angle resolved O(1s) spectrum (Fig. 3.5b) shows a slight increase in the high binding energy asymmetry, indicating adsorbed water (H_2O_{ads}) at the adlayer surface.

3.4. Discussion

Trimethylaluminum reacts with the Parylene AF-4 surface to yield aluminum bonded to oxygen, fluorine, and carbon species, with no metallic Al species evident. The aluminum-containing adlayer is stable even upon annealing to temperatures as high as 600 K, as shown by

Figure 3.7. Composition diagram of aluminum adlayer on aParylene AF-4 film.

the Al/Al(112 K) ratio in Figure 3.6. Previous experiments with the XPS system used in this study have shown a variation in absolute signal intensity of ≤ 4% for elemental spectra. The total aluminum signal remains relatively constant upon annealing to higher temperature, with a slight increase attributable to a decrease in signal attenuation because of temperature-induced desorption of hydrocarbon species formed from the decomposition of the TMA. Further evidence for hydrocarbon desorption is seen in Figure 3.6, as the decrease in the ratio of non-polymeric carbon to aluminum (C[non-polymer]/Al) with increasing temperature.

The presence of oxygen in the Al adlayer suggests the possibility of either aluminum oxyfluoride (Al–OF) or fluorinated aluminum oxide (F–AlO_x) formation upon annealing. Published values for unambiguously-assigned XPS binding energies for oxyfluoride species have not been found. Published bond energy data (Table 3.2) show the Al–F bond energy to be approximately three times that of the O–F bond (664 kJ/mol vs. 222 kJ/mol). In addition, the fluorination of an aluminum oxide ($AlO_x \rightarrow$ F–AlO_x) increases the energy of both the Al–F bond (by 97 kJ/mol vs. AlF_x) and the Al–O bond (by 70 kJ/mol vs. AlO_x).[39] Thus, under the

Table 3.2. Selected aluminum bond energies.[39]

Bond Energies (kJ mol^{-1})			
Al–Al	186	Al–C	255
Al–O	512	FAl–O	582
Al–F	664	OAl–F	761

experimental conditions described here, a fluorinated aluminum oxide (F–AlO_x) phase is thermodynamically more likely to form than either an $Al(OF)_x$ phase or a separate AlF_x phase. The low binding energy F(1s) feature (687.7 eV) must therefore be assigned to F–Al in a fluorinated aluminum oxide.

Annealing also results in increased aluminum-fluoride formation, as shown by the increasing intensities of the fitted features in both the F(1s) spectra (687.7 eV) and Al(2p) spectra (76.9 eV) (Figs. 3.4 and 3.5). It is well known[6] that x-rays have the potential to defluorinate fluoropolymers, which should be manifest in a steadily decreasing F(1s) total signal intensity. Figure 3.6 shows the F/Al ratio to be increasing much more rapidly than the total Al(2p) signal as a function of annealing. This indicates that the fluorine concentration within the aluminum adlayer increases upon annealing to higher temperature. It has been shown[8] that fluorine diffuses into aluminum films evaporated onto modified fluoropolymers; a similar situation is seen in this study, with fluorine diffusing into the aluminum adlayer. Angle-resolved spectra reveal the fluoride concentration to be decreasing toward the adlayer/vacuum interface, with a non-fluorinated aluminum oxide species concentrated near the surface. This indicates the presence of a fluorine concentration gradient consistent with fluorine diffusion into the aluminum adlayer, though the film is less than 100 Å thick; this is consistent with previous studes of TMA on Teflon®.[40] Du and Gardella[8] reported a decrease in fluorine diffusion for aluminum/fluoropolymer systems containing oxygen. The angle resolved Al(2p) spectrum (Fig. 3.5b) show aluminum carbide species to be present at the Al/polymer interface. The composition of the aluminum adlayer is shown graphically in Figure 3.7.

3.5. Summary and Conclusions

XPS was used to study the interaction between trimethylaluminum and Parylene AF-4. The data demonstrate that aluminum deposited on unmodified AF-4 by low temperature CVD is stable to elevated temperatures. At low temperature, the TMA precursor and ambient water condense on the polymer surface. Upon annealing to 300 K, the precursor decomposes and reacts with both carbon and fluorine from the polymer surface, as well as oxygen from the adsorbed water. The precursor/fluoropolymer/water reaction forms a thermally stable aluminum oxide film bonded to the polymer surface through aluminum-carbon bonds. Similar studies [29] report that TMA adds to carbon and oxygen of poly(vinyl alcohol) (PVA) to form a probable AlOC complex, attached to the polymer surface through Al–C and Al–O bonds. In this study, a fluorine concentration gradient exists across the adlayer with decreasing fluorination toward the adlayer/vacuum interface (Fig. 3.7). The aluminum defluorinates the polymer at all temperatures studied, with fluorine diffusion into the aluminum film. No metallic aluminum is observed at any time.

As integrated circuit devices become smaller, low dielectric polymers with good metal adhesion will play increasingly important roles in device design. These studies show that aluminum from chemical vapor deposition of TMA readily binds to the surface of Parylene AF-4. The aluminum oxide formed from the simultaneous adsorption of TMA and ambient H_2O at 112 K may act as a thermodynamic "trap" for fluorine, forming a thermally stable fluorinated aluminum oxide ($F–AlO_x$). This $F–AlO_x$ layer may prevent the poisoning of adjacent metal IC lines by binding fluorine diffusing out of the polymer and may also serve to block metal diffusion into the polymer.

3.6. Chapter References

1. Chang, C.-A.; Kim, Y.-K.; Schrott, A. G. *J. Vac. Sci. Tech. A* **1990**, *8*, 3304.

2. Nason, T. C.; Moore, J. A.; Lu, T.-M. *Appl. Phys. Lett.* **1992**, *60*, 186.

3. Blanchet, G. B. *Appl. Phys. Lett.* **1993**, *62*, 479.

4. Matienzo, L. J.; Zimmerman, J. A.; Egitto, F. D. *J. Vac. Sci. Tech*. **1994**, *12*, 2662.

5. Cho, C.-C.; Wallace, R. M.; Files-Sesler, L.A. *J. Electronic Mat.* **1994**, *23*, 827.

6. Rye, R. R. *J. Polym. Sci. B* **1993**, *31*, 357.

7. Shi, M.-K.; Lamontagne, B.; Martinu, L.; Semani, A. *J. Appl. Phys.* **1993**, *74*, 1744.

8. Du, Y.; Gardella, J. A. *J. Vac. Sci. Tech. A* **1995**, *13*, 1907.

9. Zhang, X.; Dabral, S.; Chiang, C.; McDonald, J. F.; Wang, B. *Thin Sol. Films* **1995**, *270*, 508.

10. You, L.; Yang, G.-R.; Knorr, D. B.; McDonald, J. F.; Lu, T.-M. *Appl. Phys. Lett.* **1994**, *64*, 2812.

11. Jeng, S. P.; Chang, M.-C.; Kroger, T.; McAnally, P.; Havemann, R. H**.** A planarized multilevel interconnect scheme with embedded low-dielectric-constant polymers for sub-quarter-micron applications. In *Digest of Technical Papers*, 1994 Symposium on VLSI Technology, Honolulu, HI, May 7–9, 1994; IEEE: 1994; 73.

12. Wang, L.; Angert, N.; Trautmann, C.; Vetter, J. *J. Adhesion Sci. Tech.*1995, *9*,1523.

13. Wary, J.; Olson, R.; Beach, W. *Semiconductor Int.* **1996**, *June*, 211.

14. *The National Technology Roadmap for Semiconductors*, Semiconductor Industry Association: San Jose, 1994.

15. Martini, D.; Sutcliffe, R.; Kelber, J. MOCVD of Cu on Teflon®-AF and Alumina-Modified Teflon®-AF. In *Low Dielectric Constant Materials III,* Proceedings of the Materials Research Society Symposium, San Francisco, CA, April 1–4, 1997; Case, C., Kohl, P., Kikkawa, T., Lee, W. W., Eds.; Materials Research Society: Pittsburgh, 1997.

16. Gorham, W. F. *J. Polym. Sci. A* **1996**, *4*, 3087.

17. Plano, M. A.; Kumar, D.; Cleary, T. The Effect of Deposition Conditions on the Properties of Vapor-Deposited Parylene AF-4 Films. In *Low Dielectric Constant Materials III,* Proceedings of the Materials Research Society Symposium, San Francisco, CA, April 1–4, 1997; Case, C., Kohl, P., Kikkawa, T., Lee, W. W., Eds.; Materials Research Society: Pittsburgh, 1997.

18. Powell, C. J. *Surf. Int. Anal.* **1995**, *23*, 121.

19. *ESCATools,* v4.6; Surface/Interface, Inc.: Sunnyvale, CA, 1995.

20. *Handbook of X-Ray Photoelectron Spectroscopy*; Wagner, C. D., Riggs, W. M., Moulder, J. S., Davis, L. E., Eds.; Perkin Elmer: Eden Prarie, MN, 1979.

21. Beamson, G.; Briggs, D.; *High Resolution XPS of Organic Polymers;* Wiley: New York, 1992.

22. You, L.; Yang, G.-R.; Lang, C.-I.; Moore, J. A.; Wu, P.; McDonald, J. F.; Lu, T.-M. *J. Vac. Sci. Tech. A* **1993**, *11*, 3047.

23. Wu, P. K.; Yang, G.-R.; McDonald, J. F.; Lu, T.-M. *J. Electronic Mat.* **1995**, *24*, 53.

24. Cadman, P.; Grossedge, G. M. *J. Mater. Sci.* **1979**, *14*, 2672.

25. Roberts, R. F.; Ryan, F. W.; Schonhorn, H.; Sessler, G. M.; West, J. E. *J. Appl. Polym. Sci.* **1976**, *20*, 255.

26. Clark, D. T.; Feast, W. J.; Kilcast, D.; Musgrave, W. K. R. *J. Polym. Sci. Polym. Chem.* **1973**, *11*, 389.

27. Clark, D. T.; Kilcast, D.; Adams, D. B.; Musgrave, W. K. R. *J. Electron Spec. Relat. Phenom.* **1972**, *1*, 227.

28. Seah, M. P. Quantification of AES and XPS. In *Practical Surface Analysis Vol. 1, Auger and X-ray Photoelectron Spectroscopy*, 2nd ed.; Briggs, D., Seah, M. P., Eds.; Wiley: New York, 1990; pp 201–255.

29. Somorjai, G. *Introduction to Surface Chemistry and Catalysis*; Wiley: New York, 1994.

30. Akhter, S.; Zhou, X.-L.; White, J. M. *Appl. Surf. Sci.* **1989**, *37*, 201.

31. Wren, A. G.; Phillips, R. W.; Torentino, C. U. *J. Colloid Interface Sci.* **1979**, *70*, 544.

32. Martensson, N.; Malmquist, P. A.; Svensson, S.; Basilier, E.; Pireaux, J. J.; Gelius, U.; Siegbahn, K. *Nouv. J. Chim.* **1977**, *1*, 191.

33. Nefedov, V. I.; Gati, D.; Dzhurinskii, B. F.; Sergushin, N. P.; Salyn, Y. V. *Zh. Neorg. Khim.* **1975**, *30*, 2307.

34. John, P. J.; Liang, J. *J. Vac. Sci. Tech. A* **1994**, *12*, 199.

35. Shi, M. K.; Lamontagne, B.; Semani, A.; Martinu, L.; Sacher, E.; Wertheimer, M. R.; Yelon, A. *J. Vac. Sci. Tech. A* **1994**, *12*, 29.

36. McGuire, G. E.; Schweitzer, G. K.; Carlson, T. A. *Inorg. Chem.* **1973**, *12*, 2450.

37. Rogers, J. W., Jr. An Electron Spectroscopic Investigation of the Interaction of Methanol and Ammonia with Clean and Partially Oxidized Aluminum Surfaces. Ph.D. Thesis, The University of Texas, 1979.

38. Rogers, J. W., Jr.; Hance, R. L.; White, J. M. *Surf. Sci.* **1980**, *100*, 388.

39. Dean, J. A.; *Lange's Handbook of Chemistry*, 14th ed.; McGraw-Hill: New York, 1992.

40. Sutcliffe, R.; Martini, D.; Pavlica, D.; Kelber, J. MO-CVD of Aluminum and Copper on Teflon®-AF. In *Advanced Metallization and Interconnect Systems for ULSI Applications, 1996,* MRS Conference Proceedings Vol.12; Havemann, R., Schmitz, J., Komiyama, H., Tsubouchi, K., Eds.; Materials Research Society: Pittsburgh, 1997.

CHAPTER 4

MODIFICATION OF PARYLENE AF-4 SURFACES USING ACTIVATED WATER VAPOR

4.1. Background

The study of low dielectric constant (low-k) polymers is a rapidly growing field, in part due to their possible use as interconnect materials in integrated circuit technology. As microelectronic devices become smaller and more complex and processing times become shorter, there is an increasing need to reduce resistance-capacitance (RC) delay and signal loss due to "cross-talk" voltages. To accomplish this, metals used for conducting lines must have lower electrical resistance, and insulating materials with lower dielectric constants must be incorporated. Low-k polymers, aerogels and xerogels are all being studied as materials to replace SiO_2 as interconnect dielectrics.

Fluorinated polymers are appealing because of their low dielectric constants, relative ease of deposition and excellent gap-filling properties. Fluoropolymers generally have dielectric constants between 1.9 and 2.1, much lower than that of SiO_2 (k = 3.9).[1–6] Issues with metal adhesion and plastic creep (cold flow), however, have limited their application in microelectronics. Parylene AF-4 (poly[α,α,α',α'-tetrafluoro-*p*-xylylene]) (Fig. 4.1) has a dielectric constant of 2.28, slightly higher than some fluoropolymers, but also has excellent thermal stability (m.p. > 773 K) and low moisture uptake (< 0.1%). The vapor deposition of polymers such as AF-4 gives a more uniform surface coverage than spin-deposition, and contamination from solvent residues does not occur as with spin-coating. Parylene AF-4 is typical of fluoropolymers in that it is relatively inert, and problems arise in the adhesion to metals. Other studies[7] have demonstrated increased polymer adhesion to aluminum due to the reaction with surface oxide or hydroxyl groups. Several techniques have been employed in the

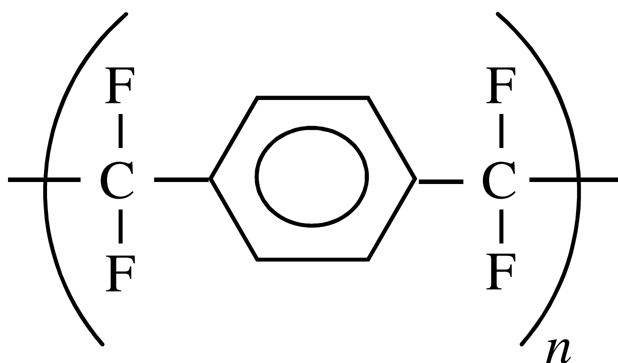

Figure 4.1. Structure of Parylene AF-4.

addition of oxygen to polymer surfaces. Methods involving plasma and ion beam modification often produce high kinetic energy species that may cause damage to polymer structures.[8–10] In this study, the surface of Parylene AF-4 was modified by exposure to ions, radicals, and neutrals produced by passing H_2O vapor across a heated tungsten filament. The resulting change in surface structure was examined and showed increased reactivity toward $Al(CH_3)_3$ at 300 K. In order to elucidate chemical changes induced by exposure to "activated" H_2O, comparisons are made to similarly exposed polystyrene. Polystyrene was chosen as a non-fluorinated analog to AF-4 due to similar structure and availability. Previous studies have used XPS to examine the effects of bombarding polystyrene surfaces with OH radicals or OH^+ ions that were separated at the dosing source;[9,11] this study, however, does not employ any techniques to isolate ions, neutrals, or radicals from the dose stream.

4.2 Experimental Methods

The Parylene AF-4 films used in this study were vapor-deposited by pyrolitic decomposition of the cyclic dimer in an experimental deposition system at Novellus Systems using the Gorham process, as described in earlier work.[12,13] The AF-4 samples used in this study were deposited at a rate of 150 Å/min to a thickness of 5000 Å on 1000 Å thick plasma-enhanced tetraethoxysilane (PETEOS) on silicon wafers. Polystyrene bulk samples were made by

compression molding of polystyrene pellets (Aldrich 18242-7) and were mechanically abraded to remove oxidized layers before insertion into UHV.

XPS and surface modifications were carried out in a UHV surface analysis system at the University of North Texas. The UHV system was evacuated with a turbomolecular pump and had a base pressure of 9×10^{-10} Torr. Typical working pressures were $1.0–2.0 \times 10^{-9}$ Torr. Sample modification was performed by passing deionized H_2O across a hot W filament, which dissociates the H_2O into a mixture of radicals and ions.[11] Prior to use, the H_2O vapor was purified by freeze-pump-thaw cycling. The composition of the gas stream exiting the doser was not examined. Dosing conditions (filament current, working distance, background H_2O pressure) were kept constant. The sample was held in direct line-of-sight of the "activated" water vapor, and the chamber was filled to a pressure of 1×10^{-5} Torr for 5 minutes, giving an exposure of 3,000 L per dose (1 L = 1×10^{-6} Torr-s). Pressure in the chamber was monitored with a nude ion gauge calibrated for N_2, mounted out of direct line-of-sight of the sample and dosing apparatus. Exposures have not been corrected for effects of directional dosing or ion gauge sensitivity. The sample was mounted on a Ta foil sample holder spot-welded to Ta leads. The sample was held in place by tabs that were cut into the Ta foil and bent over the corners of the sample. The chamber was allowed to return to an operating pressure of $\sim 1 \times 10^{-8}$ Torr prior to acquiring spectra.

XPS spectra were obtained using an unmonochromatized MgKα x-ray source (PHI model 1427) operated at 15 kV and 300 W and using a hemispherical analyzer (VG 100AX) operated in the constant pass energy mode (50 eV pass energy). Take-off angle resolved spectra were obtained by rotating the sample 60° off surface normal, relative to the analyzer. The analyzer energy scale was calibrated using Au, Ag, and Cu standards, according to the established procedure.[14] XPS data were analyzed using commercially available software[15] and

Shirley background subtraction. The variation in absolute signal intensity for the XPS system used in these experiments has been determined experimentally to be ≤ 4%. Atomic ratios were determined according to:

$$\frac{n_1}{n_2} = \frac{I_1/S_1}{I_2/S_2} \tag{4-1}$$

where n is the number of atoms of the element per cm^3, I is the number of photoelectrons detected per second, and S is the atomic sensitivity factor appropriate to the analyzer.[16] Sensitivity factors used in this experiment were specific to the analyzer and were obtained directly from the manufacturer. Exposure to x-rays is known to induce defluorination and cross-linking,[17] but sequential measurements indicate that perturbation of fluorocarbon samples due to the non-monochromatized x-ray source used in this experiment occur only for exposure times much longer than those used for typical XPS acquisition. In order to minimize x-ray induced damage, however, exposure of the sample to x-ray flux was limited to that necessary for the acquisition of spectra (i.e. the sample was moved into x-ray flux immediately before and removed immediately after analysis).

The polymer samples used in this study were affected by sample charging during XPS analysis, and all spectra required the use of charge referencing techniques. Charge referencing of polystyrene samples was accomplished by correcting the C(1s) peak due to saturated hydrocarbons to a value of 285.0 eV;[18] Parylene AF-4, however, contains no such hydrocarbons, and peaks from the C(1s) spectrum of AF-4 overlap with those from hydrocarbon contamination, hindering the use of this technique for referencing. As reported in literature,[8] the F(1s) peak of Parylene AF-4 is referenced to a value of 689.1 eV, which is consistent with published values for fluorocarbon environments.[3,15,17,18]

Atomic force microscopy was used to determine the surface roughness of the AF-4

sample and was performed at the Texas Instruments Materials Science Laboratory. The AFM (Digital Instruments) uses a photodetector to monitor a laser beam reflected from a spring cantilever mounted to the probe tip. During image acquisition, the instrument was operated in "tapping mode" where the oscillating probe encounters the surface and changes the amplitude of the vibration. The probe height is then adjusted to maintain a constant amplitude of oscillation across the surface. By mapping the voltage applied to the piezoelectric used for probe height adjustment as a function of x-y position, a topographical map is obtained. Scan areas were 1.00 μm^2, 4.00 μm^2, 25.00 μm^2 and 100.00 μm^2.

4.3 Results

4.3.1. Modification of Polystyrene

The C(1s) spectrum of unmodified polystyrene (Fig. 4.2a) contains peaks due to aliphatic

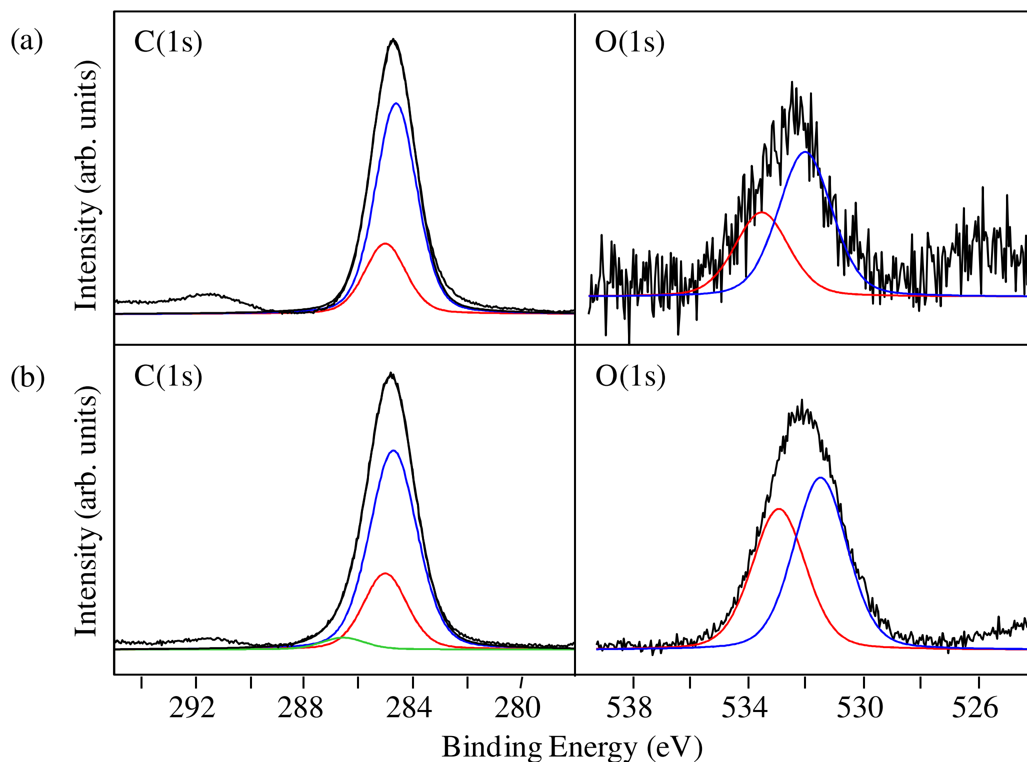

Figure 4.2. XPS spectra of polystyrene (a) before and (b) after modification.

carbons (referenced to 285.0 eV, as discussed in section II) and aromatic carbons (284.7 eV), along with a smaller peak at 291.7 eV due to the $\pi \rightarrow \pi^*$ shake-up transition of the aromatic ring system (energetic relaxation resulting in electron promotion from highest occupied to lowest unoccupied orbitals).[9,11,18] Some oxygen contamination was present in the neat polymer, with a resulting carbon/oxygen atomic ratio of ~73.7. An asymmetry in the O(1s) spectrum (Fig. 4.2a) indicates the presence of oxygen in more than one environment. By trial and error, a good visual and statistical curve fitting (minimization of chi-square value) was obtained using two peaks (each FWHM = 2.2 eV): one peak at 533.0 eV due to H_2O adsorption and another at 531.5 eV, likely from C–O–C due to reaction of the polymer with ambient environment. No elements other than carbon and oxygen were detected in the neat polystyrene.

After a single exposure (3,000 L) of polystyrene to activated H_2O, the C(1s) spectrum contains an additional peak at 286.5 eV, evidence of the presence of either C–OH bonds (286.55 eV) or C–O–C linkages (286.45 eV).[18] In previously published studies,[11] Sun et al. reported the formation of C=O and COOH functionalities (287.9 eV and 289.3 eV, respectively) upon exposure of polystyrene to doses of hydroxyl radicals of greater than one monolayer equivalent (~10 at. % oxygen). No peaks at such high binding energies were ever observed on polystyrene samples in this study.

Modification of polystyrene resulted in a slight decrease in the intensity of the aromatic carbon peak (0.76–0.72) as a fraction of the total C(1s) intensity (Table 4.1). This slight drop in aromatic carbon environment was accompanied by a decrease of ~56% in the intensity of the $\pi \rightarrow \pi^*$ shake-up peak, relative to the aromatic carbon. For simple ring cleavage, it would be expected that the opening of each ring would reduce the aromatic intensity and the $\pi \rightarrow \pi^*$ shake-up intensity by the same relative amount, leaving the ratio unchanged. The relative decrease in

Table 4.1 Carbon balance for polystyrene.

	Neat Polymer	Modified Polymer	Change
Aromatic C-H	0.76	0.72	- 0.04
Aliphatic C-H	0.24	0.24	0.00
C-O	0.00	0.04	+ 0.04
Total	1.00	1.00	0.00

the shake-up peak, however, is greater than expected for a 4% decrease in the aromatic peak, and indicates a perturbation in the shake-up excitation process of the ring system of the polymer (ring addition or cleavage).[16,18,19]

Exposure of polystyrene to activated H_2O also led to a substantial increase in the intensities of both peaks in the O(1s) spectrum, with a resulting C:O atomic ratio of 8.1, as compared to a ratio of 73.1 from the unmodified surface. The peak at 533.0 eV lies near the values given by Briggs and Beamson[20] for epoxides (533.13 eV) or ether groups adjacent to an aromatic ring system (533.25 eV). The peak at low binding energy is in the range of binding energies reported for C=O groups attached directly to aromatic ring systems. As discussed earlier, however, no C=O groups are apparent in the C(1s) spectrum. On the basis of this data, the low binding energy O(1s) peak cannot be assigned to any specific functional group.

4.3.2. Neat Parylene AF-4

The F(1s) spectrum of neat AF-4 (Fig. 4.3) contains a single peak (FWHM = 2.2 eV) referenced to 689.1 eV, as described in the experimental section. The C(1s) spectrum contains a large peak centered at a binding energy of 287.0 eV and a smaller peak at 292.2 eV; the former is assigned to the aromatic [–CH–] portion of the polymer and the latter assigned to [–CF_2–].[2,21] Both C(1s) peaks of the neat polymer have FWHM = 1.8 eV. Published studies[22,23] report peaks at 285 eV and 290 eV for Parylene AF-4. A uniform C(1s) peak shift of ~ 2.0 eV to higher

binding energy is apparent in this experiment, although the C(1s) peak-to-peak spacing (5.2 eV) is almost identical to those of published studies (5.0 eV).[22,23] Such shifting is suggestive of differences in referencing sample charging, but neither previously published study listed references for such compensation. A typical aromatic [–CH–] peak, such as that in polystyrene,

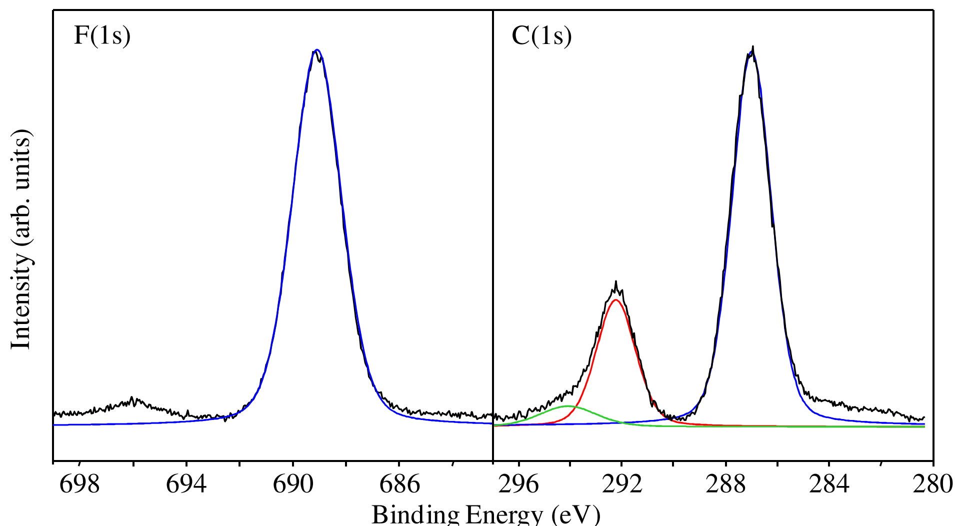

Figure 4.3. XPS spectra of neat Parylene AF-4 surface.

would be located at a binding energy of ~284.7 eV in a non-fluorinated polymer.[9,11,18] Interactions with fluorine atoms on adjacent carbons would, however, result in a shift to higher binding energy. The F(1s) to C(1s) [–CF_2–] peak spacing of 396.8 eV here agrees well with literature values of 396.8 eV to 397.0 eV for fluoropolymers. [3,17,21,24, 25]

The [$-CF_2-$] peak at 292.2 eV contains an asymmetry on the high binding energy side that is assigned to the $\pi \rightarrow \pi^*$ shake-up transition of the aromatic functionality. The position of the $\pi \rightarrow \pi^*$ peak is made on the basis of the energy separation from the main aromatic peak (7.2 eV), which closely corresponds to the separation observed for the polystyrene system (7.1 eV). A similar assignment of this feature in the C(1s) spectrum of Parylene AF-4 has been reported previously.[26] Taking into account the intensity due to shake-up, the experimental ratio of aromatic to aliphatic carbons is 3.31 ± 0.25, marginally higher than the empirical ratio of 3.00. The O(1s) spectrum (not shown) contains no distinguishable features.

4.3.3. Modification of Parylene AF-4

After an initial 3,000 L dose of activated water, there was only a slight attenuation (~3%) of the absolute intensity of the main F(1s) peak (Fig. 4.4a). No apparent change is observed in

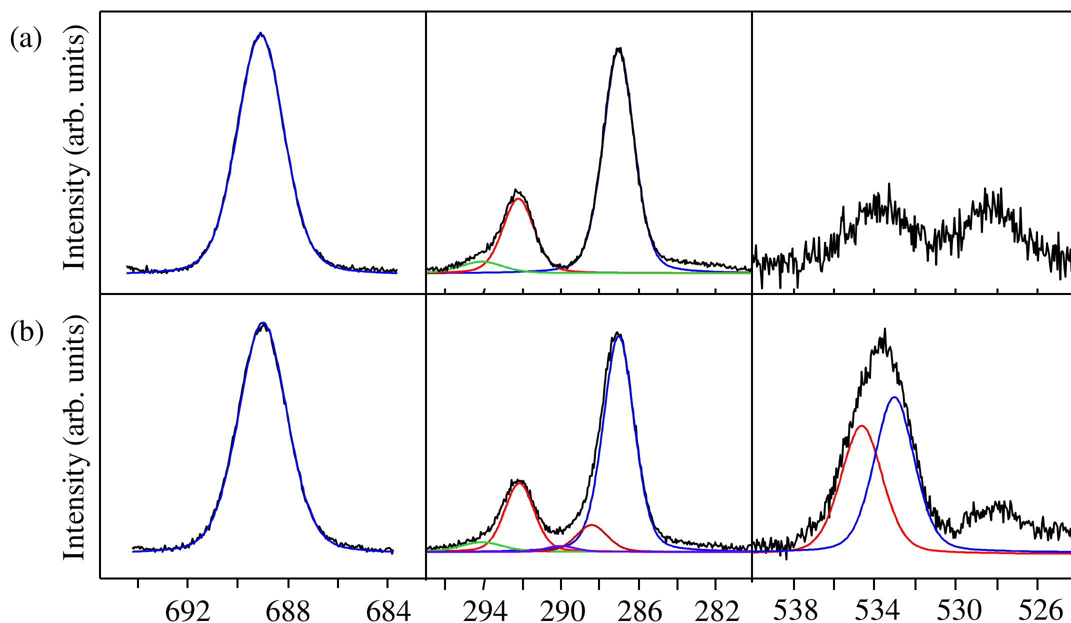

Figure 4.4. XPS spectra of Parylene sample exposed to (a) 3,000 L and (b) 24,000 L "activated" water vapor. The O(1s) feature near 528 eV binding energy is due to an oxide from the Ta sample holder.

the C(1s) spectrum, and the ratio of aromatic carbon to aliphatic carbon is only slightly decreased (Fig. 4.5). The appearance of two broad peaks in the O(1s) spectrum indicates that some oxygen has been incorporated into the sample, with a resulting C:O atomic ratio of ~52.6. Occasionally a slight sample misalignment occurs due to the sample mounting technique, and oxides of Ta (due to the Ta foil sample mount) can be observed in the O(1s) spectrum. The peak at low binding energy in the O(1s) spectrum**,** therefore, is assigned as an artifact due to metal oxide from the Ta sample holder,[16] and does not increase significantly upon successive sample modification.

After several exposures of the AF-4 sample to activated water (8 doses of 3,000 L each), the main peak in the F(1s) spectrum shows slight broadening (FWHM = 2.3 eV) and ~30% decrease in absolute intensity from the neat spectrum. The C(1s) spectrum after such modification (Fig. 4.4b) shows broadening effects manifested in additional intensity in the area between the two main peaks. Such broadening indicates the presence of additional C(1s) environments. The total absolute carbon intensity has decreased by ~12% compared to the neat spectrum. As shown in Table 4.2, both the aromatic and aliphatic carbon functionalities have decreased, as fractions of the total C(1s) signal, indicating that modification has affected both carbon environments. Two new peaks have developed in the C(1s) spectrum: one at 288.4 eV and a smaller peak at 290.0 eV. The positions of these peaks indicate defluorinated and/or

Table 4.2. Carbon balance for Parylene AF-4.

	Neat Polymer	Modified Polymer	Change
Aromatic C–H	0.76	0.71	- 0.05
$–CF_2–$	0.24	0.20	- 0.04
–C–F	0.00	0.01	+ 0.01
C–O	0.00	0.08	+ 0.08
Total	1.00	1.00	0.00

oxygenated carbon species.[3,8,21,27,28] A relative decrease of only ~8% occurred in the $\pi \rightarrow \pi^*$ shake-up peak after eight exposures (7.2% to 6.6% of the aromatic carbon peak area), much less of a decrease than that occurring in only a single modification of polystyrene (~56%).

The O(1s) spectrum of heavily modified Parylene AF-4 (Fig. 4.4b) contains a large feature centered at 534 eV (FWHM ≈ 3.4 eV). This O(1s) feature is well fit by two different peaks with binding energies of 534.6 eV and 533.0 eV with FWHM = 2.2 eV for each peak. In Figure 4.5, the atomic ratios of F, C, and O are plotted versus exposure to the activated water. The atomic concentration of fluorine, relative to carbon, decreases with exposure to activated water, indicating significant defluorination of the sample. Also shown in Figure 4.5, the addition of oxygen to the sample is manifested in an increasing O(1s) to total C(1s) ratio, which mirrors the loss of fluorine from the sample.

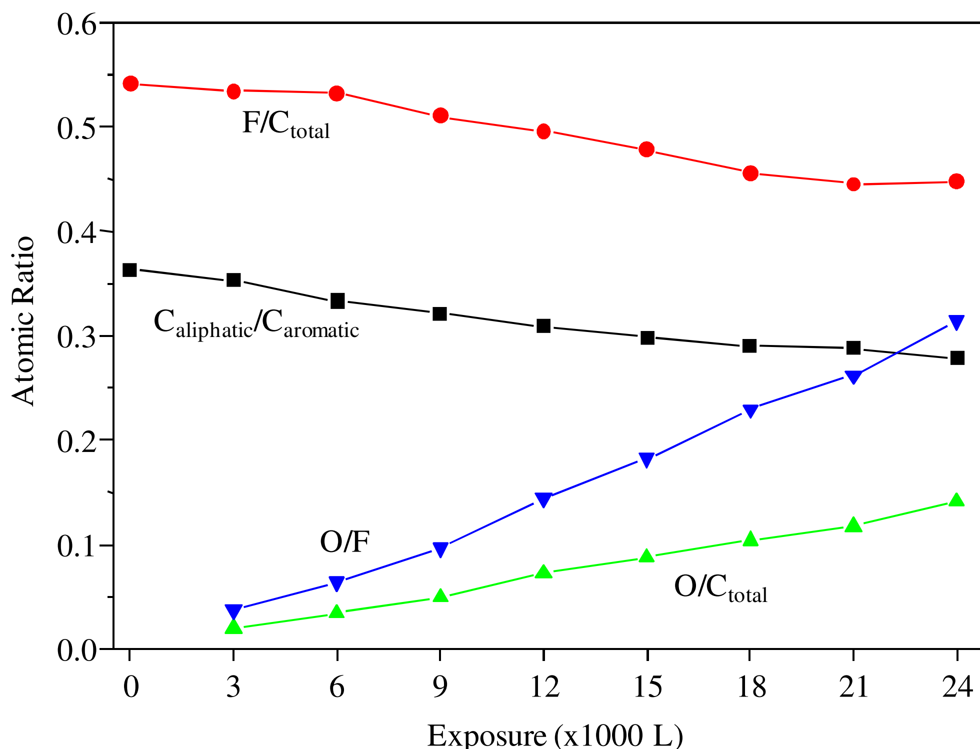

Figure 4.5. Atomic ratios of modified Parylene AF-4. Atomic ratios are corrected for spectrometer.

4.3.4. Surface Roughness of Modified AF-4

Many techniques to improve polymer adhesion, including plasma, ion beam, and chemical modification, result in significant roughening of polymer surfaces, typically on the order of 20 nm or more.[3,10,29–31] This roughening (0.02 μm) is ~10% or more of the minimum feature size for integrated circuit structures, and may pose problems in metallization schemes.

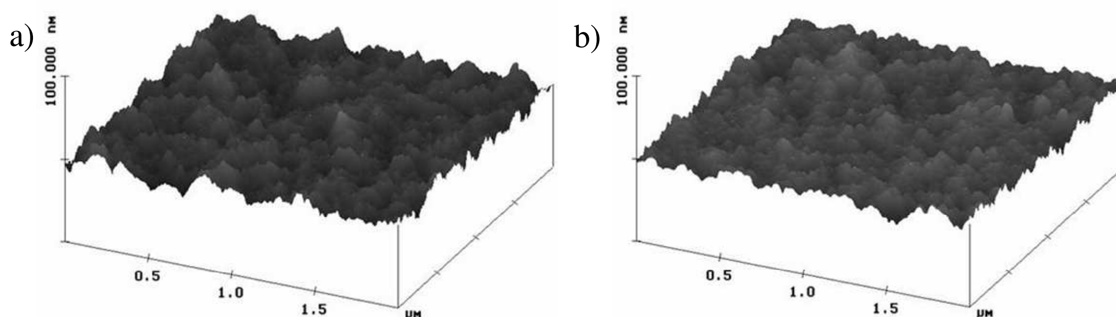

Figure 4.6. AFM images of (a) neat and (b) modified Parylene AF-4 samples.

Atomic force micrographs are shown in Figure 4.6 for two samples of Parylene AF-4 taken from the same wafer: one sample before modification and the other after eight exposures to 3,000 L of activated water. Corresponding roughness data is given in Table 4.3. The average root-mean-square (R_{rms}) of the surface roughness of the neat sample (3.2 nm) was slightly more than that of the modified sample (2.5 nm) and indicates some minor "smoothing" of the polymer surface. This is evidence that the surface of the modified sample has not been appreciably roughened by the procedure, and that modification occurs due to chemical rather than ablative effects.

Table 4.3. AFM surface roughness data for (a) neat and (b) modified Parylene AF-4 films used in this study.[a]

(a) Neat Parylene AF-4

Scan Size $(\mu m)^2$	Z_{max} (nm)	R_{avg} (nm)	R_{rms} (nm)
1	24.64	2.18	2.73
1	20.68	2.27	2.84
2	26.47	2.45	3.07
2	34.60	2.76	3.52
5	32.24	2.63	3.31
25	33.83	2.62	3.32
100	33.42	2.64	3.33
Avg.	29.41	2.51	3.16
Std. Dev.	5.45	0.22	0.29

(b) Modified Parylene AF-4

Scan Size $(\mu m)^2$	Z_{max} (nm)	R_{avg} (nm)	R_{rms} (nm)
1	16.13	2.04	2.52
1	17.66	1.80	2.26
4	20.64	2.04	2.57
4	22.51	2.02	2.52
25	22.29	2.01	2.52
25	22.95	2.18	2.73
Avg.	20.36	2.01	2.52
Std. Dev.	2.84	0.12	0.15

[a] Z_{max} is the maximum height of the profile, R_{avg} is the average of the deviations from the mean height, and R_{rms} is the root-mean-square of the roughness.

4.3.5. Trimethylaluminum Deposited Onto Modified AF-4

Trimethylaluminum shows no reaction with neat Parylene AF-4 at room temperature for doses of 3,000 L – 30,000 L TMA. After modification by as little as 3,000 L of activated water, however, the TMA reacts at room temperature (Fig. 4.7). The Al(2p) spectrum of modified AF-4 after dosing with 15,000 L TMA shows multiple Al environments, with peaks at 77.0 eV, 75.6 eV, and 74.0 eV. These peaks correspond to Al–F, Al–O and Al–C bonding, respectively, and agree with binding energy values from previous studies.[4,7,27,32] Figure 4.7 shows the gradual shift in binding energy of the centroid of the Al feature (from ~74 eV to 75.6 eV) upon increasing exposure to TMA. At low Al coverage, no Al-F bonding is apparent in the Al(2p) spectrum (Fig. 4.7a). Al($2p_{3/2}$) peak intensity vs. TMA exposure is shown in Fig. 4.8a for the modified AF-4 surface. The system does not appear to approach saturation coverage until above 15,000 L.

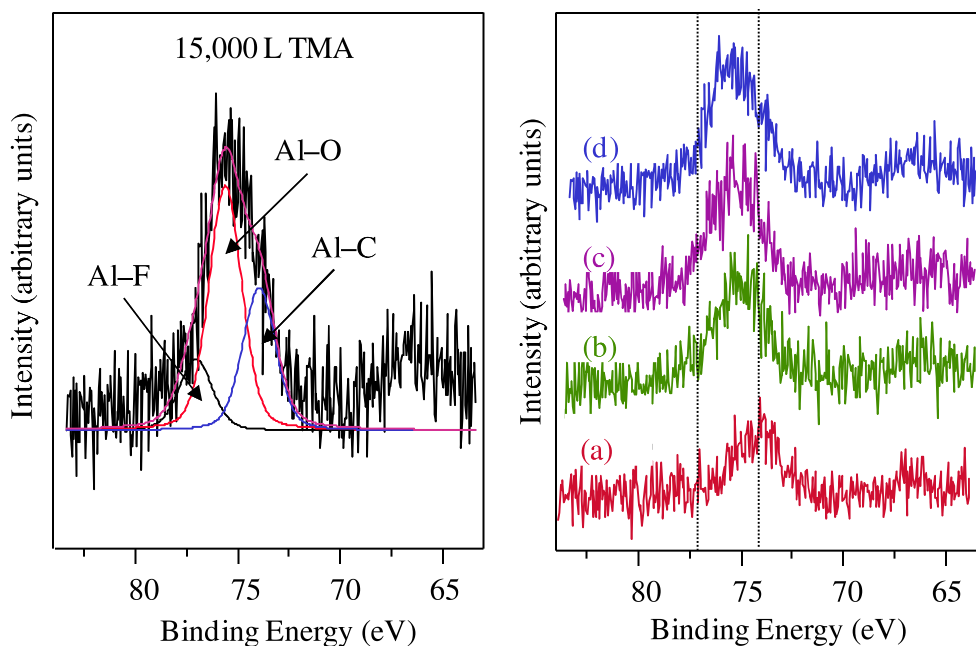

Figure 4.7. XPS Al(2p) spectra of modified Parylene AF-4 sample (3,000 L modification) after exposure to TMA at 310 K. Exposures are (a) 3,000 L (b) 6,000 L (c) 9,000 L and (d) 15,000 L TMA.

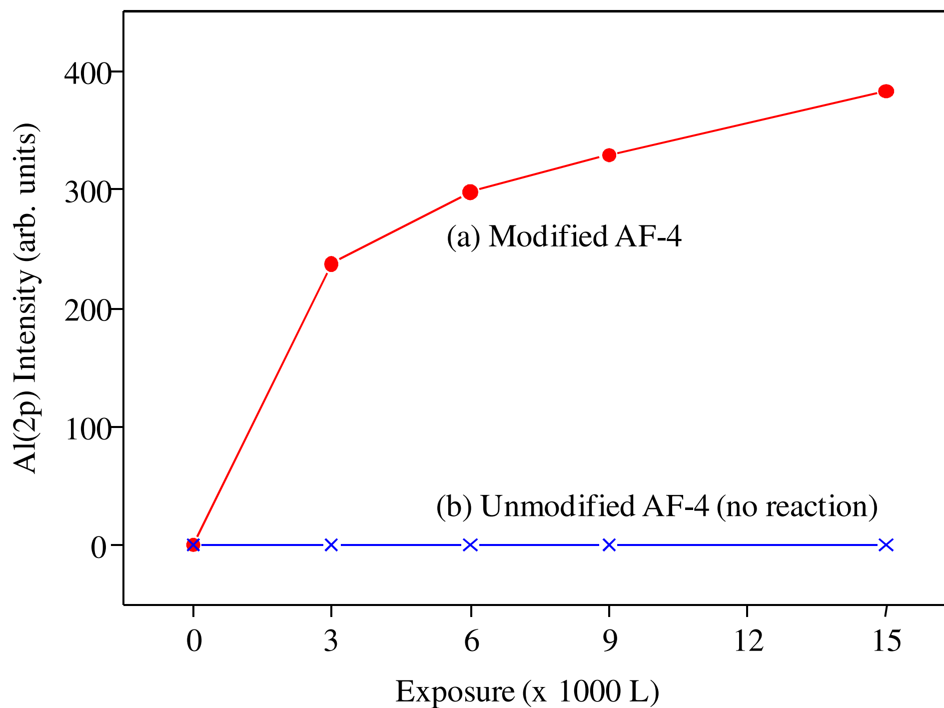

Figure 4.8. Al($2p_{3/2}$) XPS intensity versus exposure for (a) modified and (b) unmodified Parylene AF-4 exposed to activated water.

4.4. Discussion

The partially dissociated water vapor reacts with the polymer surfaces to produce oxygen bonded to carbon environments, occurring in both the parylene and polystyrene samples. The C(1s) spectrum of polystyrene is relatively simple, and it is clear that the only oxygen-containing carbon species present after modification are C–OH and/or C–O–C, appearing at a binding energy of 286.5 eV. As demonstrated by the carbon balance for polystyrene (Table 4.1), the loss of intensity of the aromatic species (- 0.04) is compensated by the gain in oxygen-containing carbon species (+ 0.04). This indicates that the aliphatic carbon species did not quantifiably participate in oxygen bonding, and that aromatic carbon species were the sole source of carbon-oxygen bonding. The C(1s) spectra in this study are similar to those given in previous studies[9,11] and are also similar to spectra of poly(4-hydroxystyrene).[17] The large decrease in the $\pi \rightarrow \pi^*$ shake-up peak (56%) upon exposure to activated water is evidence of a reduction in aromaticity in the ring system of polystyrene. Previous studies by Nowak et al.[9] found that both exposure to OH^+ ions and simple Ar^+ ion bombardment led to a $\pi \rightarrow \pi^*$ decrease in polystyrene.

In previously published studies, Sun et al.[11] reported that addition of hydroxyl radicals to polymers such as polystyrene in coverages of greater than one monolayer equivalent (~10 at. % oxygen) produced C=O and COOH functionalities. In this study, after several 3,000 L exposures of AF-4 to activated water, the polymer contains ~14 at. % oxygen, and after a single exposure polystyrene incorporates ~12 at. % oxygen from XPS data. No evidence was available in either polymer to support the existence of either C=O or COOH groups. No oxygen incorporation was attempted beyond ~14%, however; it is unclear whether the formation of other carbon–oxygen species is possible at higher doses of activated water.

After a single 3,000 L exposure, the oxygen content of the polystyrene sample increased tenfold, from O/C ≈ 1/80 before exposure to O/C = 1/8. The O(1s) peak appears slightly more symmetrical than that of the polymer before exposure, but the spectrum is again well fit using both peaks observed in the unmodified polymer. Briggs and Beamson[20] have reported an O(1s) binding energy of 533.63 eV for poly(4-hydroxystyrene), and Nowak et al.[9] reported a binding energy of 533.4 eV for polystyrene samples exposed to OH^+ ions. The O(1s) peak occurring at 533.0 eV in this study likely occurs from hydroxyl addition to the aromatic ring system, though it is roughly 0.5 eV lower than such previously reported values. The low binding energy peak at 531.5 eV does not correlate with any reported values from similar substances but probably results from adsorbed or absorbed water. The entire O(1s) spectrum appears to be shifted to lower binding energy by 0.5 eV due to sample charging issues.

A single exposure of AF-4 to 3,000 L activated water produced no apparent changes in the C(1s) spectrum. After eight exposures of 3,000 L each, significant defluorination was observed. Possible causes of defluorination include reactions with hydroxyl or hydrogen free radicals or ions resulting from the dissociation of water. Figure 4.5 demonstrates that the loss of fluorine from AF-4 occurs at approximately the same rate as the addition of oxygen, but since hydrogen radicals and ions are also attacking the polymer, this cannot be taken as direct evidence for reaction between oxygen and [$-CF_2-$] species. The small peak at 290.0 eV in the C(1s) spectrum of modified AF-4 probably represents a carbon species bearing a single fluorine [−CF−],[8,27,28] resulting from free radical hydrogen addition to the polymer. The carbon balance of AF-4 (Table 4.2) after modification (8 x 3,000 L) shows that both aromatic C–H and aliphatic [$-CF_2-$] bonds have decreased (0.04 and 0.05, respectively) as fractions of the total carbon, indicating reaction at both carbon species. Since the defluorinated [−CF−] peak at 290.0 eV

accounts for only 0.01 as a fraction of the carbon signal, the remaining fraction of 0.03 from the decrease in [$-CF_2-$] must appear under the oxygenated peak at 288.4 eV, strong evidence that reaction with oxygen has taken place at both aliphatic and aromatic carbon sites.

After exposure to a single 3,000 L dose of activated H_2O, the O/C ratio in the AF-4 sample is only ~1/50, much lower than that of polystyrene after one dose (~1/8). Only after eight 3,000 L exposures does the O/C ratio of AF-4 reach that of polystyrene after a single exposure. The more moderate rate of oxygen incorporation into AF-4 is evidence that the oxidation of the fluoropolymer surface occurs much more slowly than that of the non-fluorinated polystyrene. Because of the polarity of the C–F bond, $-CF_x$ groups should withdraw electrons from the aromatic ring system, thus deactivating the ring toward electrophilic substitution by OH^+ species.[33] Since the [–CH–] groups in polystyrene inductively donate electrons and activate the aromatic ring, the large difference in reactivity between Parylene AF-4 and polystyrene is not unexpected. A decrease in $\pi \rightarrow \pi^*$ shake-up peak intensity of only ~8%, relative to the aromatic carbon intensity, occurred after eight exposures of AF-4 to activated water. This is a stark contrast to the 56% decrease in polystyrene after only a single exposure, and may also indicate that carbocation/radical stability affects the presence of the $\pi \rightarrow \pi^*$ shake-up peak due to the presence of radicals in the aromatic rings.

The O(1s) spectrum of heavily modified AF-4 (Fig. 4.3b) is almost identical to that of modified polystyrene (Fig. 4.5b), but is shifted toward higher binding energy by 1.5 eV. Peak widths in the fitted O(1s) spectrum are nearly identical between the modified polymers (FWHM = 2.3 eV for AF-4, 2.2 eV for polystyrene), as are the ratios of the two O(1s) components, suggesting that the polymers contain identical oxygen groups. Presumably the binding energy shift in AF-4 is due to secondary fluorine effects from neighboring [$-CF_2-$] and [–CF–]

groups,[17,28,34] but the possibility of different oxygen functionalities in the parylene cannot be completely eliminated.

Modification of polystyrene indicates oxygen addition exclusively to the aromatic carbons, in agreement with previous work by Sun et al.[11] Similar evidence demonstrates oxygen addition at both aromatic and aliphatic carbon sites in AF-4. The decreasing aliphatic/aromatic carbon ratio of AF-4, upon successive exposures to activated water, indicates that aliphatic [–CF_2–] carbons may undergo some reaction. Otherwise, an increase in this aliphatic/aromatic ratio would be expected. The sequential (as opposed to simultaneous) addition of oxygen to the different carbon species would result in changing ratios of the two O(1s) peaks and, therefore, a change in the line shape of the O(1s) signal. No such change is apparent. A plot of aliphatic/aromatic carbon ratio vs. exposure (Fig. 4.5), with sequential oxygen addition, should also result in a non-uniform slope. Sequential oxygen addition to different carbon species may thus be ruled out.

Previous studies[7] have demonstrated that exposure of Parylene AF-4 to trimethylaluminum at low temperatures, and in the presence of ambient water vapor, produces an AlO_x layer bound to the polymer through Al–C and Al–O bonds, due to the co-condensation of TMA and H_2O on the sample. Upon increased exposure of the modified AF-4 to TMA, as seen in Figure 4.8, there is a shift in the Al($2p_{3/2}$) spectra toward higher binding energy. This shift is indicative of the breaking of low binding energy Al–CH_3 bonds from the precursor and formation of Al–O and Al–F bonds on the polymer surface. It is possible that once the Al from the precursor has reacted with all available surface oxygen sites, the incoming Al bonds with the existing AlO_x and with F from the underlying polymer. As indicated by Figure 4.8, saturation of Al on the modified polymer surface did not occur at the exposures in this study.

4.5. Summary and Conclusions

Parylene AF-4 and polystyrene polymers were modified by dosing with water vapor passed over a hot W filament, resulting in oxygen addition to the polymer surfaces. XPS spectral evidence indicates that oxygen incorporation into polystyrene occurred exclusively at aromatic carbon sites, while the incorporation into AF-4 did not occur with such selectivity. Oxygen x-ray photoelectron spectra of the two modified polymers were comparable (apart from a shift to higher binding energy due to secondary fluorine effects in AF-4) indicating that similar reactions occurred. The rate of oxygen uptake from exposure to "activated" water was substantially less for AF-4 than for polystyrene, but even the more modest oxygen incorporation observed for AF-4 led to increased room temperature reactivity between the polymer and trimethylaluminum. Atomic force microscopy showed no significant roughening of the parylene sample due to exposure to activated water. Parylene AF-4 modified by exposure to 3,000 L of "activated" H_2O showed significantly enhanced reactivity toward MOCVD of TMA at 300 K. At low Al exposures, no Al–F was observed, although Al–F formation was observed at higher exposures.

These results demonstrate that oxygen incorporation into fluoropolymers is possible using a simple dosing apparatus. The surface oxidation allows enhanced surface reactivity toward aluminum metallization. A comparison of these results with those of other investigators[9,11] indicates that electrostatic filtering of charged species from the gas stream may significantly alter the types of oxygen-containing species incorporated into the polymer. By utilization of low-kinetic-energy techniques that allow relatively low penetration into the polymer bulk, the possibility exists to modify only the surface of polymers, thus enhancing reactivity at the surface and leaving bulk properties unchanged.

4.6. Chapter References

1. Singer, P. *Semiconductor Int.* **1996**, *19*, 88.

2. Chang, C.-A.; Kim, Y.-K.; Schrott, A. G. *J. Vac. Sci. Technol. A* **1990**, *8*, 3304.

3. Cho, C.-C.; Wallace, R. M.; Files-Sesler, L. A. *J. Electronic Mat.* **1994**, *23*, 827.

4. Du, Y.; Gardella, J. A. *J. Vac. Sci. Technol. A* **1995**, *13*, 1907.

5. Murarka, S. P. *Solid State Technol.* **1996***, 39*, 83.

6. Nason, T. C.; Moore, J. A.; Lu, T.-M. *Appl. Phys. Lett.* **1992**, *60*, 1866.

7. Sutcliffe, R.; Lee, W. W.; Gaynor, J. F.; Luttmer, J. D.; Martini, D.; Kelber, J.; Plano, M. A. *Appl. Surf. Sci.* **1998**, *126*, 43.

8. Wells, R. K.; Ryan, M. E.; Badyal, J. P. S. *J. Phys. Chem.* **1993**, *97*, 12879.

9. Nowak, P.; McIntyre, N. S.; Hunter, D. H.; Bello, I.; Lau, W. M. *Surf. Int. Anal.* **1995**, *23*, 873.

10. Hopkins, J.; Boyd, R. D.; Badyal, J. P. S. *J. Phys. Chem.* **1996**, *100*, 6755.

11. Sun, J. Q.; Bello, I.; Bederka, S.; Lau, W. M. *J. Vac. Sci. Technol. A* **1996**, *14*, 1382.

12. Gorham, W. F. *J. Polym. Sci. A* **1996**, *4*, 3087.

13. Plano, M. A.; Kumar, D.; Cleary, T. The Effect of Deposition Conditions on the Properties of Vapor-Deposited Parylene AF-4 Films. In *Low Dielectric Constant Materials III,* Proceedings of the Materials Research Society Symposium, San Franciso, CA, April 1–4, 1997; Case, C., Kohl, P., Kikkawa, T., Lee, W. W., Eds.; Materials Research Society: Pittsburgh, 1997.

14. Powell, C. J. *Surf. Int. Anal.* **1995**, *23*, 121.

15. *ESCATools,* v4.6; Surface/Interface, Inc.: Sunnyvale, CA, 1995.

16. Moulder, J. F.; Stickle, W. F.; Sobol, P. E.; Bomben, K. D. *Handbook of X-ray Photoelectron Spectroscopy*; Physical Electronics: Eden Prairie, MN, 1995.

17. Rye, R. R. *J. Polym. Sci. B, Polym. Phys. Ed.* **1993**, *31*, 357.

18. Beamson, G.; Briggs, D. *High Resolution XPS of Organic Polymers;* Wiley & Sons: New York, 1992.

19. Seah, M. P. Quantification of AES and XPS. In *Practical Surface Analysis Vol. 1, Auger and X-ray Photoelectron Spectroscopy*, 2nd ed.; Briggs, D., Seah, M. P., Eds.; Wiley: New York, 1990; pp 201–255.

20. Briggs, D.; Beamson, G. *Anal. Chem.* **1993**, *65*, 1517.

21. Matienzo, L. J.; Zimmerman, J. A.; Egitto, F. D. *J. Vac. Sci. Technol. A* **1994**, *12*, 2662.

22. Wu, P. K.; Yang, G.-R.; McDonald, J. F.; Lu, T.-M. *J. Electron. Mater.* **1995**, *24*, 53.

23. You, L.; Yang, G.-R.; Lang, C.-I.; Moore, J. A.; Wu, P.; McDonald, J. F.; Lu, T.-M. *J. Vac. Sci. Technol. A* **1993**, *11*, 3047.

24. Cadman, P.; Gossedge, G. M. *J. Mater. Sci.* **1979**, *14*, 2672.

25. Roberts, R. F.; Ryan, F. W.; Schonhorn, H.; Sessler, G. M.; West, J. E. *J. Appl. Polym. Sci.* **1976**, *20*, 255.

26. Harrus, A. S.; Plano, M. A.; Kumar, D.; Kelly, J. Parylene AF-4: A Low Material Candidate for ULSI Multilevel Interconnect Applications. In *Low-Dielectric Constant Materials II*, Proceedings of the Materials Research Society Symposium, Boston, MA, Dec. 2–3, 1996; Lagendijk, A., Treichel, H., Uram, K. J., Jones, A. C., Eds.; Materials Research Society: Pittsburgh, 1997.

27. Shi, M.-K.; Lamontagne, B.; Martinu, L.; Selmani, A. *J. Appl. Phys.* **1993**, *74*, 1744.

28. Clark, D. T.; Feast, W. J.; Kilcast, D.; Musgrave, W. K. R. *J. Polym. Sci., Polym. Chem. Ed.* **1973**, *11*, 389.

29. Tan, B. J.; Fessehaie, M.; Suib, S. *Langmuir* **1993**, *9*, 740.

30. Graziani, E. I.; McKeown, N. B.; Kalman, P. G.; Thompson, M. *Inter. Biodeter. Biodeg.* **1992***, 30*, 217.

31. Baglin, J. E. E. *Nucl. Instr. Meth. Phys. Res.* **1992**, *B65*, 119.

32. John, P. J.; Liang, J. *J. Vac. Sci. Technol. A* **1994**, *12*, 199.

33. McMurry, J. *Organic Chemistry,* 3rd ed.; Brooks/Cole: Pacific Grove, CA, 1992.

34. Clark, D. T.; Kilcast, D.; Adams, D. B.; Musgrave, W. K. R. *J. Electron Spec. Relat. Phenom.* **1972**, *1*, 227.

CHAPTER 5

FORMATION OF SI-C_X FILMS AND THEIR INTERACTIONS WITH H_2O AND CU

5.1. Introduction

Because of the introduction of Cu into integrated circuit (IC) architectures, the demand has grown for low-dielectric-constant materials that can be readily incorporated into Cu systems. Cu diffusion is rapid through SiO_2 dielectrics,[1–3] and suitable low-dielectric-constant (low-k) materials and Cu barrier materials are needed to prevent this diffusion and the subsequent poisoning of insulating layers and gate structures by Cu atoms. In addition, as each added material layer occupies a finite volume (as well as adding processing steps), the ever-decreasing feature sizes of ICs require the use of low-k materials as interlayer dielectrics (ILDs) as well as extremely limited thicknesses of diffusion barrier or adhesion promoting layers. Constantly shrinking devices sizes and increasing packing densities of transistors have spurred the investigation into both Cu barrier and adhesion-promoting materials with thicknesses on the order of monolayers rather than hundreds of Angstroms.

This research describes the formation of thin Si-C_x films and their subsequent investigation for simultaneous use as both Cu diffusion barriers and Cu-to-dielectric adhesion promoters. Carbon-doped silicon oxide films have recently become important in high-volume manufacturing (HVM) due to their stability, insulating properties, and relatively simple deposition by plasma processes. Previous works[4] have demonstrated that Si-C_x films may have potential as Cu diffusion barriers. This work describes the in-situ formation of Si-C_x films by electron beam bombardment, investigation of the films' Cu-diffusion-barrier properties via x-ray photoelectron spectroscopy (XPS), and the possibility of tailoring their surface-layer functional groups in order to increase their compatibility with fluorinated, low-k polymer layers.

Plasma processes are often used in IC manufacturing for the deposition of ILD materials. These plasma systems contain complex environments of radical and charged reactive gas species and are difficult to study directly. Simple, controlled studies have previously been performed[5] that emulate a portion of the reactions within a plasma while allowing a more controlled environment. Similarly, I have chosen to deposit thin films in ultra-high vacuum (UHV) by simple low-temperature adsorption of reactants followed by exposure to an electron-beam, which mimics some reactions within a complex plasma deposition.

5.2. Experimental

Experiments were carried out under ultra-high vacuum (UHV) conditions. As described in earlier works,[6–8] the UHV system has two chambers separated by a gate valve (Fig 5.1). Turbo

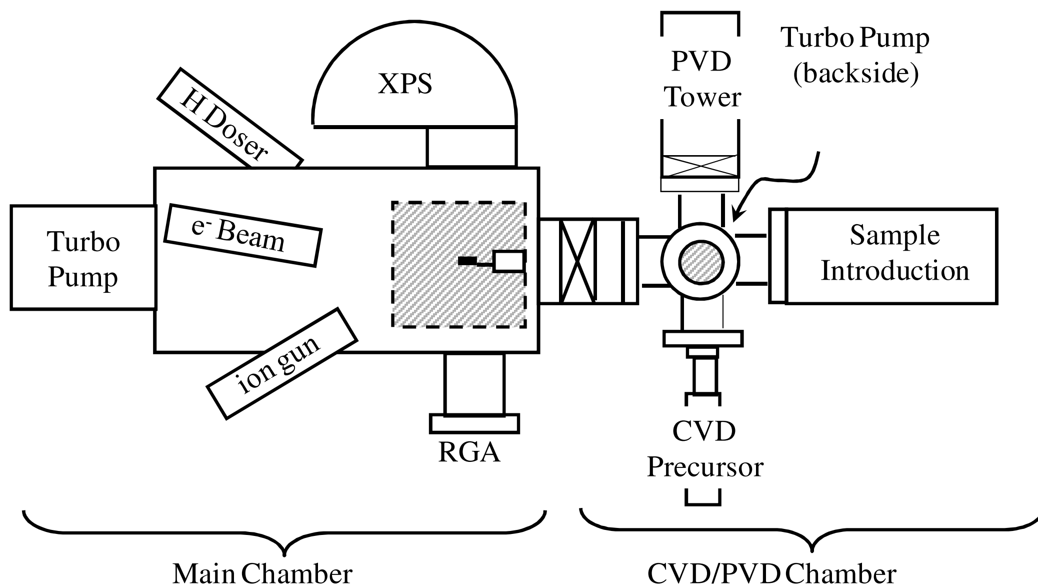

Figure 5.1. Schematic of UHV/XPS chamber.

molecular pumps were used to evacuate both chambers, and typical working pressures for the main and CVD/PVD chambers were 1 x 10^{-10} Torr and 1 x 10^{-8} Torr, respectively. Pressures in the UHV chambers were monitored by nude ion gauges calibrated for N_2 and located out of

direct line-of-sight of the samples in order to avoid any ion-induced surface modifications. Substrates were 1 cm^2 samples of polycrystalline Cu, polycrystalline Ta, or 1000 Å SiO_2 (on Si wafers). Samples were either welded directly to Ta wire leads (for the case of Ta foil) or held in place using a Ta foil sample holder. Sample temperatures were controlled from 90-1000 K by a combination of resistive heating of the sample or holder and liquid nitrogen cooling. For temperature measurement, a thermocouple junction was welded either directly to the top of the sample (for Ta) or to the top side of the sample holder.

Prior to vapor deposition, metal samples were cleaned by Ar^+ sputtering until a minimum of carbon and oxygen were detected on the surface by XPS analysis. Chemical vapor deposition (CVD) was achieved through a direct dosing tube positioned ~3 cm from the sample surface. Gas exposures were not calibrated for effects of directional dosing or ion gauge sensitivity and are given in terms of Langmuirs, where 1 L = 1 x 10^{-6} Torr-sec. Dosing was with commercially available liquid vinyltrimethylsilane (VTMS, 97%, Aldrich) that was purified by freeze-thaw pumping prior to evaporation into the UHV chambers. Gas purities and desorbing species were evaluated using a residual gas analyzer (RGA) mounted in the main chamber. Due to the dual-chamber UHV setup, “co-deposited” films were alternating depositions of VTMS and H_2O using either a two-layer (e.g., H_2O/VTMS/Cu) or four-layer (e.g., H_2O/VTMS/ H_2O/VTMS/Cu) deposition sequence at ~90 K. In order to determine the effect of deposition sequence on oxygen incorporation, precursors were deposited in 2-layer and 4-layer sequences with either H_2O or VTMS directly adsorbed on the Cu surface. Electron bombardment of the samples was performed using an ELG-2A electron gun (Kimball Instruments) set at 500 V and 3 μA emission current. The current to the sample was approximately 9 μA as measured by a picoammeter. Direct current magnetron sputter deposition of Cu was performed using a Mini-mak 1.33”

diameter sputter source operated at 150 W using a 500 W d.c. power supply. Pure Ar carrier gas was used during sputter deposition at a pressure of 15 mTorr, and the target material was pure (99.995 %) Cu. The estimated sputter deposition rate was ~0.1 Å/min, based on x-ray photoelectron spectroscopy (XPS) thickness calculations.

XPS characterization was performed in the main UHV chamber using a non-monochromatized Mg Kα x-ray source (Phi 1427) operated at 15 kV and 300 W and with a hemispherical analyzer (VG 100AX) operating in constant pass energy mode (50 eV pass energy). Typical XPS spectra were obtained with the analyzer normal to the sample surface, and angle-resolved spectra were obtained by rotating the sample to an angle of 60º from surface normal. The analyzer binding energy (BE) scale was calibrated with Cu, Au, and Ag standards using the published procedure.[9] XPS data were analyzed using commercially available software and Shirley background subtraction. Atomic ratios were determined according to:

$$\frac{n_1}{n_2} = \frac{I_1 / S_1}{I_2 / S_2} \qquad (5\text{-}1)$$

where n is the number of atoms of the element per cm^3, I is the number of photoelectrons detected per second, and S is the atomic sensitivity factor for each element appropriate to the analyzer.[10] Overlayer thickness calculations were based on the attenuation of the substrate XPS intensity, using $Si(2p_{3/2})$ for SiO_2 substrates, $Cu(2p_{3/2})$, or $Ta(4f_{7/2})$ in the following equation:

$$d = \lambda_A(E_B)\ln(I_B^{\infty}/I_B) \qquad (5\text{-}2)$$

where I_B^{∞}/I_B is the ratio of the unattenuated signal of substrate B to the attenuated signal and $\lambda_A(E_B)$ is the calculated mean free path of the substrate photoelectron of interest through the overlayer A.[11] The mean free path of a $Cu(2p_{3/2})$ photoelectron was calculated to be ~23 Å, using an estimated $Si\text{-}C_x$ film density of ~1.6 g/ml.

5.3. Results and Discussion

5.3.1. Film Composition

Similar to that reported in earlier works,[4] VTMS precursor was condensed onto Cu, Ta, or SiO_2/Si substrates held at low temperature (≤ 95 K) in UHF and subsequently exposed to an electron beam in order to crosslink the precursor molecules. The C(1s), Si($2p_{3/2}$), and O(1s) XPS

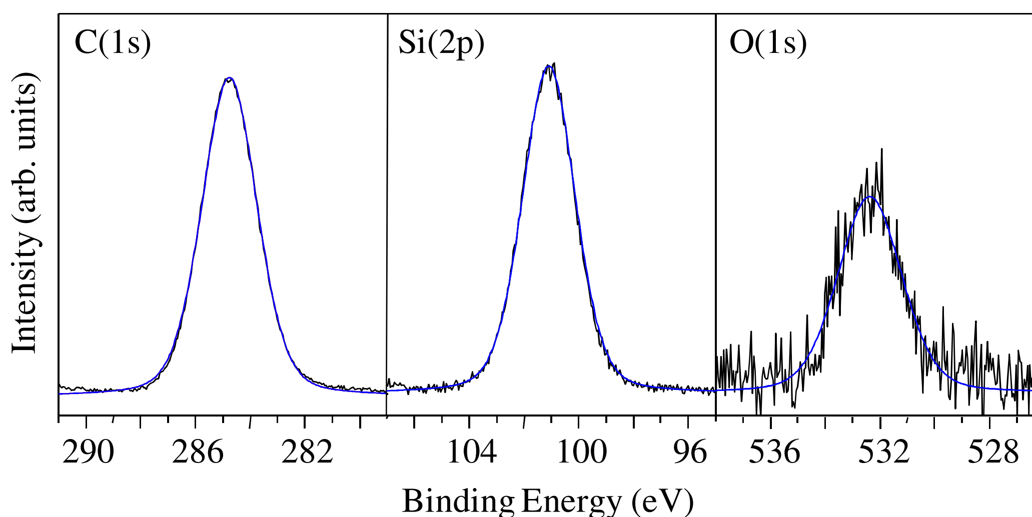

Figure 5.2. XPS spectra of a typical Si-C_x film.

spectra of the resulting films are shown in Fig. 5.2. The small oxygen peak at 532.3 eV in the O(1s) spectrum is likely due to adsorbed or absorbed water, similar to that observed in previous UHV polymer studies,[6,7] although the binding energy is somewhat lower than typical literature values for H_2O.[12] The C(1s) spectrum contains a single peak at 284.7 eV (FWHM = 2.4 eV), and the Si(2p) spectrum a single peak at 101.1 eV (FWHM = 2.3 eV). The single XPS peak of each species indicates that each spectrum contains only a single chemical environment, although differentiation between C–Si and C–C species is extremely difficult using XPS. The C:Si ratio of the pure Si-C_x films was 3.79 ± 0.10, less than the ratio of 5 expected from the pure VTMS

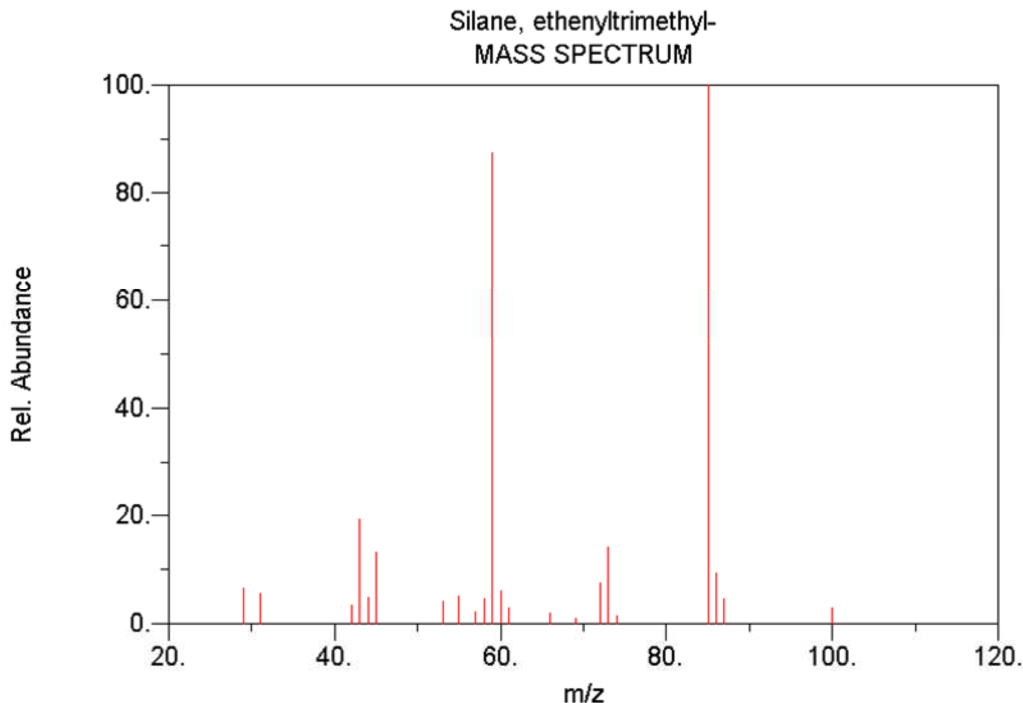

Figure 5.3. Mass spectrum of ethenetrimethylsilane (vinyltrimethylsilane, or VTMS). Reprinted with permission from NIST Standard Reference Database 69. Copyright 2005 National Institute of Standards and Technology.[12]

precursor. As in previous experiments, a C:Si ratio of ~5 was never observed, even upon low-temperature XPS examination of the VTMS precursor prior to e-beam exposure. This is evidence of decomposition of the VTMS precursor during dosing or within the dosing apparatus, likely caused by the loss of a methyl group. The reference mass spectrum of VTMS (Figure 5.3) contains a base peak at m/z = 85 a.u., consistent with the formation of the stable $(CH_3)_2Si^+(CH{=}CH_2)$ species, resultant from the loss of a methyl group, similar to our experimental results.

5.3.2. Stability in Air/H_2O

A Si-C_x film of ~50 Å thickness was deposited onto a Cu foil substrate and allowed to equilibrate to room temperature in UHV. Single XPS peaks were observed in the C(1s) and Si(2p) spectra at 284.7 eV and 101.1 eV, respectively, and very little oxygen was observed

(Fig. 5.4a). The sample was then removed from UHV into the ambient environment for 30 minutes (relative humidity ≈ 48%) and returned to the UHV chamber. Following this short ambient exposure, the O(1s) spectrum (Fig. 5.4b) indicates a slight increase in the total oxygen in the sample, from 2% to 8% of the film composition. The post-exposure O(1s) spectrum contains two peaks at 530.4 eV and 532.5 eV. The low-energy oxygen peak originates from the oxidation of the Cu substrate from Cu metal to Cu_2O; the corresponding shift in Cu(L_3VV) Auger line

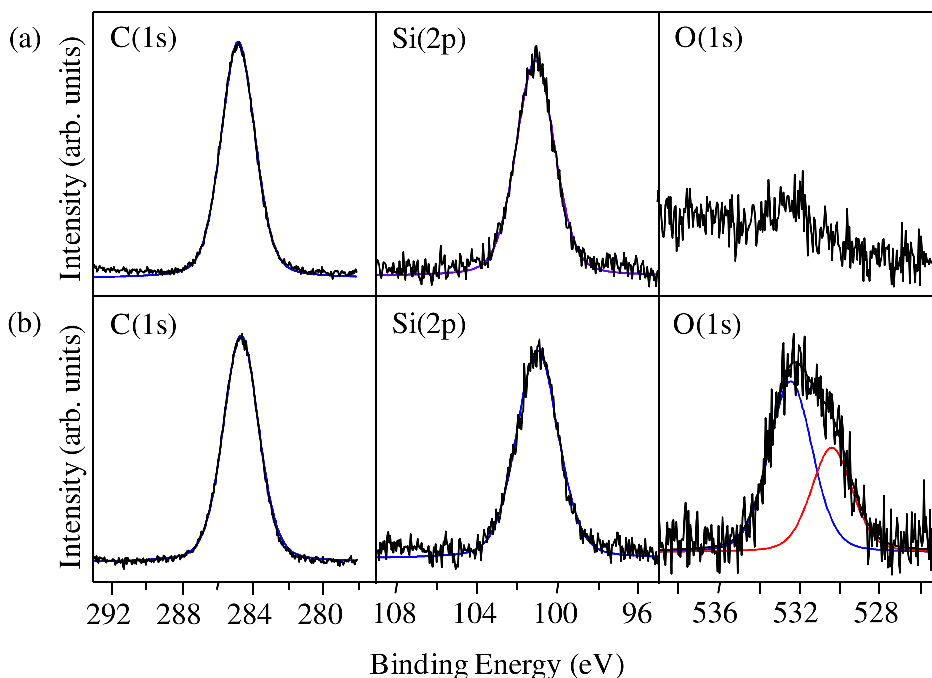

Figure 5.4. XPS spectra of 50 Å Si-C_x film on Cu substrate (a) in UHV and (b) after exposure to ambient environment for 30 minutes.

shape upon exposure (not shown) was also seen. Because of the lack of Si–O peak in the Si(2p) spectrum, the high-energy O(1s) peak at 532.5 eV is again evidence of adsorbed or absorbed water rather than Si–O formation (at similar binding energies of 532.5–532.9 eV). The lack of high binding energy peaks in the C(1s) spectrum is supporting evidence that the film is unreactive to atmospheric oxygen within the short ambient exposure.

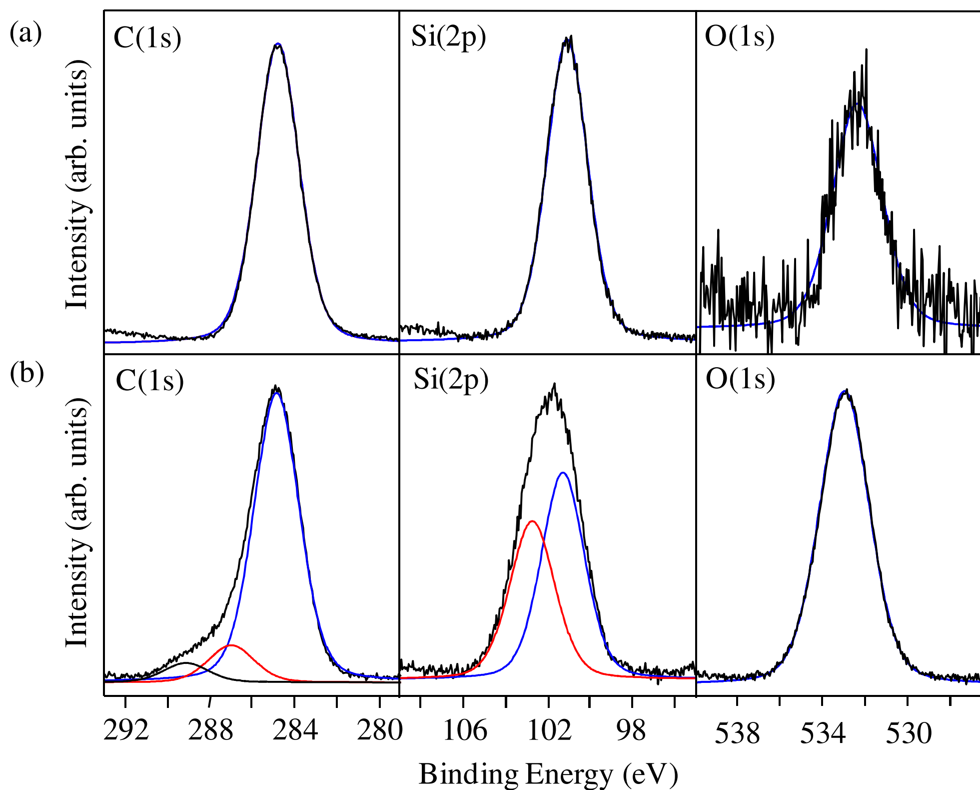

Figure 5.5. Si-C_x Film (~100 Å) on Cu substrate (a) in UHV and (b) after 38 days in air.

A similar sample of ~100 Å Si-C_x/Cu, roughly double the thickness of the original sample, was allowed to remain in ambient conditions for > 30 days and, contrary to the original sample, showed definite signs of oxidation in both the Si(2p) and C(1s) spectra (Fig. 5.5). The high binding energy Si–O peak at 102.7 eV in the Si(2p) spectrum now makes up 44% of the total Si($2p_{3/2}$) intensity. The two new high binding energy peaks observed in the C(1s) spectrum were at 287.0 eV and 289.1 eV, likely from C–O and C=O bonding, respectively.[10] The O(1s) spectrum after 38 days of exposure consists of a single peak at 532.9 eV, corresponding to the O–Si bonding seen in the Si(2p) spectrum. No low-energy O(1s) peak was present in this sample after exposure to ambient, indicating that the film thickness was sufficient to fully protect the Cu substrate from oxidation.

In order to test the reactivity exclusively with water vapor (rather than with O_2), a third sample of ~50 Å Si-C_x/Cu was heated from room temperature to 700 K in the presence of 600 L H_2O vapor (1 x 10^{-6} Torr, 10 min.), which was backfilled into the UHV chamber. This sample showed no evidence of either film oxidation or of water uptake, as measured by increased O(1s) intensity or the observance of high binding energy C(1s) or Si(2p) peaks.

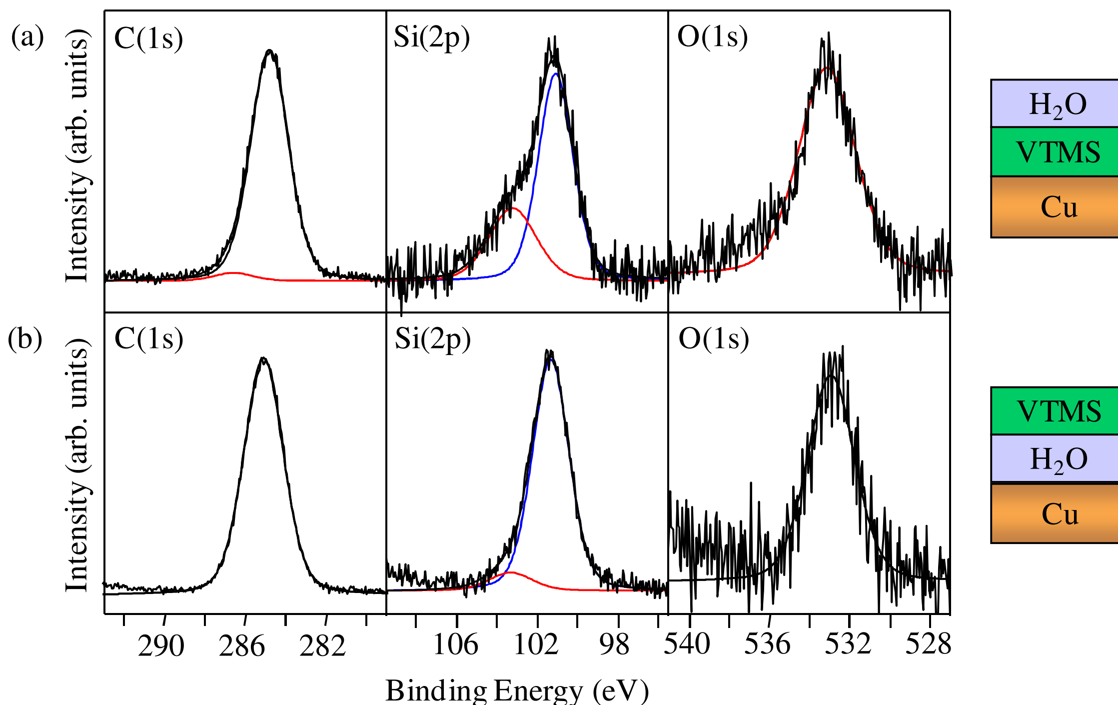

Figure 5.6. XPS spectra of films formed by 2-layer deposition sequences. (a) 30 L exposures with VTMS directly on Cu and (b) 30 L exposures with H_2O directly on Cu.

5.3.3. Addition of Oxygen to films

Although these Si-C_x films are apparently stable to oxidation during relatively short exposures to air and H_2O, oxygen has been added directly into the films by low temperature "co-adsorption" of the VTMS precursor and H_2O followed by e-beam exposure. This co-adsorption was actually an alternating series of adsorptions of VTMS and H_2O precursors onto metal substrates at low temperature (~90 K) by either a two-layer or four-layer ("stacked") sequence

(Figs. 5.6 and 5.7). For two-layer films formed by low-temperature adsorption of VTMS onto a Cu substrate followed by H_2O adsorption, peaks at 101.1 eV and 103.3 eV were observed in the Si(2p) spectra resulting from Si–C and Si–O bonding, respectively (Fig. 5.6a).[10] The high binding energy Si–O peak comprised about 32% of the total Si(2p) peak intensity, indicating a significant amount of oxygen incorporation into the films. A small high binding energy peak (not shown) also appears in the C(1s) spectra of the films at 286.6 eV, due to C–O bond formation. The resulting C:Si atomic ratio of 3.6 in the oxygenated films is similar to that of the original Si-C_x films (C:Si ≈ 3.8).

In the films formed from reversing the H_2O/VTMS dosing sequence (adsorbing H_2O directly on the metal substrate followed by VTMS adsorption) a Si–O peak again appears at 103.3 eV in the Si(2p) spectrum but with much lower intensity (~10% of total Si), and with no corresponding C–O peaks (Fig. 5.6b). Almost identical results were obtained from four-layer

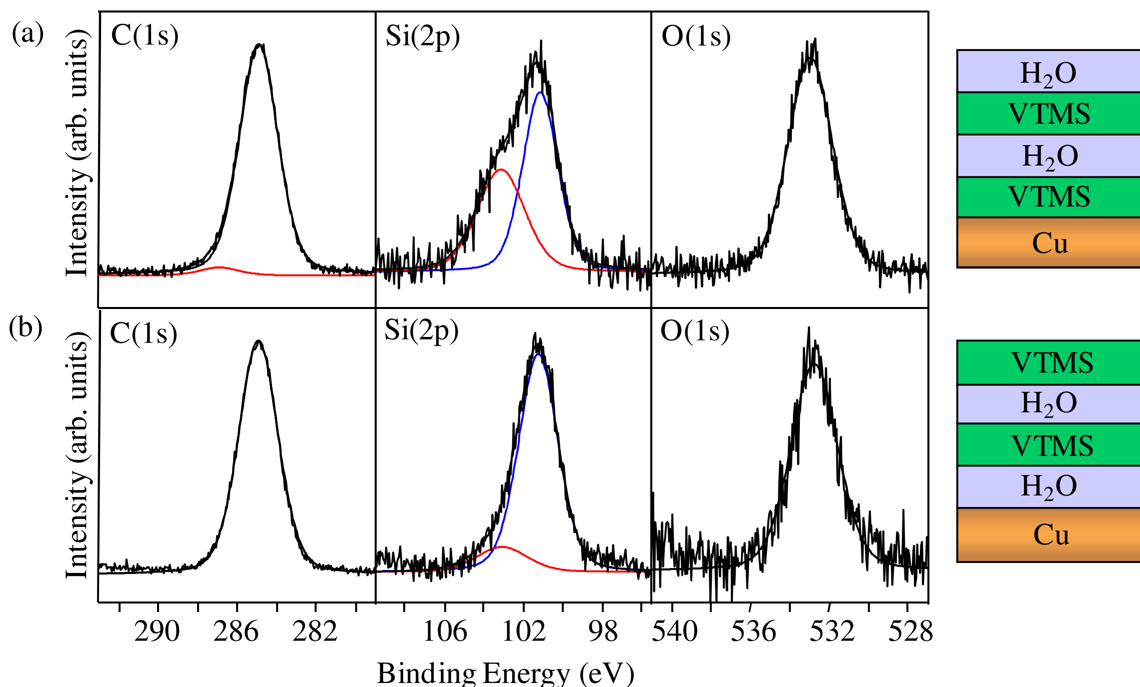

Figure 5.7. XPS spectra of films formed by 4-layer deposition sequences. (a) 5 L exposures with VTMS directly on Cu and (b) 15 L exposures with H2O directly on Cu.

films (Fig. 5.7), where films formed from the adsorption of the VTMS precursor on top of the adsorbed H_2O showed evidence of very little Si–O bond formation (and no C–O bonding), while Si–O formation resulting from H_2O at a film's surface was substantial. Overall, films formed with H_2O layers covering the VTMS also showed significantly decreased film thickness/density than the inverse films. This suggests that during e-beam bombardment, H_2O layers adsorbed atop the VTMS layer attenuate the electron beam reaching the VTMS precursor, thereby decreasing the amount of cross linking between the VTMS molecules for a given e-beam exposure. In addition, the electrons passing through H_2O and reaching the underlying VTMS must encounter the H_2O/VTMS interface, resulting in a larger percentage of the film's cross linking occurring in the presence of water molecules and accounting for a greater percentage of oxygen incorporated in the films.

5.3.4. Annealing of Si(O)C Films

Figure 5.8 shows the Si(2p) spectra of a film formed by e-beam bombardment of a four-layer structure (H_2O/VTMS/H_2O/VTMS/Cu). In each of the Si(2p) spectra, peaks appear at 101.1 and 103.1 eV, though in different ratios depending on anneal temperature. The low binding energy peaks at 101.1 eV are identical to those of the typical Si-C_x films and the high binding energy peaks at 103.3 eV arise from Si–O bonding.[10] At ~90 K, the O(1s) spectrum (not shown) contains a single peak at 533.6 eV, corresponding to adsorbed H_2O, as described earlier. Upon annealing to 300 K there was an apparent desorption of weakly bound oxygen and/or H_2O, resulting in a decrease in both the Si(2p) Si–O peak and the O(1s) peak (not shown). After the 300 K anneal, the O(1s) peak has shifted by 0.7 eV toward lower binding energy to 532.9 eV, which is within the reported values of 532.5–532.9 eV for Si–O bonding in SiO_2.[10] This BE shift

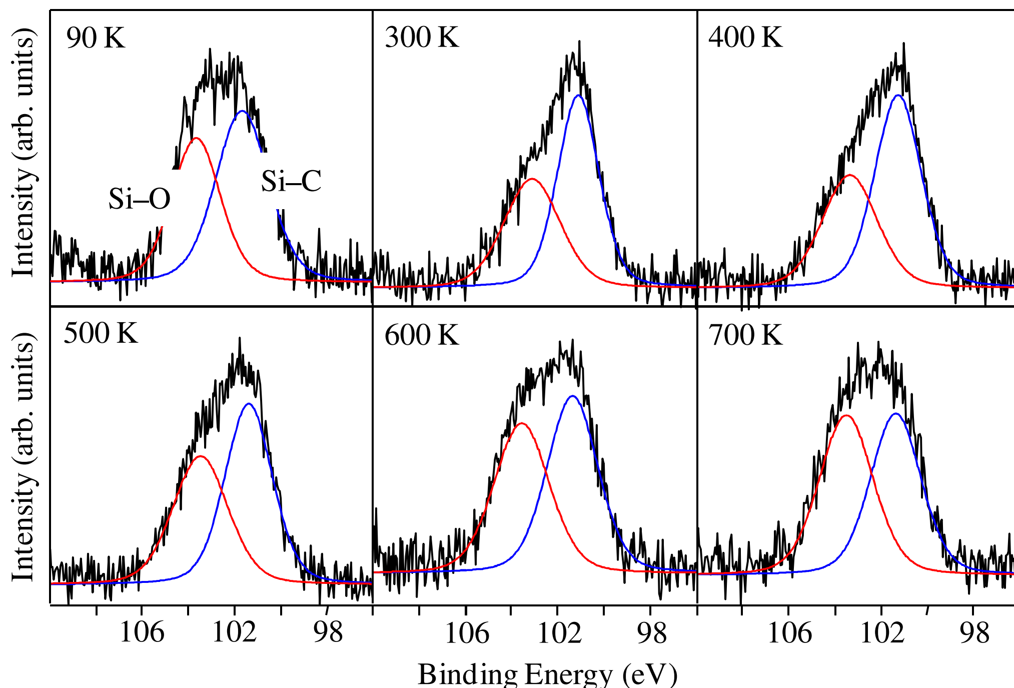

Figure 5.8. Si(2p) spectra of Si(O)C films made from coadsorbed VTMS and H_2O (alternating layers of 5 L each).

indicates a change in the oxygen in the analyzed films from H_2O at 533.6 eV to bound O–Si at 532.9 eV.

For the oxygen-containing Si(O)C films, increased anneal temperature in the range of 300–700 K led to increased Si–O bond formation, as shown by increasing intensities of the peaks at 103.1 eV in the Si(2p) spectra. The O(1s) intensity remained relatively constant through the range of 300–700 K annealing temperatures, indicating no major oxygen loss from the films. At 700 K, ~51% of the total Si(2p) intensity from the film was from Si–O bonding. A decrease in the C:Si atomic ratios from 3.47 (at 300 K) to 2.90 (at 700 K) is evidence of the loss of C in the films from the breaking of Si-C bonds and subsequent formation of Si-O bonds at elevated temperatures.

5.3.5. Cu Interactions with Si-C_x Films

Sputter deposition was utilized in order to investigate the interactions of small amounts of deposited Cu with Si-C_x films of 50–100 Å thickness on silicon. A series of Cu depositions (2

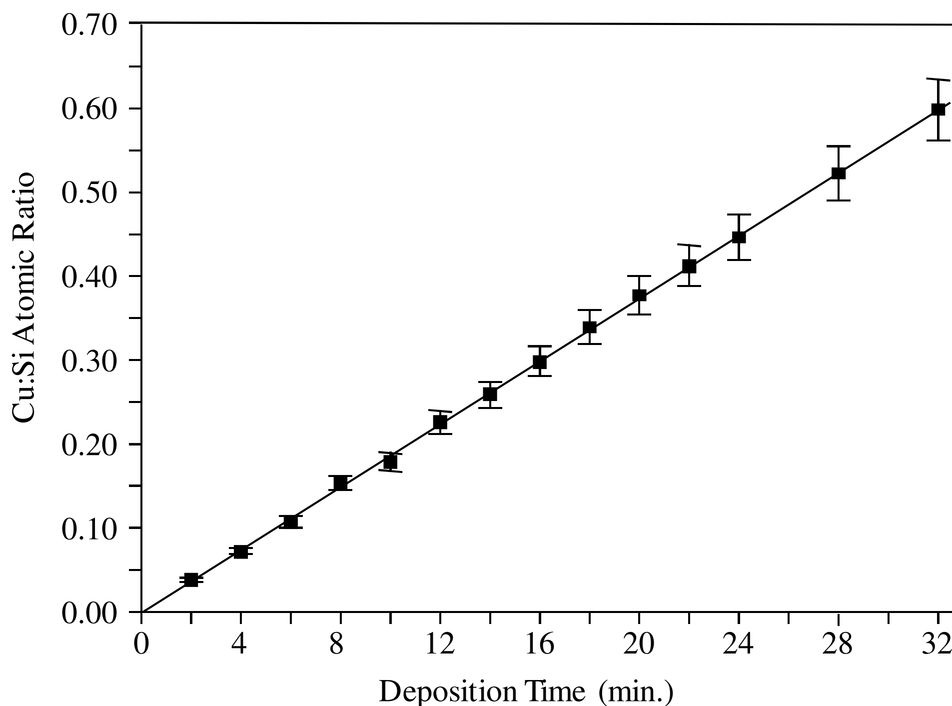

Figure 5.9. Deposition curve for Cu sputter deposited onto 50 Å Si-C_x. Sputter deposition rate was ~0.1 Å/min.

minutes each, ~0.05 monolayers/min) were performed on each Si-C_x sample in the CVD/PVD chamber. After each sputter deposition, the sample was transferred into the main UHV chamber for XPS analysis and returned to the CVD/PVD chamber for further deposition. The atomic ratio vs. deposition time plot in Figure 5.9 indicates weak interaction between Cu and Si-C_x substrates. Strong metal–substrate interactions, as previously observed between Cu and Al_2O_3,[14] result in an initial conformal Cu layer, followed by subsequent layer-by-layer growth of the Cu (Frank–van der Merwe growth). This conformal overlayer growth is indicated by a sudden change in the slope of the Cu(2p):Si(2p) atomic ratio vs. time plot at the point where one monolayer is completed and another begins.[8,13,14] No abrupt change in slope was ever witnessed

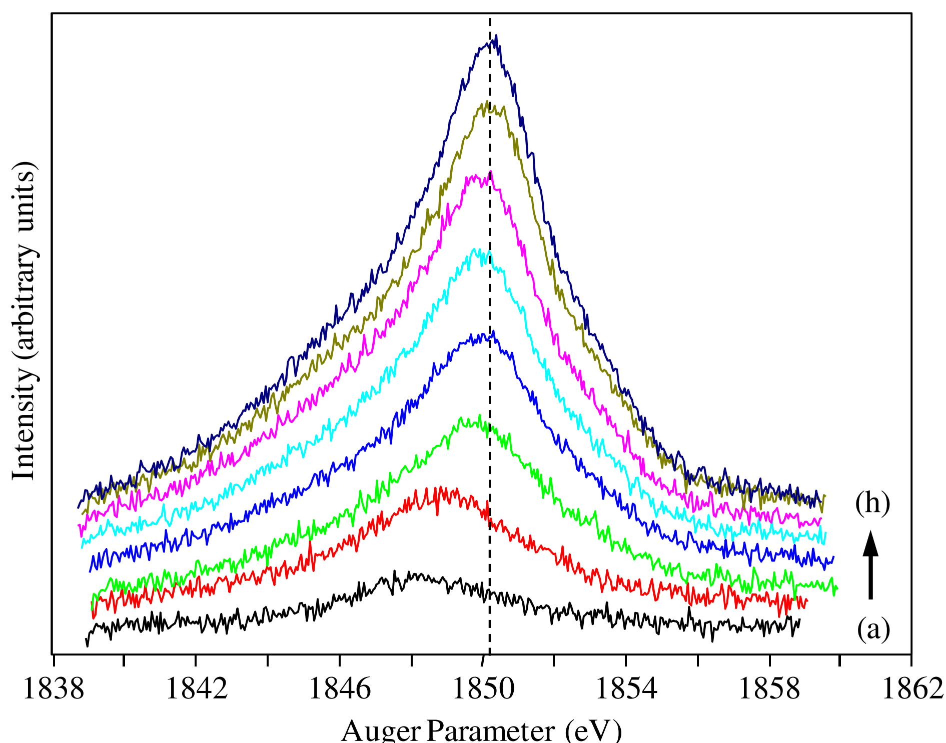

Figure 5.10. Cu (L_3VV) Auger peak after sputter deposition of Cu onto a Si-C_x film. (a) 4 min. (b) 8 min. (c) 12 min. (d) 16 min. (e) 20 min. (f) 24 min. (g) 28 min and (h) 32 min.

during these experiments with Cu on Si-C_x films, indicating that Cu deposition resulted in either the formation of three-dimensional clusters or implantation into the film. Previous experiments also resulted in appreciable amounts of Cu(I) due to charge transfer from the deposited Cu to the substrate, as seen by changes in the x-ray excited Auger $L_3M_{4,5}M_{4,5}$ (or simply L_3VV) lineshape.[14] A slight change in line shape with deposition time was noticed in this experiment, as shown in Fig. 5.10, but was likely due to native Cu oxide formation while in the sputter chamber rather than charge transfer to the film substrate.

The modified Auger parameter has been shown to be very sensitive to the oxidation state of Cu and is given as:

$$\alpha = KE_{Auger} + BE_{Cu2p} \qquad (5\text{-}3)$$

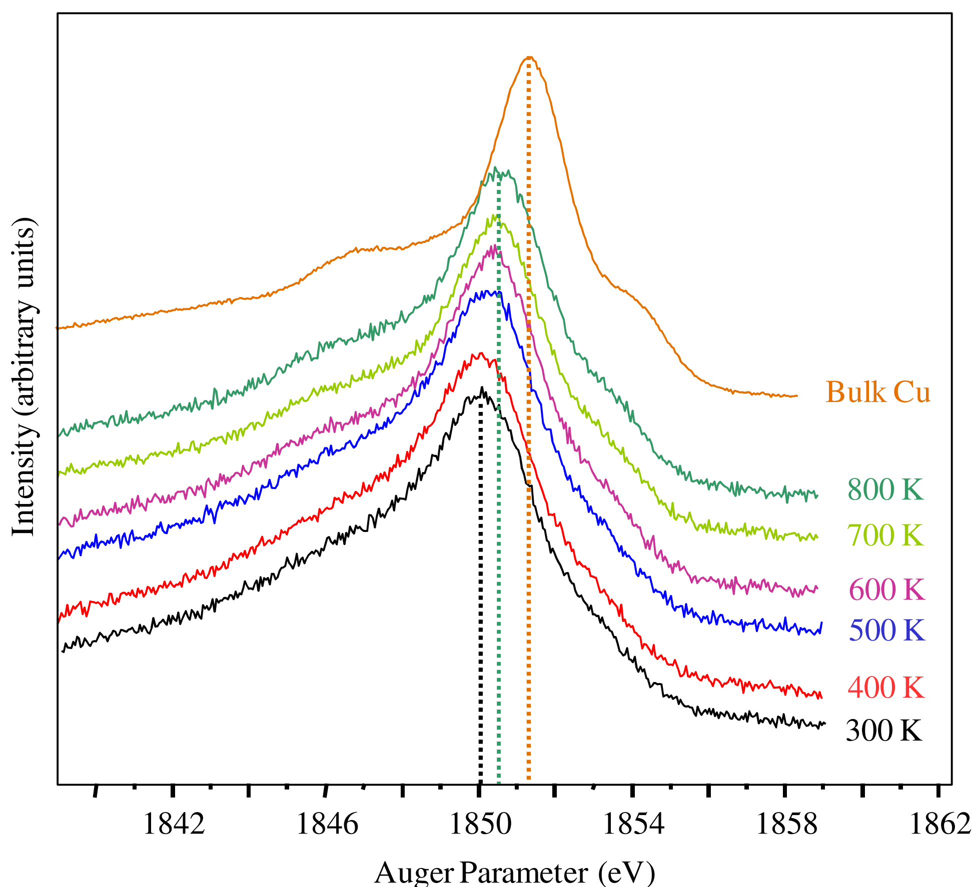

Figure 5.11. Shift in Cu Auger parameter with annealing temperature (a)–(f) and bulk Cu foil (g).

After 4 minutes (~0.5 monolayer) of deposition the Auger parameter was 1848.9 eV, similar to values reported for Cu(I) (1848–1849 eV).[10] After 32 minutes deposition time, the Cu Auger parameter had shifted to a value of 1850.1 eV, still lower than the value of metallic Cu (α = 1851.3 eV). It has been previously demonstrated that Auger kinetic energy is affected by final state hole–hole interactions, and that localization effects occur due to limited charge screening by small particles.[15] The increase in Cu Auger parameter with deposition time is indicative of an increase in particle size - further evidence that Cu islanding is occurring on the Si-C_x surface.

After Cu deposition, the Si-C_x sample was annealed in 100 K increments at 10 minutes each to a final temperature of 800 K. Figure 5.11 shows the shift in Auger parameter with increased anneal temperature, referenced to the value of bulk Cu(0). At 800 K the Auger

parameter has increased slightly to 1850.6 eV, indicating continued growth or aggregation of the Cu islands with increased temperature. No Cu silicide was ever detected by XPS in these studies.

5.4. Conclusions

Studies were carried out on Si-C_x film samples formed in UHV by e-beam bombardment of VTMS precursor adsorbed onto metal substrates. Results show that films with C:Si ratios of ~4:1 are formed that are stable to oxidation under ambient conditions for short periods (> 30 min.) but undergo some oxidation during long exposures to air (≤ 38 days). Although very little oxygen was incorporated using solely VTMS precursor, oxygen was added to the films by co-adsorbing H_2O prior to e-beam bombardment.

Previous studies showed Si-C_x films to be stable to ≥ 1000 K; similarly, oxygen-containing Si(O)C_x films were shown to be stable to ≥ 700K (the highest temperature tested). Serial annealing of the Si(O)C_x films to increasing temperatures resulted in increased Si–O bond formation, while oxygen concentrations in the films remained relatively constant at temperatures between 300 K and 700 K. At elevated temperatures (> 300 K), Si–C bonding was replaced by Si–O bond formation, with a corresponding decrease in C:Si ratios and increase in Si–O peaks intensity in XPS. Thus, depending on the co-adsorbed species used, properties of the resulting films may be tailored for stress, dielectric, or bonding properties by co-deposition of differing amounts and species of oxygen.

Cu was sputter-deposited onto 50–100 Å Si-C_x films in very small increments (~0.1 Å/min, or ~0.05 monolayers/min), and XPS measurements indicate Volmer–Weber growth of the Cu (formation of 3D nuclei), rather than formation of distinct monolayers of surface coverage. This island growth is evidence of low Cu–film interaction and poor adhesion of the

Cu; this is in distinct contrast to 50–100 Å Si-C_x films formed directly on Cu, which were stable to > 600 K. Upon anneal at temperatures of 400–800 K, the Cu Auger parameter gradually shifted toward that of bulk Cu, indicating further growth or coalescence of Cu islands. Due to the industry preference of dielectric films and barrier layers with good Cu adhesion properties, some surface modification techniques would likely be necessary for integration of Si-C_x into current or future dual-damascene processing.

5.5. Chapter References

1. Rodriguez, O.; Cho, W.; Saxena, R.; Plawsky, J. L.; Gill, W. N. *J. Appl. Phys.* **2005**, *98*, 24108.

2. McBrayer, J. D.; Swanson, R. M.; Sigmon, T. W. *J. Electrochem. Soc.* **1986**, *133*, 1242.

3. Shacham-Diamand, Y.; Dedhia, A.; Hoffstetter, D.; Oldham, W. G. *J. Electrochem. Soc.* **1993**, *140*, 2427.

4. Chen, L.; Kelber, J. A. *J. Vac. Sci. Technol. A* **1999**, *17*, 1968.

5. Chen, J.G.; Colaianni, M. X.; Weinberg, W. H.; Yates, J. T. *Surf. Sci.* **1992**, *279*, 223.

6. Sutcliffe, R.; Lee, W. W.; Gaynor, J. F.; Luttmer, J. D.; Martini, D.; Kelber, J.; Plano, M. A. *Appl. Surf. Sci.* **1998**, *126*, 43.

7. Martini, D.; Shepherd, K.; Sutcliffe, R.; Kelber, J. A.; Edwards, H.; Martin, R. S. *Appl. Surf. Sci.* **1999**, *141*, 89.

8. Shepherd, K.; Niu, C.; Martini, D.; Kelber, J. A. *Appl. Surf. Sci.* **2000**, *158*, 1.

9. Powell, C.J.; Jablonski, A.; Tilinin, I. S.; Tanuma, S.; Penn, D.R. *J. Electr. Spectrosc. Relat. Phenom.* **1999**, *98*, 1.

10. Moulder, J. F.; Stickle, W. F.; Sobol, P. E.; Bomben, K. D. *Handbook of X-ray Photoelectron Spectroscopy*; Physical Electronics: Eden Prairie, MN, 1995.

11. Seah, M. P. Quantification of AES and XPS. In *Practical Surface Analysis Vol. 1, Auger and X-ray Photoelectron Spectroscopy*, 2nd ed.; Briggs, D., Seah, M. P., Eds.; Wiley: New York, 1990; pp 201–255.

12. NIST Mass Spec Data Center, S.E. Stein, director, Mass Spectra. In *NIST Chemistry WebBook, NIST Standard Reference Database Number 69*; Linstrom, P. J., Mallard,

W.G., Eds.; National Institute of Standards and Technology: Gaithersburg, MD, 2005. (http://webbook.nist.gov).

13. Argile, C.; Rhead, G. E. *Surf. Sci. Reports* **1989**, *10*, 277.

14. Niu, C.; Shepherd, K.; Martini, D.; Tong, J.; Kelber, J. A.; Dennison, D. R.; Bogicevic, A. *Surf. Sci.* **2000**, *465*, 163.

15. Jennison, D. R.; Kelber, J. A.; Rye, R. R. *Phys. Rev. B* **1982**, *25*, 1384.

LIST OF REFERENCES

Akhter, S.; Zhou, X. -L.; White, J. M. *Appl. Surf. Sci.* **1989**, *37*, 201.

Akhter, S.; Zhou, X.-L.; White, J. M. *Appl. Surf. Sci.* **1989**, *37*, 201.

Argile, C.; Rhead, G. E. *Surf. Sci. Reports* **1989**, *10*, 277.

Baglin, J. E. E. *Nucl. Instr. Meth. Phys. Res.* **1992**, *B65*, 119.

Beamson, G.; Briggs, D.; *High Resolution XPS of Organic Polymers;* Wiley: New York, 1992.

Benndorf, C.; Caus, H.; Egert, B.; Seidel, H.; Thieme, F. *J. Electron Spec. Rel. Phenom.* **1980**, *19*, 77.

Bent, B. E.; Nuzzo, R. G.; Dubois, L. H. *J. Am. Chem. Soc.* **1989**, *111*, 1634.

Blanchet, G. B. *Appl. Phys. Lett.* **1993**, *62*, 479.

Briggs, D.; Beamson, G. *Anal. Chem.* **1993**, *65*, 1517.

Briggs, D.; Rivière, J. C. Spectral Interpretation. In *Practical Surface Analysis Vol. 1, Auger and X-ray Photoelectron Spectroscopy*, 2nd ed.; Briggs, D., Seah, M. P., Eds.; Wiley: New York, 1990; pp 86–141.

Buck, W. H.; Resnick, P. R. Properties of Amorphous Fluoropolymer Based on 2,2-Bistrifluoromethyl-4,5-Difluoro-1,3-Dioxole. Proceedings of the183rd Meeting of the Electrochemical Society, Honolulu, HI, May 16–23, 1993.

Cadman, P.; Grossedge, G. M. *J. Mater. Sci.* **1979**, *14*, 2672.

Carley, A. F.; Roberts, M. W. *Proc. R. Soc. London A* **1978**, *363*, 403.

Catherine, Y.; Turban, G. *Thin Solid Films* **1979**, *60*, 193.

Chang, C.-A.; Kim, Y.-K.; Schrott, A. G. *J. Vac. Sci. Tech. A* **1990**, *8*, 3304.

Chen, J. G.; Colaianni, M. X.; Weinberg, W. H.; Yates, J. T. *Surf. Sci.* **1992**, *279*, 223.

Chen, L.; Kelber, J. A. *J. Vac. Sci. Technol. A* **1999**, *17*, 1968.

Cho, C.-C.; Wallace, R. M.; Files-Sesler, L.A. *J. Electronic Mat.* **1994**, *23*, 827.

Clark, D. T.; Feast, W. J.; Kilcast, D.; Musgrave, W. K. R. *J. Polym. Sci. Polym. Chem.* **1973**, *11*, 389.

Clark, D. T.; Kilcast, D.; Adams, D. B.; Musgrave, W. K. R. *J. Electron Spec. Relat. Phenom.* **1972**, *1*, 227.

Cohen, S. L.; Liehr, M.; Kasi, S. *Appl Phys. Lett.* **1991**, *60*, 50.

Creighton, J. R.; Parmeter, J. E. *Crit. Rev. Solid State Mater. Sci.* **1993**, *18*, 175.

Dean, J. A.; *Lange's Handbook of Chemistry*, 14th ed.; McGraw-Hill: New York, 1992.

Deplancke, M. P.; Powers, J. M.; Vandentop, G. J.; Salmeron, M.; Somorjai, G. A. *J. Vac. Sci. Technol. A* **1991**, *9*, 450.

Donnelly, V. M.; Gross, M. E. *J. Vac. Sci. Tech. A* **1993**, *11*, 66.

Drüsedau, T. P; Lohmann, M.; Klabunde, F.; John, T.-M. *Surf. Coat. Technol.* **2000**, *133*, 126.

Du, M.; Opila, R. L.; Case, C. *J. Vac. Sci. Technol. A* **1998**, *16*, 155.

Du, Y.; Gardella, J. A., Jr. *J. Vac. Sci. Tech. A* **1995**, *13*, 1907.

ESCATools, v.4.2; Surface/Interface, Inc.: Mountain View, CA.

ESCATools, v.4.6; Surface/Interface, Inc.: Sunnyvale, CA, 1995.

Fleming, R. *The CEA Online Tutorial*. http://www.cea.com/cai/rbstheo/cairtheo.htm (accessed May, 2000), Charles Evans & Associates.

Giorgis, F.; Giuliani, F.; Pirri, C. F.; Tresso, E.; Conde, J. P.; Chu, V. *J. Non-Cryst. Solids* **1998**, *227*, 465.

Girolami, G. S.; Jeffries, P. M.; Dubois, L. H. *J. Am. Chem. Soc.* **1993**, *115*, 1015.

Gorham, W. F. *J. Polym. Sci. A* **1996**, *4*, 3087.

Graziani, E. I.; McKeown, N. B.; Kalman, P. G.; Thompson, M. *Inter. Biodeter. Biodeg.* **1992**, *30*, 217.

Grill, A.; Patel, V. *J. Appl. Phys.* **1999**, *85*, 3314.

Guinn, K. V.; Donnelly, V. M.; Gross, M. E.; Baiocchi, F. A. *Surf. Sci.* **1993**, *295*, 219.

Han, H. W.; Lee, N.-E. *Thin Solid Films* **2005**, *475*, 144.

Handbook of X-Ray Photoelectron Spectroscopy; Wagner, C. D., Riggs, W. M., Moulder, J. S., Davis, L. E., Eds.; Perkin Elmer: Eden Prarie, MN, 1979.

Harrus, A. S.; Plano, M. A.; Kumar, D.; Kelly, J. Parylene AF-4: A Low Material Candidate for ULSI Multilevel Interconnect Applications. *In Low-Dielectric Constant Materials II;* Lagendijk, A., Treichel, H., Uram, K. J., Jones, A. C., Eds.; MRS Symposium Proceedings Vol. 443; Materials Research Society: Warrendale, PA, 1997; pp 21–33.

Havemann, R. H.; Jain, M. K.; List, R. S.; Ralston, A. R.; Shih, W.-Y.; Jin, C.; Chang, M. C.; Zielinski, E. M.; Dixit, G. A.; Singh, A.; Russell, S. W.; Gaynor, J. F.; McKerrow, A. J.; Lee, W. W. Overview of Process Integration Issues for Low K Dielectrics. In *Low-Dielectric Constant Materials IV*; Chiang, C., Ho, P. S., Lu, T.-M., Wetzel, J. T., Eds.; MRS Symposium Proceedings vol. 511; Materials Research Society: Warrendale, PA, 1998.

Higashi, G. S. *Appl. Surf. Sci.* **1989**, *43*, 6.

Hopkins, J.; Boyd, R. D.; Badyal, J. P. S. *J. Phys. Chem.* **1996**, *100*, 6755.

International Technology Roadmap for Semiconductors, 1999 Ed.; Semiconductor Industry Association: San Jose, CA, 1999.

Jeng, S. P.; Chang, M.-C.; Kroger, T.; McAnally, P.; Havemann, R. H**.** A planarized multilevel interconnect scheme with embedded low-dielectric-constant polymers for sub-quarter-micron applications. In *Digest of Technical Papers*, 1994 Symposium on VLSI Technology, Honolulu, HI, May 7–9, 1994; IEEE: 1994; 73.

Jennison, D. R.; Kelber, J. A.; Rye, R. R. *Phys. Rev. B* **1982**, *25*, 1384.

Jirka, I. *Surf. Sci.* **1990**, *232*, 307.

John, P. J.; Liang, J. *J. Vac. Sci. Tech. A* **1994**, *12*, 199.

Kim, D.-H.; Wentorf, R. H.; Gill, W. N. *J. Vac. Sci. Technol. A* **1994**, *12*, 153.

Kim, M. T.; Lee, J. *Thin Solid Films* **1997**, *303*, 173.

Kim, Y.-K.; Chang, C.-A.; Schrott, A. G. *J. Appl. Phys.* **1990**, *67*, 251.

Kishi, K.; Ikeda, S. *Bull. Chem. Soc. Jpn.* **1972**, *46*, 341.

Lee, W. W. *Thin Solid Films* **1995**, *262*, 39.

Lee, W. W.; Ho, P. S. *Mater. Res. Soc. Bulletin* **1997**, *22*, 19.

Lee, M.-S.; Bent, S. F. *J. Vac. Sci. Technol. A* **1998**, *16*, 1658.

Lee, W.-Y. *J. Appl. Phys.* **1980**, *51*, 3365.

Loboda, M. J.; Seifferly, J. A.; Dall, F. C. *J. Vac. Sci. Technol. A* **1994**, *12*, 90.

Martensson, N.; Malmquist, P. A.; Svensson, S.; Basilier, E.; Pireaux, J. J.; Gelius, U.; Siegbahn, K. *Nouv. J. Chim.* **1977**, *1*, 191.

Martini, D.; Shepherd, K.; Sutcliffe, R.; Kelber, J. A.; Edwards, H.; Martin, R. S. *Appl. Surf. Sci.* **1999**, *141*, 89.

Martini, D.; Sutcliffe, R.; Kelber, J. MOCVD of Cu on Teflon®-AF and Alumina-Modified Teflon®-AF. In *Low Dielectric Constant Materials III,* Proceedings of the Materials Research Society Symposium, San Franciso, CA, April 1–4, 1997; Case, C., Kohl, P., Kikkawa, T., Lee, W. W., Eds.; Materials Research Society: Pittsburgh, 1997; pp 61–67.

Matienzo, L. J.; Zimmerman, J. A.; Egitto, F. D. *J. Vac. Sci. Tech. A.* **1994**, *12*, 2662.

McBrayer, J. D.; Swanson, R. M.; Sigmon, T. W. *J. Electrochem. Soc.* **1986**, *133*, 1242.

McGuire, G. E.; Schweitzer, G. K.; Carlson, T. A. *Inorg. Chem.* **1973**, *12*, 2450.

McIntyre, N. S.; Chan, T. C. Uses of Auger Electron and Photoelectron Spectroscopies in Corrosion Science. In *Practical Surface Analysis Vol. 1, Auger and X-ray Photoelectron Spectroscopy*, 2nd ed.; Briggs, D., Seah, M. P., Eds.; Wiley: New York, 1990; pp 485–529.

McMurry, J. *Organic Chemistry*, 3rd ed.; Brooks/Cole: Pacific Grove, CA, 1992.

Moulder, J. F.; Stickle, W. F.; Sobol, P. E.; Bomben, K. D. *Handbook of X-ray Photoelectron Spectroscopy*; Physical Electronics: Eden Prairie, MN, 1995.

Murarka, S. P. *Solid State Technol.* **1996**, *39*, 83.

Naik, M. B.; Gill, W. N.; Wentorf, R. H.; Reeves, R. R. *Thin Solid Films* **1995**, *262*, 60.

Nason, T. C.; Moore, J. A.; Lu, T.-M. *Appl. Phys. Lett.* **1992**, *60*, 1866.

The National Technology Roadmap for Semiconductors, 1994 ed.; Semiconductor Industry Association: San Jose, 1994.

Nefedov, V. I.; Gati, D.; Dzhurinskii, B. F.; Sergushin, N. P.; Salyn, Y. V. *Zh. Neorg. Khim.* **1975**, *30*, 2307.

Nguyen, T.; Charneski, L. J.; Hsu, S. T. *J. Electrochem. Soc.* **1997**, *144*, 2829.

NIST Mass Spec Data Center, S.E. Stein, director, Mass Spectra. In *NIST Chemistry WebBook, NIST Standard Reference Database Number 69*; Linstrom, P. J., Mallard, W.G., Eds.; National Institute of Standards and Technology: Gaithersburg, MD, 2005. (http://webbook.nist.gov).

Niu, C.; Shepherd, K.; Martini, D.; Tong, J.; Kelber, J. A.; Dennison, D. R.; Bogicevic, A. *Surf. Sci.* **2000**, *465*, 163.

Nowak, P.; McIntyre, N. S.; Hunter, D. H.; Bello, I.; Lau, W. M. *Surf. Int. Anal.* **1995**, *23*, 873.

Nuesca, G. M.; Kelber, J. A. *Thin Solid Films* **1995**, *262*, 224.

Nuesca, G.; Prasad, J.; Kelber, J. A. *Appl. Surf. Sci.* **1994**, *81*, 237.

Pan, F.-M.; Huang, J.-L.; Liaw, C.-F. *J. Vac. Sci. Technol. A* **1993**, *11*, 3076.

Perry, W. L.; Chi, K. M.; Kodas, T.; Hampden-Smith, M.; Rye, R. *Appl. Surf. Sci.* **1993**, *69*, 94.

Plano, M. A.; Kumar, D.; Cleary, T. The Effect of Deposition Conditions on the Properties of Vapor-Deposited Parylene AF-4 Films. In *Low Dielectric Constant Materials III,* Proceedings of the Materials Research Society Symposium, San Francisco, CA, April 1–4, 1997; Case, C., Kohl, P., Kikkawa, T., Lee, W. W., Eds.; Materials Research Society: Pittsburgh, 1997; pp 213–218.

Powell, C. J. *Surf. Int. Anal.* **1995**, *23*, 121.

Powell, C.J.; Jablonski, A.; Tilinin, I. S.; Tanuma, S.; Penn, D.R. *J. Electr. Spectrosc. Relat. Phenom.* **1999**, *98*, 1.

Rhead, G. E.; Barthès, M.-G.; Argile, C. *Thin Solid Films* **1981**, *82*, 201.

Roberts, R. F.; Ryan, F. W.; Schonhorn, H.; Sessler, G. M.; West, J. E. *J. Appl. Polym. Sci.* **1976**, *20*, 255.

Rodriguez, O.; Cho, W.; Saxena, R.; Plawsky, J. L.; Gill, W. N. *J. Appl. Phys.* **2005**, *98*, 24108.

Rogers, J. W., Jr. An Electron Spectroscopic Investigation of the Interaction of Methanol and Ammonia with Clean and Partially Oxidized Aluminum Surfaces. Ph.D. Thesis, The University of Texas, 1979.

Rogers, J. W., Jr.; Hance, R. L.; White, J. M. *Surf. Sci.* **1980**, *100*, 388.

Rye, R. R. *J. Polym. Sci. B* **1993**, *31*, 357.

Ryu, C.; Lee, H.; Kwon, K.-W.; Loke, A. L. S.; Wong, S. S. *Mater. Res. Soc. Symp. Proc.* **1998**, **14**, 75.

Sacher, E. *Prog. Surf. Sci.* **1994**, *47*, 273.

Seah, M. P. Quantification of AES and XPS. In *Practical Surface Analysis Vol. 1, Auger and X-ray Photoelectron Spectroscopy*, 2nd ed.; Briggs, D., Seah, M. P., Eds.; Wiley: New York, 1990; pp 201–255.

Seekamp, J.; Bauhofer, W. *J. Non-Cryst. Solids* **1998**, *227*, 474.

Seki, K.; Frye, J. M.; Okabe, H.; Halpern, J. B. *J. Cryst. Growth* **1993**, *132*, 25.

Sekiguchi, A.; Kobayashi, T.; Hosokawa, N.; Asamaki, T. *J. Vac. Sci. Technol. A* **1990**, *8*, 2976.

Shacham-Diamand, Y.; Dedhia, A.; Hoffstetter, D.; Oldham, W. G. *J. Electrochem. Soc.* **1993**, *140*, 2427.

Shepherd, K.; Niu, C.; Martini, D.; Kelber, J. A. *Appl. Surf. Sci.* **2000**, *158*, 1.

Shi, M.-K.; Lamontagne, B.; Belmani, A.; Martinu, L. *J. Vac. Sci. Tech. A* **1994**, *12*, 44.

Shi, M.-K.; Lamontagne, B.; Martinu, L.; Semani, A. *J. Appl. Phys.* **1993**, *74*, 1744.

Shi, M. K.; Lamontagne, B.; Selmani, A.; Martinu, L.; Sacher, E.; Wertheimer, M. R.; Yelon, A. *J. Vac. Sci. Technol. A* **1994**, *12*, 29.

Singer, P. *Semiconductor Int.* **1996**, *19*, 88.

Somorjai, G. *Introduction to Surface Chemistry and Catalysis*; Wiley: New York, 1994.

Stapinski, T.; Ambrosone, G.; Coscia, U.; Giorgis, F.; Pirri, C. F. *Physica B* **1998**, *254*, 99.

Strongin, D. R.; Comita, P. B. *J. Phys. Chem.* **1991**, *95*, 1329.

Sun, J. Q.; Bello, I.; Bederka, S.; Lau, W. M. *J. Vac. Sci. Technol. A* **1996**, *14*, 1382.

Sutcliffe, R.; Lee, W. W.; Gaynor, J. F.; Luttmer, J. D.; Martini, D.; Kelber, J.; Plano, M. A. *Appl. Surf. Sci.* **1998**, *126*, 43.

Sutcliffe, R.; Martini, D.; Pavlica, D.; Kelber, J. MO-CVD of Aluminum and Copper on Teflon®-AF. In *Advanced Metallization and Interconnect Systems for ULSI Applications, 1996,* MRS Conference Proceedings Vol.12; Havemann, R., Schmitz, J., Komiyama, H., Tsubouchi, K., Eds.; Materials Research Society: Warrendale, PA, 1997; pp 437–447.

Tan, B. J.; Fessehaie, M.; Suib, S. *Langmuir* **1993**, *9*, 740.

Tsubouchi, K.; Masu, K. *Vacuum* **1995**, *46*, 1249.

Vasile, M. J.; Bachman, B. J. *J. Vac. Sci. Technol. A* **1989**, *7*, 2992.

Wagner, C. D.; Zatko, D. A.; Raymond, R. H. *Anal. Chem.* **1980**, *52*, 1445.

Wang, L.; Angert, N.; Trautmann, C.; Vetter, J. *J. Adhesion Sci. Tech.*1995, *9*,1523.

Wary, J.; Olson, R.; Beach, W. *Semiconductor Int.* **1996**, *June*, 211.

Wasa, K.; Hayakawa, S. *Handbook of Sputter Deposition Technology*; Noyes: Park Ridge, NJ, 1992.

Wells, R. K.; Ryan, M. E.; Badyal, J. P. S. *J. Phys. Chem.* **1993**, *97*, 12879.

Wren, A. G.; Phillips, R. W.; Tolentino, C. U. *J. Colloid Interface Sci.* **1979**, *70*, 544.

Wu, P. K.; Yang, G.-R.; McDonald, J. F.; Lu, T.-M. *J. Electronic Mat.* **1995**, *24*, 53.

Wu, P. K.; Dabral, S.; Yang, G.-R.; Gittleman, B.; Li, C.; McDonald, J. F.; Lu, T.-M. *J. Appl. Phys.* **1996**, *80*, 5759.

Xu, J.; Choyke, W. J.; Yates, J. T. *Appl. Surf. Sci.* **1997**, *120*, 279.

You, L.; Yang, G.-R.; Lang, C.-I.; Moore, J. A.; Wu, P.; McDonald, J. F.; Lu, T.-M. *J. Vac. Sci. Tech. A* **1993**, *11*, 3047.

You, L.; Yang, G.-R.; Knorr, D. B.; McDonald, J. F.; Lu, T.-M. *Appl. Phys. Lett.* **1994**, *64*, 2812.

Zhang, X.; Dabral, S.; Chiang, C.; McDonald, J. F.; Wang, B. *Thin Sol. Films* **1995**, *270*, 508.